2020

Fully Compressible Hydrodynamic Simulation of Non-Equidiffusive Premixed Flames Propagation in Channels

Olatunde A. Abidakun
West Virginia University, oaabidakun@mix.wvu.edu

2020

Fully Compressible Hydrodynamic Simulation of Non-Equidiffusive Premixed Flames Propagation in Channels

Olatunde A. Abidakun

Fully Compressible Hydrodynamic Simulation of Non-Equidiffusive Premixed Flames Propagation in Channels

Olatunde Ayodeji Abidakun

Dissertation submitted

to the Statler College of Engineering and Mineral Resources

at West Virginia University

in partial fulfilment of the requirements for the degree of

Doctor of Philosophy in

Mechanical Engineering

V'yacheslav Akkerman, Ph.D., Chair

Hailin Li, Ph.D.

Patrick Browning Ph.D.

Songgang Qiu, Ph.D.

Hayri Sezer, Ph.D.

Department of Mechanical and Aerospace Engineering

Morgantown, West Virginia

2020

Keywords: Lewis number, premixed combustion, obstructed channels, non-equidiffusive flame, flame oscillations, flame acceleration, deflagration to detonation transition, computational simulation, Bychkov mechanism, open channels.

ABSTRACT

Fully Compressible Hydrodynamic Simulation of Non-Equidiffusive Premixed Flames Propagation in Channels

Olatunde Ayodeji Abidakun

Premixed combustion remains of fundamental interest in energy generation and propulsion systems as well as in implementation of safety measures for residential and industrial accidental fire explosions. While the fast pace and complex nature of the combustion process has previously necessitated the analytical and computational studies to employ the simplifying assumption of equidiffusivity, when the Lewis number defined as the thermal-to-mass diffusivities ratio is unity ($Le = 1$), the ongoing advancements in technology and the requirements for efficiently operating combustors over a wide range of conditions make the combustion process more non-equdiffusive ($Le \neq 1$) than ever. The impact of non-equidiffusivity on the dynamics and morphology of a flame, and thereby on the combustion efficiency, becomes aggravated by the interactions with combustor geometric parameters as well as thermochemical properties of the fuel mixture.

Therefore, by representing combustors as channels with various extreme conditions (open channels, when both ends are open, or semi-open, when one end is closed, while the other one remains open), boundary conditions (non-slip or free slip, adiabatic or isothermal walls) and internal structures (obstructed or unobstructed), the current work addresses the effects of non-equidiffusivity and its interplays with other parameters on flame propagation in channels. Specifically, propagation of non-equidiffusive flames in channels is investigated by means of the computational simulations of the reacting flow equations with fully-compressible hydrodynamics and Arrhenius chemical kinetics. A detailed parametric study is performed for the Lewis numbers in the range $0.2 \leq Le \leq 2$; the channel half-width $10 \leq R/L_f \leq 48$, where L_f is the thermal flame thickness; the blockage ratios, α, being from 0 to $2/3$; and the spacing between the obstacles being $1/4 \leq \Delta Z/R \leq 1$.

The diffusional-thermal combustion instability, associated with $Le < 1$, and the flame thickening at $Le > 1$ are found to play a major role in determining the flame dynamics in a channel. Regarding finger flame acceleration in semi-open channels with adiabatic slip walls, it is shown that the $Le > 1$ flames accelerate slower than equidiffusive ones. In contrast, the $Le < 1$ flames acquire stronger distortion, associated with the diffusional-thermal combustion instability, and thereby accelerate much faster than at $Le = 1$. Increased surface area of the flame front and thus, a higher burning rate and stronger acceleration is also obtained in wider channels. Presence of equally spaced obstacles in such channel produced higher acceleration, with the increase being more significant at $Le < 1$ and high blockage ratio.

When both ends of the channels are open, the flames show oscillations, acceleration or a sequence of both, depending on other parameters. For a channel with adiabatic non-slip walls, the oscillation amplitude and frequency decreases with Le, and the low-Le flames exhibiting different morphologies. A drastic change in flame dynamics is however seen for channel with isothermal wall. In narrow channels with small blockage ratios, the oscillations amplitude and frequency changes with Le, with the frequency decreasing and the amplitude increasing as Le grows from 0.3 to 2. In other conditions, a transition from flame oscillations to its sudden acceleration or propagation at constant velocity, is singularly influenced by the Lewis number, or by Le coupling to the geometric parameters. The delay time before the onset of flame acceleration, especially at $Le < 1$, also varies as channel width and the blockage ratio changes. In all cases, the Lewis number shows both quantitative and qualitative effects on flame propagation in obstructed channel.

To my beloved wife, Esther Abidakun, and my daughters, Tola and Bola Abidakun.

ACKNOWLEDGEMENTS

I would like to express my sincere gratitude to my advisor, Dr. Vyacheslavv Akkerman for his guidance and support through the course of this program, and for always being committed to helping me succeed. His in-depth knowledge of the subject field and expert guidance has helped me grow professionally.

My profound appreciation also goes to the National Science Foundation, the West Virginia Higher Education Policy Commission for the support and the financial resources provided for me during the period of my PhD program. I also appreciate the WVU Division of Diversity, Equity and Inclusion for the support made available to me through the Chancellor Scholarship Program.

My sincere appreciation goes to all the members of my dissertation committee: Dr. Hailin Li, Dr. Patrick Browning, Dr. Songgang Qiu and Dr. Hayri Sezer. Their relentless support, constructive criticism and timely response is highly appreciated.

I also thank my colleagues: Abdulafeez Adebiyi, Gbolahan Idowu, Mohammed Alkhabaz, Furkan Kodakoglu, Samuel Ogunfuye, Sunita Pokharel, Ansan Pokharel, Alain Islas Montero, and Lateef Kareem, who helped me get started on my research and who have been of tremendous support over time. I appreciate you all.

Finally, I express deepest appreciation to my beloved wife Esther Abidakun, my daughters Tola Abidakun and Bola Abidakun, all members of the extended Abidakun and Akano families, for their unconditional love, sacrifices, support and encouragement during this program. Your contributions in making this a success are invaluable and highly appreciated.

Table of Contents

List of Tables

List of Figures

List of Symbols

English Letters

a	Thermal diffusivity
C_V	Specific heat capacity at constant volume
C_P	Specific heat capacity at constant pressure
c_0	Speed of the sound in the unburned fuel mixture
c_{tip}	Speed of sound associated with the flame tip
D	Mass diffusivity of deficient reactant
E_a	Activation energy
L_b	Markstein length
Le	Lewis number (ratio of thermal diffusivity to mass diffusivity)
L_f	Flame thickness
m	Molecular weight
Ma	Mach number
Mk	Markstein number
$\bar{n}$	Normal vector
P	Pressure
P_f	Initial pressure
Pr	Prandtl number
Q	Specific energy released in a chemical reaction
r_f	Radial position of the flame as function of time
R	Channel half-width
Re	Flame Reynolds number
R_u	Universal gas constant
Sc	Schmidt number
S_L	Laminar flame speed
T	Temperature
T_f	Initial fuel mixture temperature
T_{ad}	Adiabatic flame temperature
u	Velocity component
U_{tip}	Flame tip velocity
U_W	Corrugated flame velocity or burning rate
U_1	Flow velocity at burned extreme end
U_2	Flow velocity at cold extreme end
X_i	Specie mole fraction
Y	Mass fraction of the fuel mixture.
Z_f	Flame tip position
z	Axial direction

Greek Letters

α	Blockage ratio
γ	Specific heat ratio
Θ	Thermal expansion ratio
ΔZ	Obstacle spacing
τ	Scaled time
τ_R	Reaction time constant
σ	Exponential acceleration rate
λ	Thermal conductivity
ρ	Density
η	Dynamic viscosity
ν	Kinematic viscosity
e	Energy release per unit volume
ξ	Reduced low pressure inverse viscosity

1 Introduction

1.1 Overview

The usual saying of fire being a good servant, and a bad master indicates a clear recognition of the positive and destructive tendencies of combustion by humanity. Indeed, fire has proven to be a good servant in many respects, when handled appropriately, as it occupies the central stage in human civilization. Without it, many accomplishments attained in the history of mankind would be a mirage. From the medieval period till the present day, its usefulness has spanned many areas of human endeavors, ranging from cooking, heating, and lighting, to powering rockets [1]. Another interesting application of combustion is in the synthesis of advanced nanomaterials, that is, the technique popularly called combustion synthesis or self-propagating high-temperature synthesis (SHS) [2].

On the other hand, when out of control, combustion can lead to catastrophic incidents. Unwanted combustion often results in urban and wildland fires, explosion in locations like power plants and coal mines [3,4]. Destruction of properties and loss of human lives always accompany combustion, whenever it becomes uncontrollable and results in explosion. These potential adverse effects of combustion, as well as the need to fully harness the energy available through combustion, while reducing pollution and the accompanying health concerns to the barest minimum, makes combustion studies essential. Based on this premise, promotion/facilitation of combustion where it is useful; and its prevention and control when it may have catastrophic tendency, become crucial.

Generally, combustion involves a redox reaction between a combustible (fuel) and an oxidizer to form an oxidized product. Methane, propane, hydrogen, wood and coal are common examples of fuel, and typical oxidizer includes pure oxygen or oxygen present in air, and fluorine. Depending on the stage at which fuel and oxidizer are mixed, combustion can be classified into premixed and non-premixed. In premixed combustion, the fuel and oxidizer are perfectly mixed at the molecular level before ignition. Spark ignition (SI) engines, lean-premixed gas turbine combustors, and gas-leak explosions, are examples of applications and situation in which premixed combustion is encountered. In situation when there is no prior mixing of the fuel and oxidizer before their involvement in the reaction zone, the process is termed non-premixed (diffusion) combustion, with burning of candle wax and diesel (compression ignition) engine being typical examples [5].

1.2 Motivation and Objectives

Reasonable percentage of world energy is still derived from burning of fuel, in one form or another, and this will possibly remain so, for many years to come. In the USA, about 80 % of the total energy consumed in 2017 [6], and about 63 % of electricity generation in 2019 [7] are from fossil fuels. However, stringent emission regulations and the push towards improved efficiency has placed higher requirements on the combustion process, which originally, is a very complex one. The complex nature of combustion requires the involvement of many subject areas, such as thermodynamics, fluid mechanics, chemical kinetics, and heat and mass transfer, all coming into play in its analysis [8]. In some cases, it requires accounting for phase changes in conditions ranging from atmospheric to supercritical conditions [9]. In view of this complexity, analyzes of the combustion processes have often been achieved by taking simplifying assumptions. Many of these assumptions include: considering one-step reaction, isobaric approximation, infinitely thin flame, equidiffusion of mass and heat in the flame front, i.e. the unity Lewis number, $Le = 1$.

Further advancements that have been recorded in many areas, ranging from micro combustion in powering micro devices [10,11] to detonations in powering rockets [12], or in providing understanding for designing devices to enable prevention and control in case of unwarranted explosion [13,14], demonstrated that we can no longer rely on these assumptions to address ensuing challenges. For instance, engines and combustors are being designed to operate over a wide range of equivalence ratios (the ratios of the actual fuel-to-oxidizer ratio to the stoichiometric ones), with a capability to burn varieties of fuels, including blends of hydrocarbons, hydrogen, biofuel and syngas, to mention a few [15]. Many other approaches, such as exhaust gas recirculation [16], diluted combustion [17,18], re-ignition of the combustion process in case of extinction in critical situation [19], all geared towards improving efficiency, safe operation and reducing pollutants emission, have placed more constraint on an extent to which these assumptions can be relied upon.

Of special interest among the simplifying assumptions is that of equidiffusivity, $Le = 1$, which is directly related to the reactivity of the fuel-oxidizer mixtures. Obviously, this assumption can no longer be expected to hold in all practical situations, as many of the measures being taken to extend the application of combustion or improve performance, directly or indirectly affects either or both the thermal and mass transport. For instance, $Le < 1$ for lean hydrogen-air mixture, and conversely, $Le > 1$ for a fuel-rich hydrogen. The reverse is the case for propane and other heavier

hydrocarbon, so $Le < 1$ and $Le > 1$ correspond to rich and lean mixtures, respectively. However, dilution with such gas as He, Ar or CO_2 alters the thermal and mass transfer properties of the fuel-oxidizer mixtures and consequently, their Lewis number [18]. Tables 1.1 - 1.3 show the changes recorded in the values Lewis number of the fuel-oxidizer mixtures based on the level of dilution and other operating conditions.

Table 1.1: Lewis number of H_2-air mixtures diluted with He, Ar and CO_2 [18].

Dilution (%v)	Lewis number
0%	1.02
20% He	0.962
40% He	0.980
60% He	1.013
20% Ar	1.324
40% Ar	0.956
60% Ar	0.679
20% CO_2	1.380
40% CO_2	0.853
60% CO_2	0.528

Table 1.2 Effective Lewis number of multicomponent fuel-air mixture diluted with CO_2 [15]

Pressure (MPa)	Temperature (K)	CO_2 ratio in fuels (%)	Le_{eff}
0.5	298	0	1.603
0.5	298	10	1.560
0.5	298	20	1.515
0.5	298	30	1.469
0.1	298	0	1.040
0.1	298	10	1.021
0.1	298	20	0.999
0.1	298	30	0.975
0.1	298	40	0.946
0.1	375	0	1.025
0.1	375	10	1.006
0.1	375	20	0.984
0.1	375	30	0.956
0.1	375	40	0.931
0.1	450	0	1.020
0.1	450	10	1.000
0.1	450	20	0.978
0.1	450	30	0.952
0.1	450	40	0.923

Table 1.3 Effective Lewis number of diffusion flame of CH_4 and C_3H_8 – air mixtures diluted with He and Ar [20]

Dilution (%v)	CH_4-air	C_3H_8-air
0%		
20% He	0.489	0.379
40% He	0.700	0.696
60% He	1.028	1.461
20% Ar	1.085	0.775
40% Ar	1.041	0.949
60% Ar	1.004	1.270

Another important factor is a configuration of the combustor or the enclosure in which the combustion process occurs. The interactions between the flame and the geometric parameters is of importance in determining the dynamics and morphology of the flames. The enclosures can be of different shapes and configurations, with each producing different effects on the flame. An enclosure, where both ends of the channel are open can produce flame that oscillates, accelerates or a sequence of both [21–24]. Also, in enclosure where one end is close and the other is open, flame acceleration (FA) and deflagration-to-detonation (DDT), if length permits, are often experienced, with the acceleration rate being influenced by the channel width and channel internal structures [25–27]. Flow-flame interactions and impact of acoustic becomes paramount when both ends of the channel are close, and thus, produce a different effect on the flame [28–30]. The type thermal boundary condition [31], or mechanistic boundary condition [32] also contributes to determining the flame behavior.

The effect of these interactions is expected to be even more substantial for non-equidiffusive flames. Therefore, the main aim of the present work is to investigate and analyze what impact non-equidiffusivity and its interactions with geometric parameters would have on a flame propagating in a channel, with channel providing a good representation of many enclosure where combustion occurs. Therefore, providing an understanding of the flame behavior caused by non-equidiffusive burning in channels, and also creating approaches essential for the promotion or mitigation of flame acceleration as required in practical situations.

Hence, the specific objectives of this work are to…

i. Investigate the impact of non-equidiffusivity on FA occurring at the early stage of burning in a pointy-ignited flame propagating from the close end to the open end of a pipe;
ii. Scrutinize the effects of channel obstruction on the propagation of non-equidiffusive flames in enclosures where one end is closed, and the other end is open;

iii. Explore the propagation mechanisms of non-equidiffusive flames in channels with both ends open, considering a frictional interaction between a flame and the channel walls; and
iv. Analyze the effects of obstacles and non-equidifusivity, as well as their interplay, on flame propagation in obstructed channel with both ends open.

1.3 Structure of the Dissertation

The remaining part of this dissertation is arranged as follows: Chapter 2 presents the relevant literature overview related to non-equidiffusive burning and flame propagation in channels. In chapter 3, the computational methodology employed in this study are described. This includes the presentation of the hydrodynamic and transport equations, brief description of the grid resolution tests, validation of the computational platform by experimental data, description of the parametric studies, and finally, a description of how the flame was characterized. In chapter 4, the impact of non-equidiffusivity on finger FA in semi-open channel with adiabatic and free slip walls is analyzed. Chapter 5 contains the results and discussions on the effect of Lewis number on FA in obstructed semi-open channels, describing the impacts of the channel width, blockage ratio, obstacle spacing and their interplay with the Lewis number. Propagation of non-equidiffusive flames in channels with both ends open and adiabatic, non-slip walls is discussed in chapter 6. In chapter 7, the morphology and dynamics of non-equidiffuve flames propagating in adiabatic fully open channels laden with equally spaced obstacles are scrutinized. Finally, chapter 8 contains the conclusions of this work and presents the recommended directions for the future works.

2 Literature Review

2.1 Premixed Combustion

Premixed combustion, encountered in various applications, such as in spark ignition (SI) engines [33], lean-premixed gas turbine combustors [34], pulse-detonation engines [35], or in the situations such as gas-leak explosions [36] requires that the fuel and oxidizer are perfectly mixed at the molecular level before ignition. As the premixture ahead of the flame is being consumed, there is generation of combustion waves in the unburnt premixture. The travelling velocity of the generated waves with respect to a stationary reference frame can be in the subsonic or supersonic range. Depending on the velocity of these waves, the premixed combustion process is categorized into two distinguishable modes, which are deflagration (flame) and detonation [8].

2.1.1 Deflagration (Flame)

In most engineering applications or industrial explosions, combustion is often initiated from a weak ignition source. Deflagration represents the process following weak ignition of a combustible mixture. In this combustion mode, a chemical reaction, which occur at near constant pressure, propagates at a subsonic velocity, and it occur mainly due to thermal conduction and diffusion between the burnt gas and the pre-mixture ahead of the flame front. The chemical reaction wave velocities for deflagration are of the order of 1 m/s [35], signifying a strongly subsonic flow. A small scale deflagration experiment conducted by Rocourt *et al*. [37] on the influence of reactivity, volume and congestions on the deflagration process of hydrogen-air mixtures in cylindrical pipe with congested volume revealed an impact on the flame speed and overpressure. The volume was however reported to have a weaker effect on the flame, compared to the effect of congestion with different number of obstacle layers. In large obstructed channel, the computational simulation of FA by Kessler *et al*. [38] have revealed that flame stretching and folding, flame-front wrinkling caused by turbulent eddies and fluid-dynamic instabilities, and flame-surface creation by shock-flame interactions are the stages of acceleration for stoichiometry methane-air mixture combustion. Final choking velocity attained by the flames is reported to be the same for all geometric configurations and only depends on properties of the gas mixture.

2.1.2 Detonation

Unlike deflagration, the combustion reaction in detonation propagates due to rapid shock and compression waves, with the shock wave and the trailing reaction zone coupled [1]. The reaction front in fuel-air mixture propagates with a typical velocity of the order of 2 km/s; and it can be as high as 3 km/s in oxy-fuel detonations [35]. This high velocity is also accompanied by the pressure rise, by a significant factor of 10~20, being responsible for the damages caused by the accidental explosions [35]. The computational work on propagation of regular detonation waves in narrow channel by Chinnaya *et al*. [39] revealed that the detonation wave speed decreases as compared to the Chapman-Jouguet (CJ) detonation velocity, due to the wall dissipative effects, with transverse instabilities being damped by the reduced channel height. The development of the thermo-diffusive boundary layers behind the leading shock wave is also reported in Ref. [39].

Rudy *et al*. [40] performed a large-scale experiment involving detonation propagation in the uniform and non-uniform hydrogen-air mixtures in a partially confined enclosure, which was open at the bottom. Detonation was reported to propagate in a uniform, stoichiometry mixture only if

the mixture layer height exceeds a threshold of approximately 3 cm. For non-uniform hydrogen–air mixture, where H_2 concentration slope is approximately -1.1% per cm, the critical hydrogen concentration at the top of the layer is approximately 26 % and the mean detonation layer height is close to 8.5 cm.

Han *et al*. [41] identified pulsating instability and cellular structure analyzing propagation of globally planar detonations in free space. The pulsations are found to include three stages, namely: (i) rapid decay of the overdrive; (ii) approaching the Chapman-Jouguet state and emergence of the weak pulsations; and (iii) formation of the strong pulsations. The three stages are also characterized by different cellular structures such as (i) no cell formation; (ii) formation of small-scale, irregular cells, and (iii) formation of regular large-scale cells, respectively. The average shock pressure in the detonation front has been reported to consist of fine-scale oscillations, reflecting the collision dynamics of the triple-shock structure and large-scale oscillations affected by the global pulsation.

2.1.3 Deflagration-to-Detonation Transition (DDT)

DDT incorporates the sequence of events occurring when an accelerating flame is transitioning into a detonation. It represents all events relating to the creation of the conditions for the onset of the detonation up to the actual onset of detonation. It is known to appear as a sudden explosion in the vicinity of the flame, which could occur in the region containing the turbulent flame, or in the compressed, preheated premixture between the leading shock wave and the flame front [1,42].

Han *et al*. [43] conducted a computational study to understand the specific mechanism of DDT and subsequent detonation propagation modes in micro and macro channels. It was reported DDT proceeds differently in the two channels due to viscous effect. The DDT in micro channel is found to be controlled by viscosity, while establishment of a turbulent flame is the controlling factor in macro channel. The entire DDT process in a micro channel is reported to consist of (i) exponential FA due to viscous stretch; (ii) linear FA due to compressibility; (iii) abrupt FA to overdriven detonation due to direct ignition of the unreacted gas by the strong and curved leading shock; and finally, (iv) steady detonation with a velocity below the CJ value. On the other hand, the DDT process in a macro channel takes a different route, including: initially slow FA due to combustion instability; transition to turbulent flame with precursor compression wave; overdriven detonation due to local explosion induced by a strong shock; and cellular detonation with the average velocity close to the CJ value.

An experimental study of DDT limits, which defines the quasi-detonation regime, in obstacles-filled tube was conducted by Cross and Ciccarelli [44] using hydrogen-air and ethylene-air as fuel mixtures at atmospheric pressure. The experiment was conducted to determine if the DDT limits are dictated by the DDT event or by the quasi-detonation wave propagation requirements, using a traditional and a modified experimental set up. It was reported that the DDT limit depends to great extent on the ratio of the orifice-plate diameter to the detonation cell size. It is also indicated that the DDT limits obtained depends largely on the detonation propagation mechanism, and not the initiation process. The process of DDT in obstructed small channels with decreasing blockage ratio was reported by Goodwin *et al*. [45], and their results have revealed different causes for DDT for different range of blockage ratios. Specifically, for the blockage ratios in the range of 0.35 – 0.5, creation of hot spots in a gradient of reactivity that forms behind a Mach reflection was cited as the cause. On the other hand, shock collisions that increase the temperature, pressure and density of the unburnt material was reported for the blockage ratios in the range 0.05 – 2. Both mechanisms are reported to be in effect at a higher blockage ratio of 0.8.

The experimental work on DDT in stoichiometry hydrogen-methane-air mixtures in obstructed tubes of various blockage ratios and obstacle spacing by Porowski & Teodorczyk [46] revealed that DDT occurred for blockage ratios ranging from 0.4 to 0.6. Higher obstacle densities was reported to cause quasi-detonation regime for mixtures containing from 30 % to 50 % of methane, with the velocities of 1500 m/s. Hydraulic resistance as a mechanism for DDT was investigated by Brailovsky and Sivashinsky [47], where it was stated that hydraulic resistance causes a gradual precompression and preheating of the unburned gas adjacent to the advancing deflagration. This condition was reported to lead to a localized thermal explosion triggering an abrupt transition from deflagration to detonation. Thomas [48] identified the conditions required for the development of detonation in ethylene-oxygen and hydrogen-methane-oxygen mixtures at elevated temperatures and pressures. The study [48] also included methane-ammonia-oxygen mixture at standard initial temperature and temperature. The results indicate that at the fuel lean limit, neither increasing temperature nor pressure has any significant effect on the limit of establishment of detonation.

2.2 Premixed Flame Structure

By the nature of premixed combustion, burnt matter and premixture exists on opposite sides of the flame front being a discontinuity between them. As a result, the structure of the flame is determined

by such phenomena as convection, transport, that is, heat and mass diffusion, and chemistry [49]. As illustrated in Fig. 2.1, a flame structure is made up of the reaction zone and the flame front, and there exists variations of the fuel concentration, temperature, and reaction rate, across the flame (Fig. 2.2). In representing the premixed flame, various approaches are employed, depending on the level of complexity and details desired. In the first approach, which is also the simplest, the flame is considered as an interface separating two fluids (flame sheet). In the second case, the flame sheet is expanded to contain a preheat zone, with consideration given to the transport properties in the flame. While, in the third approach, illustrated by Fig. 2.3, the thermal and molecular diffusions is taken into consideration [8].

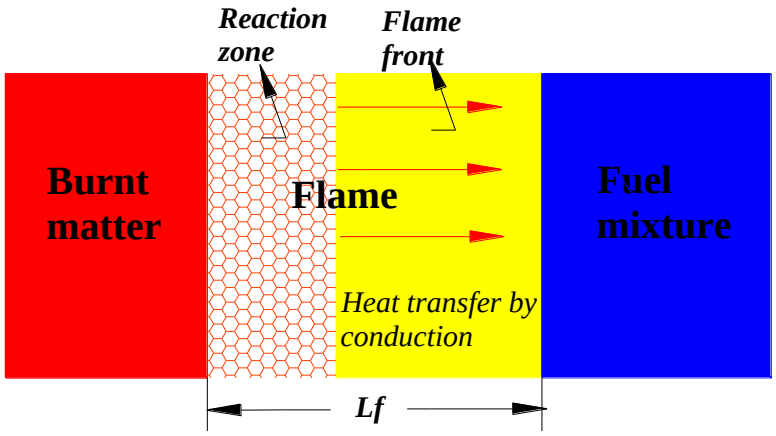

Figure 2.1: Premixed flame configuration.

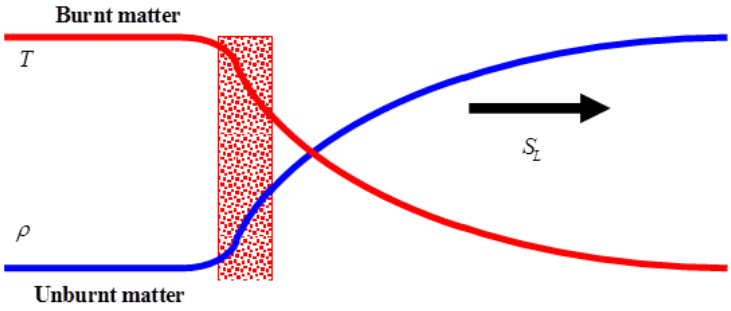

Figure 2.2: Characteristic temperature and density distribution inside a planar flame.

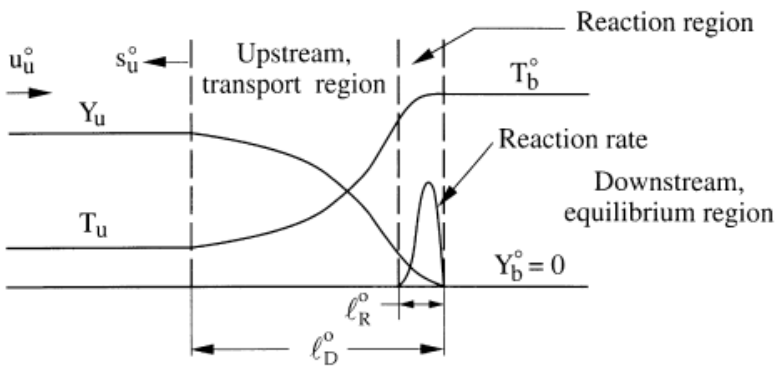

Figure 2.3: Reaction level flame structure [49].

2.3 Flame Propagation in Channels

The process of FA in a channel can occur through variety of mechanisms [4], which include: acceleration caused by formation of a finger-shaped flame front [50,51], that caused by friction at the walls [43,52], and that due to obstructions in the channel [53–55].

2.3.1 Flame propagation in Semi-open channels

In a semi-open channel with free-slip walls, where there is no friction-based flame-wall interaction, responsible for producing a curved flame front that can cause a flame to accelerate, a time-limited acceleration mechanism is exhibited. This FA, which results in a formation of a tulip flame was first experimentally studied by Clanet and Searby [50], who revealed different stages of the flame propagation process in this scenario. The interaction between the flame front and gas dynamics was found to result in a formation of finger-shaped flame, and later a "tulip flame" due to inversion of the flame front curvature. The process through formation of a finger-shaped flame and a tulip flame was reported by Ponizy *et al*. [56] to be a purely hydrodynamic phenomenon, due to the competition between the backward movement of deflected burned gases expanding from the lateral flame skirts and the forward movement of unburned gases.

The finger flame acceleration process was also studied computationally by Bychkov *et al*. [51] and provided detailed description on the acceleration mechanism as follows. Specifically, a hemi-spherical flame embryo is initiated at the closed end of a pipe. At the first stage, it exhibits uniform outward expansion in all directions. At the second stage, the "axial tip" of the flame front receives a significant push from the coupled effects of expanding burnt gas and flow restriction in the lateral or radial direction. Such a push results in a formation of a finger-like shape of the flame front,

leading to an increased surface area of the front and, consequently, higher acceleration. This goes on until a "skirt" of the flame front contacts a sidewall, at which instant acceleration stops, resulting in the flame skirt catching up with the flame tip, to form an almost flat shape of the front and eventually overtakes it to form a concave flame. The impact of gas compression on this acceleration process was studied by Valiev *et al*. [57], with the result that gas compression reduces the acceleration rate and the maximum flame tip velocity, and thereby moderates FA noticeably. Similar to previous works, Ref. [57] showed that finger FA is followed by formation of a ''tulip flame", which indicates termination of the early acceleration process. Experimental results on hydrogen-oxygen mixtures with considerable initial values of the Mach number, reported in the same study, revealed finger FA with the acceleration rate much smaller than that found previously for hydrocarbon flames.

For semi-open channels with non-slip walls, the friction-based acceleration mechanism is in effect. Uneven flow of burnt gas in a channel results in a flame curvature and leads to the Darrieus-Landau (DL) instability. This causes further increase in the surface area of the flame front and, subsequently, promoted FA. The effects of thermal expansion on the multiplicity of the steady flame propagation regimes in cylindrical channel, considering both axisymmetric and non-axisymmetric configurations, was reported in Ref. [58]. The results show that axisymmetric flames, concave towards the burnt gas, are more unstable against the three-dimensional (3D) perturbations than convex flames, and the non-axisymmetric property of the flame is also found to push back the critical flashback limits at larger flow rate. Flame propagation and DDT in micro-channels with one end closed is reported in Ref. [59], with the focus on the final saturation stages in the process of flame acceleration. It is shown that an intermediate stage with quasi-steady velocity may occur, noticeably below the Chapman-Jouguet deflagration speed. The intermediate stage is followed by additional FA and subsequent saturation to the Chapman-Jouguet deflagration regime. Viscous heating at the channel wall was also found to provide additional velocity.

The acceleration mechanism encountered in the semi-open obstructed channels produces the fastest known regime of burning [42]. While flame propagation through obstacles is oftentimes associated with turbulence, shocks, or hydraulic resistance [1], Bychkov *et al.* [54] identified and scrutinized a conceptually laminar, shockless mechanism of ultrafast flame acceleration in semi-open channels or tubes equipped with a toothbrush-like array of obstacles. This mechanism relies mainly on the delayed burning of fuel premixture in the pockets between adjacent obstacles which

eventually results in a stronger push of the flame front. The impact of surface friction on the acceleration process was studied by Adebiyi *et al*. [60] employing an obstructed cylindrical pipe. The authors reported a minor impact of surface friction on acceleration. Also, Ciccarelli *et al*. [61] demonstrated the role of shock-flame interactions on FA in a channel filled with obstacles on the top and bottom walls. Special attention has been paid to the later stage of FA, when compression waves and, eventually, a shock wave, are formed ahead of the flame. The interactions between the flame front and the reflected shock waves is reported to govern the later stage of the flame acceleration process and to provide oscillations of the flame tip velocity.

Gamezo *et al*. [55] worked on the effects of obstacle spacing on FA and DDT in obstructed channels using hydrogen-air mixture. It was reported that higher number of obstacles per unit length create more perturbations, causing a quicker increase in the flame surface area, and therefore a faster flame acceleration. Also, DDT is reported to occur more easily when the obstacle spacing is large enough for the shock waves caused by the fusion of the incident and reflected shock waves (Mach stems) to form between the obstacles. Three flame acceleration regimes were reported to be caused by this effect, and they are: detonation ignition when a Mach stem formed by the diffracting shock collides with an obstacle; there is no detonation because Mach stems do not form, and lastly, detonation when leading shock becomes strong enough to ignite a detonation by direct collision with the top of an obstacle.

An experimental work of Ciccarelli *et al*. [62] on the effect of the obstacle size and spacing on the initial stage of FA in obstructed tube revealed that the flame run-up distance decreased with the blockage ratio as well as with the mixture reactivity. For higher blockage ratio, FA was also reported to be highest when the obstacle spacing is in the range of one tube diameter. Also, Boeck *et al*. [63] reported the experimental study on FA for stoichiometric H_2/O_2 flames in an obstacle laden rectangular channel. The results showed the occurrence of vortex shedding off obstacle edges over long time-scales in the slow-flame regime. The fast-flame regime is marked by the presence of compression waves, which interact with the flame and cause macroscopic deformation of the flame and the small-scale wrinkling. Similarly, Toedorczyk *et al*. [64] investigated, experimentally, the deflagration and DDT of hydrogen-air mixtures in a small rectangular channel with obstacles on the bottom wall. It was found [64] that while a large blockage ratio provides the turbulizing effects on the flame, such an effect appeared destructive to the flame propagation. The

optimum obstacle separation distance required for DDT was also reported to be larger for the channels with high blockage ratios.

2.3.2 Flame Propagation in Channels with both Ends Open (Fully-Open Channels)

Flame propagation in a channel where both ends are open is oftentimes qualitatively different from that of semi-open channels [21,24]. This is primarily because a flame-generated flow a fully-open channel is distributed between the upstream and the downstream flows. Akkerman *et al*. [24] investigated the propagation of premixed flames in pipes with non-slip walls and both ends open. The results showed a flame front oscillating due to flame-wall interaction. The flame oscillations involved the variations of the curved flame shape and velocity. The oscillation period was found to depend on the channel width, with the oscillations being weak in narrow channel, and stronger in wider channels. Di Stazio *et al*. [65] conducted an experimental study on oscillating methane-air flames in micro-combustors and reported an existence of various flame propagation regimes such as stable flames, oscillating flames with repetitive extinction and ignition, and oscillating weak flames.

Bychkov *et al*. [22] showed that flames in open/vented obstructed cylindrical pipes accelerate strongly, but at a slower rate than in semi-open pipes. On the other hand, the study [21] reported a nonlinear quasi-steady oscillations of the burning rate, with the oscillation period growing with the blockage ratio but decreasing with thermal expansion ratio. The authors of Ref. [21] also identified the possibility of FA to replace the oscillations in wider channels. Both experimental and numerical results [66] revealed the existence of slowly propagating flame, which undergoes instant acceleration without generating shock waves. The authors [66] reported pressure oscillations, flame-obstacles interactions, and hydrodynamic resistance as the cause of the sudden acceleration.

2.4 The Lewis Number

The Lewis number and the thermal expansion ratio are two of the main dimensionless parameters describing premixed flames, and they are important to characterize the reactivity, diffusivity and exothermicity of the premixtures. The Lewis number Le is also coupled to the flame Markstein length $L_m = MkL_f$, as it affects the flame response to curvature and stretch. Here, the Markstein number Mk describes the effect of local heat release of a propagating flame on the flame curvature. The practical implications of Le on the combustion process includes the impact on the ease of

ignition [67], and possibility of flame extinction during its propagation [68], as well as to determine the flame speed and thickness $L_f = \eta/Pr\rho_f S_L$. The Lewis number is determined based on the ratio of the thermal diffusivity to the mass diffusivity of the deficient reactant, namely, as the fuel or oxidizer species for lean and rich mixtures, respectively,

$$Le_i = \frac{a}{D} = \frac{\lambda}{\rho D c_p} = \frac{Sc}{Pr}, \tag{2.1}$$

where α is the thermal diffusivity of the fuel-air mixture, λ the thermal conductivity, c_p the specific heat capacity at constant pressure, Sc the Schmidt number, Pr the Prandtl number, and D, which can be represented as D_{ij} or $D_{i,mix}$, being the mass diffusivity of the deficient reactants. In the situations where nitrogen (N_2) is assumed to be the abundant specie, D_{ij} connotes the mass diffusion of the deficient reactant i towards N_2, j, at the free stream temperature. In other cases, such as a H_2-air mixture, the mixture-average coefficient of mass diffusion, $D_{i,mix}$ is adopted,

$$D_{i,mix} = \left(1 - Y_{i,mix}\right)\left(\sum_{\substack{s=1 \\ s\neq i}}^{N} \frac{X_s}{D_{is}}\right), \tag{2.2}$$

where Y is the mass fraction and χ is the molar fraction of each specie, s, in the mixture. The use of $D_{i,mix}$ instead of D_{ij} has been shown to yield the Lewis number in closer agreement with the experimentally determined ones [69]. However, the determination of Le when multiple fuels are blended together can be quite complex, especially for a lean mixture [69–71].

Behavior of non-equidiffusive flames in channels accelerating due to wall friction have been studied by Bilgili *et al.* [72], with drastic promotion of flame acceleration observed for the $Le < 1$ mixtures, as compared to equidiffusive burning, and moderation of acceleration encountered when $Le > 1$. Kurdyumov [73] reported a possibility of symmetric and non-symmetric flames at various Le in narrow adiabatic channels, with the stability analysis performed [73]. It is shown that an increase in the flow rate leads to a loss of stability with subsequent formation of the non-symmetric solutions for the symmetric flames with low Le, while the Poiseuille flow produces a stabilization effect for high-Le flames. Kagan and Sivashinky [74] studied the effect of Le on flame propagation through the vortical flows and reported that in the presence of volumetric heat losses, the stirring will invariably promote extinction and reduce the flammability limits, provided $Le > 1$. At $Le < 1$ this holds only for the sufficiently strong stirring, whereas the moderate stirring actually expands

the flammability limits. At $Le > 1$, the deficient reactant is fully consumed up to the quenching point, while at $Le < 1$, prior to the total extinction, a part of the deficient reactant will escape the reaction zone and remain unconsumed. Chakraborty *et al.* [75] showed formation of a multicellular flame with a "funnel-like" shape when $Le \ll 1$ in the presence of high heat loss, while at $Le > 1$, the Le-dependence of the reaction rate is reversed as the heat loss increases.

Zhou et al. [76] studied the impacts of Le on the ball-like lean limit for methane-air, methane-hydrogen-air and hydrogen-air mixtures. The authors of Ref. [76] reported formation of cellular-like methane-air flames with only the leading edge of the lean limit located inside the recirculation zone, while for the two other mixtures, the ball-like lean limit flames have been observed, with the entire flame located inside a recirculation zone. Yoon *et al.* [77] studied the effects of Le on the generation of acoustic instability in downward-propagating flames. It was shown [77] that for $Le < 1$, where the reaction rate increases with reducing reaction zone thickness, a relatively strong sound is produced under the same coupling constant (a product of the Zeldovich number and the Mach number) because the chemical reaction rate becomes very sensitive to the gas temperature fluctuations in the acoustic field. It was also reported [77] that a larger coupling constant is required to generate the primary acoustic instability as Le grows. Subsequently, Berger *et al*. [78] found a periodic sequence of formation/destruction of the flame fingers caused by the diffusional-thermal instability in the lean hydrogen flames. Salusbury and Bregthorson [68] investigated the impact of Le on a stretched, laminar, premixed counter-flow flame, focusing on the flame speed and the extinction limit. Specifically, the flame extinction at a lower stretch rate has been observed in the $Le > 1$, propane-air mixture, while the extinction appeared limited to a reduced residence time for the $Le \ll 1$, hydrogen-air flame.

Patel and Chakraborty [67] analyzed the effects of Le on the evolution of the flame curvature in the expanding turbulent premixed flames and found that the overall burning rate and the extent of flame wrinkling grows with decreasing Le. Higher tendency of wrinkling is found prevalent for the $Le < 1$, due to the occurrence of the thermo-diffusive instability. It was also stated that flame propagation at $Le < 1$promotes flame curvature, while propagation tends to smoothen the surface of the $Le \geq 1$ flames. It was also revealed that the maximum values of the temperature and reaction rate increase with decreasing fuel Le during the period of external energy deposition. The initial value of the fuel Lewis number was also shown to have significant effects on the extent of burning of stratified mixtures following localized ignition, as the burning rate decreases with Le.

Chakraborty and Cant 2009a and b also a positive correlation between the surface density function and tangential strain rate. A positive correlation is also obtained between curvature and SDF for the $Le < 1$ flames, negative correlation is obtained for the $Le > 1$ flames, while a weak correlation exists at $Le = 1$. As for the effects of the Lewis number on the scalar transport in turbulent flames, it is reported [79] that the condition $Le \ll 1$ exhibit counter gradient transport, while the extent of the gradient transport increase with increasing global Lewis numbers [80,81].

2.5 Relevant Flame Acceleration Theory

At the early stage of burning in unobstructed channels with slip walls, the acceleration mechanism of interest is termed finger flame acceleration, i.e. formation of a finger-shaped flame front with an increasing surface area. The evolution of the flame tip, shown in Fig. 2.4, is described by [51]

$$\frac{d\xi_{tip}}{d\tau} - (\Theta - 1)\xi_{tip} = \Theta. \tag{2.3}$$

Taking the initial condition $\xi_{tip}(0) = 0$, the solution to Eq. (2.3) reads

$$\xi_{tip} = \frac{\Theta}{\Theta - 1}\{exp[(\Theta - 1)\tau] - 1\}, \tag{2.4}$$

where ξ_{tip} is the dimensionless axial coordinate for the flame tip, and $\tau = S_L t/R$ is the scaled time. Equations representing the flame tip and acceleration as affected by gas compression are [57]

$$\frac{d\xi_{tip}}{d\tau} = -Ma\gamma(\Theta - 1)^2\xi_{tip}^2 + \sigma_{1,pl}\xi_{tip} + \Theta_1, \tag{2.5}$$

with

$$\sigma_{1,pl} = (\Theta - 1)\big[1 - Ma\big(\Theta + 2(\gamma - 1)(\Theta - 1)\big)\big], \tag{2.6}$$

$$\Theta_1 = \Theta - Ma(\gamma - 1)(\Theta - 1)^2. \tag{2.7}$$

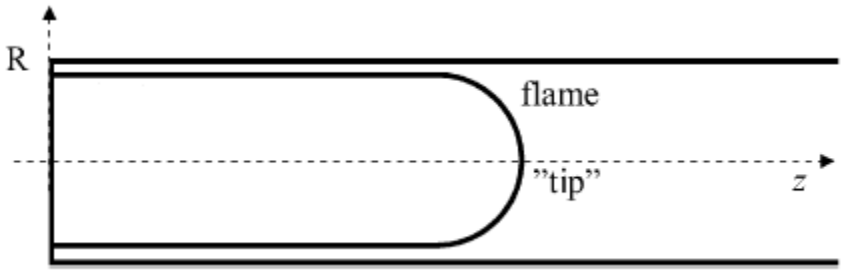

Figure 2.4 Evolution of a finger flame in a channel.

At the early stage, $\xi_{tip} \to 0$, the flame acceleration is moderated by the linear terms of Eq. (2.5), and the solution becomes

$$\xi_{tip} = \frac{\Theta_1}{\sigma_{1,pl}}\left[\exp\left(\sigma_{1,pl\tau}\right) - 1\right], \tag{2.8}$$

with the solution given as

$$\xi_{tip} = \frac{2\Theta_1[\exp(\sigma_2\tau) - 1]}{(\sigma_2 - \sigma_{1,pl})exp\sigma_2\tau) + (\sigma_2 + \sigma_{1,pl})}, \tag{2.9}$$

where

$$\sigma_2 \equiv \sqrt{\sigma_{1,pl}^2 + 4Ma\gamma\Theta_1(\Theta - 1)^2}, \tag{2.10}$$

and Ma is the initial Mach number and γ is the specific heat ratio.

For semi-open channel with obstacles, the flame tip position and acceleration at the early stage, where incompressibility assumption appears reasonable, are given by [52,54]

$$\frac{Z_f}{(1-\alpha)R} = \frac{\Theta}{\Theta - 1}[exp(\sigma S_L t/R - 1)], \tag{2.11}$$

$$\sigma = \frac{\Theta - 1}{1 - \alpha}, \tag{2.12}$$

and at the later stage where the effect of gas compression becomes significant [82] as

$$Z_f = \frac{2\Theta_1 S_L[exp(\sigma_1 t) - 1]}{(\sigma_2 - \sigma_1)exp(\sigma_2 t) + (\sigma_2 + \sigma_1)}, \tag{2.13}$$

$$\sigma_2 = \sqrt{\sigma_1^2 + 4Ma\mathrm{X}\Theta_1\sigma_0^2}, \tag{2.14}$$

$$\sigma_1 = \sigma_0\left[1 - Ma\left(\frac{\Theta}{1-\alpha} + 2(\gamma - 1)(\Theta - 1)\right)\right], \tag{2.15}$$

where Ma is the initial Mach number and γ is the specific heat ratio.

For an obstructed channel with both ends open [22], the flame tip position Z_f and the scaled acceleration rate of the flame tip σ_0 for inviscid flow are given by

$$Z_f = \frac{\Theta R}{\sigma_0}\{exp(\sigma_0 S_L t/R) - 1\}, \tag{2.16}$$

$$\sigma_0 = \frac{\Theta - 1}{\sqrt{(\Theta + 1)}(1 - \alpha)}. \tag{2.17}$$

Considering viscous effects, the flame tip position obeys the equation [22]

$$\frac{dZ_f}{dt} \approx \frac{\sigma S_L}{R}\left[Z_f + \frac{T}{\sigma}\right] \approx U_2\left(Z_f, Re\right) + S_L. \tag{2.18}$$

where U_2 is the exit velocity of fuel mixture at channel exit $z = L$.

3 Research Methodology

The present research work is centered on analyzing the roles of nonequidiffusivity in propagation of premixed flames in channels of various geometric configurations. The investigation is carried out by means of computational simulations of reacting flow equations, with fully-compressible hydrodynamics and Arrhenius chemical kinetics. The simulated equations are that of mass, momentum, energy and species transport in their 2D forms, as a rectangular channel used is reduced to a 2D problem.

3.1 The Governing Equations and Numerical Approach

The basic governing equations which represents the conservation equations of mass, momentum, energy and species take the form:

$$\frac{\partial}{\partial t}\rho + \frac{\partial}{\partial x_i}(\rho u_i) = 0, \tag{3.1}$$

$$\frac{\partial}{\partial t}(\rho u_i) + \frac{\partial}{\partial x_j}\left(\rho u_i u_j + \delta_{ij}P - \gamma_{i,j}\right) = 0, \tag{3.2}$$

$$\frac{\partial}{\partial t}\left(\rho e + \frac{1}{2}\rho u_i u_j\right) + \frac{\partial}{\partial x_i}\left(\rho u_i h + \frac{1}{2}\rho u_i u_j u_j + q_i - u_j \gamma_{i,j}\right) = 0, \tag{3.3}$$

$$\frac{\partial}{\partial t}(\rho Y) + \frac{\partial}{\partial x_i}\left(\rho u_i Y - \frac{\eta}{S_c}\frac{\partial Y}{\partial x_i}\right) = -\frac{\rho Y}{\tau_R} exp\left(-E_a/R_p T\right), \tag{3.4}$$

where Y is the mass fraction of the fuel mixture, $e = QY + C_V T$ and $h = QY + C_P T$ are the specific internal energy and enthalpy, respectively; $Q = C_P T_f(\Theta - 1)$ the energy release in the reaction, and C_V, C_P the specific heats at constant volume and pressure, respectively. Both the unburned and burnt matters are assumed to be two-atomic ideal gases of the same constant molecular weight, m, with $C_V = 5R_p/2m$, $C_p = 7R_p/2m$, the universal gas constant $R_p = 8.314\ \mathrm{J/(mol \cdot K)}$ and the equation of state

$$P = \rho R_p T/m. \tag{3.5}$$

The stress tensor $\gamma_{i,j}$ and the energy diffusion vector q_i are given by

$$\gamma_{i,j} = \eta\left(\frac{\partial u_i}{\partial x_j} + \frac{\partial u_j}{\partial x_i} - \frac{2}{3}\frac{\partial u_k}{\partial x_k}\delta_{i,j}\right), \tag{3.6}$$

$$q_i = -\eta\left(\frac{C_P}{Pr}\frac{\partial T}{\partial x_i} + \frac{Q}{Sc}\frac{\partial Y}{\partial x_i}\right), \tag{3.7}$$

where $\eta = \rho\nu$ is the dynamic viscosity in the fuel mixture, Pr and Sc are the Prandtl and Schmidt numbers, respectively.

Equation (3.4) describes an irreversible one-step Arrhenius reaction of the first order, with the activation energy E_a and the constant of time dimension τ_R. A conventional unit of velocity dimension is the unstretched laminar flame velocity S_L. A useful unit of length dimension is the thermal flame thickness, which is conventionally defined as $L_f \equiv \eta_f/\rho_f S_L \mathrm{Pr}$. All channel half-widths, *R*, in this study are therefore measured in terms of L_f.

The governing equations presented above are solved with an in-house solver which is based on the cell-centered, finite volume approach. The ordinary differential equations obtained from the finite volume discretization are explicitly solved using the 4th-order Runge-Kutta method, with the implementation carried out in Fortran and C programming languages. The solver is the 2nd-order accurate in time, 4th-order accurate in space for the convective terms, and 2nd-order accurate in space for the diffusive term. The code is based on the ideal gas equation of state (IG EoS), with the Sutherland formulation used to calculate the viscosity. The embryo of this solver was first developed at Volvo Aero Co. by Dr. Eriksson, and later revised and updated by many research groups, including the groups of Drs. Liberman (Uppsala University), Bychkov (Umea University), Valiev (Tsinghua University) and Akkerman (West Virginia University).

3.2 Channel Geometry

Given the effects of geometric parameters on the propagation of flames, channels with various geometries are considered in this work to represent enclosures like pulse detonation engines, gas turbines, oil and gas pipelines, relieve pipes, coal mine passage and underground tunnel.

3.2.1 Semi-Open Channels

The first case of channel geometry considered is that in which one end is closed and the other end remains open, with ignition being initiated at the close end. In addition, the internal surface of the side walls is either smooth (Fig. 3.1) or contains obstacles to form the obstructions along the channel walls (Fig. 3.2). The obstructed channel is further defined by the ratio of the channel internal diameter that is blocked by the obstacles, the blockage ratio, α, and the spacing between adjacent obstacles, ΔZ.

Figure 3.1: Schematic of a semi-open channel with smooth walls.

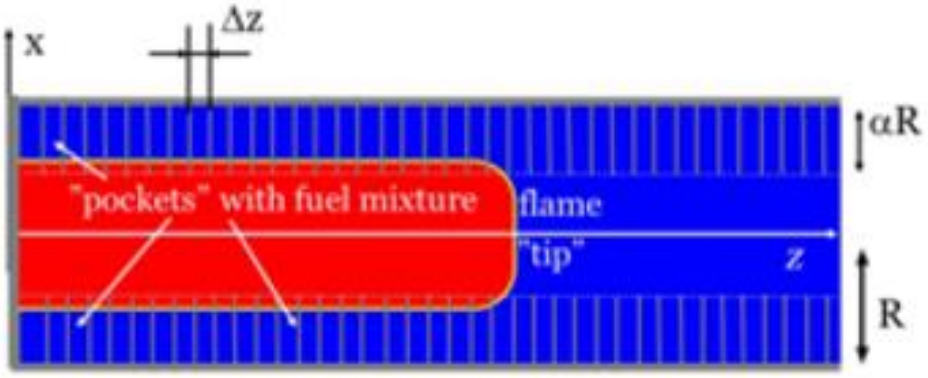

Figure 3.2: Schematic of a semi-open channel with evenly spaced obstacles on the internal wall surface.

3.2.2 Fully-Open Channels

The second type is when the channel is open at both ends, thus, permitting distributed flow of the content. The internal wall is also considered to be either smooth (Fig. 3.3) or obstructed (Fig. 3.4).

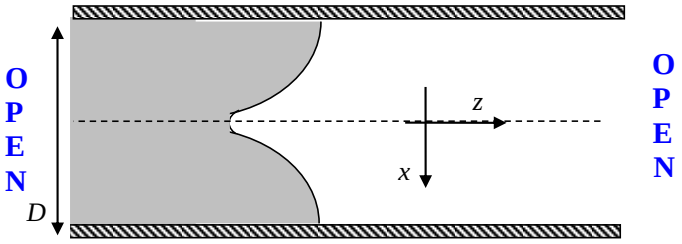

Figure 3.3: Schematic illustration of a channel with both ends open.

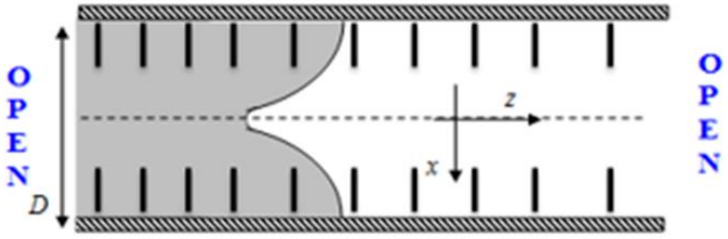

Figure 3.4: Schematic of an obstructed channel with both ends open.

3.3 Boundary Conditions

The type of boundary conditions imposed at the interface between a propagating flame and other surfaces depends on the specific objective that is to be achieved in each case, and it determines the type of flame-surface interactions occurred. Therefore, various thermal and mechanistic boundary conditions are considered in the present study.

3.3.1 Boundary Conditions at the Channel Walls

Possible extreme cases of thermal boundary conditions are considered in this work. The thermal boundary conditions are adiabatic, $\mathbf{n} \cdot \nabla T = 0$, or isothermal, $T_w = (T_{in} + T_{out})/2$, with T_w being the isothermal wall temperature calculated as the average value at the mid-point from both surface boundaries. Also, the mechanistic boundary conditions at the walls are free-slip, $\mathbf{n} \cdot \mathbf{u} = 0$, or nonslip, $\mathbf{u} = 0$, where $\mathbf{n}$ is a normal vector at a surface.

3.3.2 Boundary Conditions at the Channel Ends

Depending on a channel geometry being considered, different conditions are encountered at the channel ends. When a channel end is closed, the same boundary conditions at the channel walls applies. In contrast, different sets of boundary conditions are applied at the open end of the channel. Nonreflecting boundary conditions, $P = P_{amb}$, $\rho = \rho_f$, $(u_x, u_y) = 0$ and $Y = 1$ are applied to prevent the propagating flame from interacting with reflecting shocks.

3.4 The Ignition Model

The initial flame structure is imitated by the Zeldovich-Frank-Kamenetskii (ZFK) solution [84],

$$Y = \big(\Theta - T/T_f\big)/(\Theta - 1), \qquad P = P_f, \qquad u_x = 0, \qquad u_z = 0, \tag{3.9}$$

such that the mass fraction of the fuel mixture Y (which is the reaction progress variable) is $Y = 0$ in the burnt matter and $Y = 1$ in the fresh fuel mixture. The pressure P in the channel is equal to the initial fuel mixture P_f and the velocity components are set to zero at the beginning. Such a solution is shown for both planar and spherical ignition in Figs. 3.5 and 3.6, respectively. The temperature profiles in the domain before and after a planar flame front are

$$T = T_f + T_f(\Theta - 1)exp\big(z/L_f\big) \qquad if \quad z > 0 \tag{3.24}$$

$$T = \Theta T_f \qquad if \quad z < 0 \tag{3.25}$$

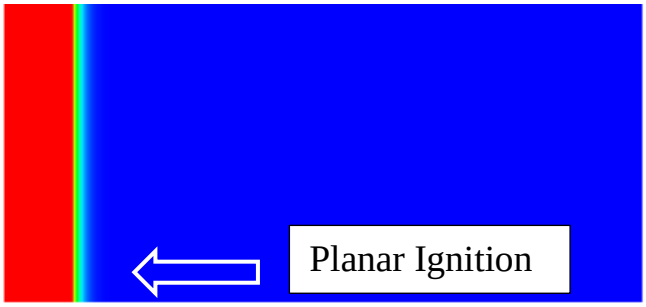

Figure 3.5: Planar ignition of fuel premixture in obstructed channel.

For a hemispherical flame, the temperature profile in the domain created from a point ignition is

$$T = T_f + (T_b - T_f) exp\left(\left(-\sqrt{(x^2 + z^2)} + r_f\right)/L_f\right) \quad if \quad z^2 + x^2 \geq r_f^2 \tag{3.26}$$

$$T = \Theta T_f \quad if \quad z^2 + x^2 < r_f^2 \tag{3.27}$$

where r_f is the initial flame radius position and T_b is the temperature of the burned matter.

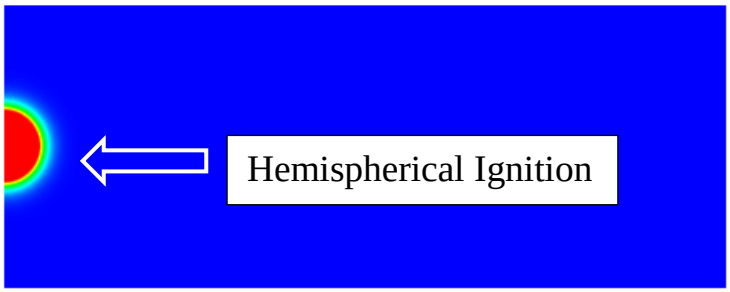

Figure 3.6: Hemispherical ignition of channel with smooth wall.

3.5 Grid/Mesh Generation

Given the wide disparity in dimension between the flame thickness and the length of the channel, the solver used in this work adopts a dynamic and self-adaptive mesh generation approach. The mesh around the flame is made finer to allow adequate resolution of the flame front. In order to save computational resources, the finer mesh is confined to the travelling flame front with the surrounding mesh being about 2% coarser. An illustration of the adaptive mesh is shown in Fig. 3.7. After adequate resolution tests, a minimum grid size of 0.2 L_f is found to adequately resolve the flame front, and it is adopted in this work. Therefore, the computational grid used in this work consists of square cells of size 0.2 L_f × 0.2 L_f. Figure 3.8 and Table 3.1 show different parameters describing a flame propagating in a semi-open channel with smooth wall for grid size ranging from 0.1 to 0.8 L_f. It is seen that no significant improvement is achieved below the grid size of 0.2 L_f.

Similar result is also presented for an obstructed channel in Fig. 3.9 where a mesh size of 0.2 L_f is also found appropriate

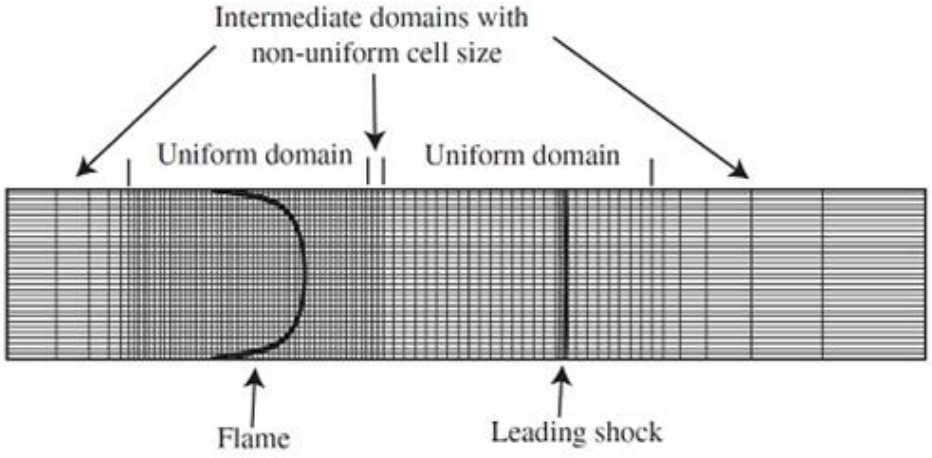

Figure 3.7: Schematic of the grid used in the numerical simulations [57]

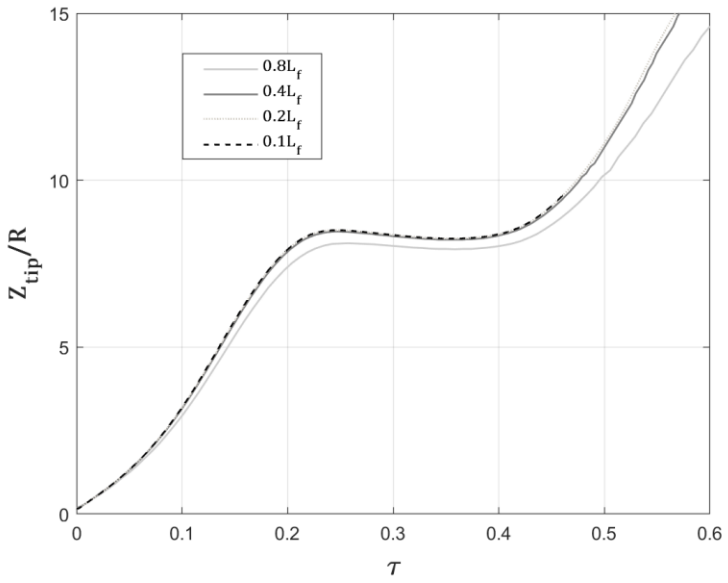

Figure 3.8: Resolution Test: The scaled tip position Z_{tip}/R versus the scaled time $\tau = U_f t/R$ for Le $= 0.2$, $R = 20$ and various mesh sizes.

Table 3.1: Resolution test for semi-open channel.

$\Delta z_f/L_f$	$U_{w,max}/U_f$	$\Delta U_{w,max}/U_f$	$\tau_{U_w,max}$	$\lvert\Delta\tau_{U_w,max}\rvert$	Z_{tip}/R	$\lvert\Delta Z_{tip}/R\rvert$
0.8	7.0053	-	0.1446	-	7.3983	-
0.4	7.5247	0.5194	0.1390	0.0056	7.8568	0.4585
0.2	7.5904	0.0657	0.1373	0.0017	7.9227	0.0659
0.1	7.5914	0.0010	0.1374	0.0001	7.9262	0.0035

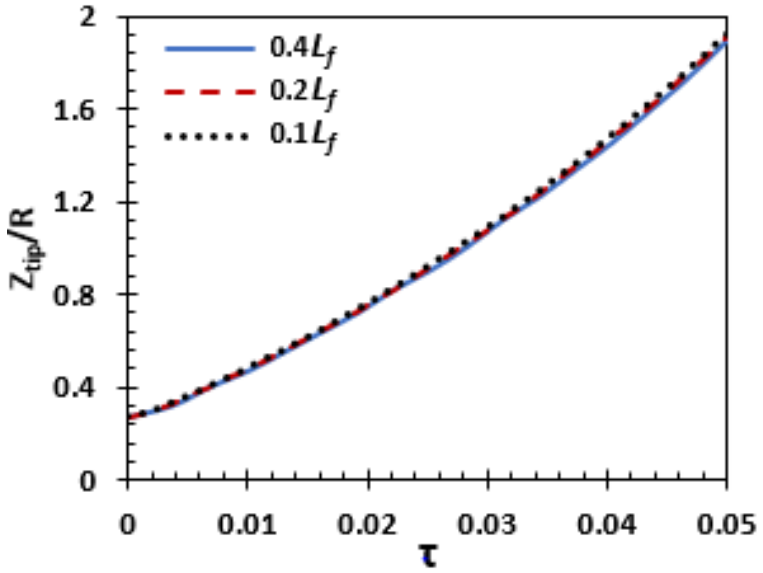

Figure 3.9: Resolution Test: The scaled flame position versus the scaled time for α = 1/3, Le = 0.2 and various square mesh sizes.

3.6 Validations

The validity and accuracy of the solver used in this work has previously been evaluated through experimental study of ethylene-oxygen combustion in a smooth tube of diameters 0.25 and 0.5 mm with 1.5 m long. The scaled tip velocity versus the scaled time were calculated numerically and compared to the experimental results shown in Figs. 3.10 and 3.11. Further validation of the solver is performed by comparing the simulation results for semi-open obstructed channel with the experimental results of Sahoo [85]. The simulation result is for $\Theta = 8$ flame propagating in $24L_f$ wide channel with a blockage ratio of 2.3, with $L_f = 4.0 \times 10^{-5}$m and $S_L = 0.364$ m/s. The experiment was conducted using stochiometric methane/air burning in a 7.5 cm x 7.5 cm channel and 2 m in length, with the obstacle spacing of $1/16$ of the channel width and with a blockage ratio of 2/3. The simulation result is in good agreement with the experimental result (see Fig. 3.12).

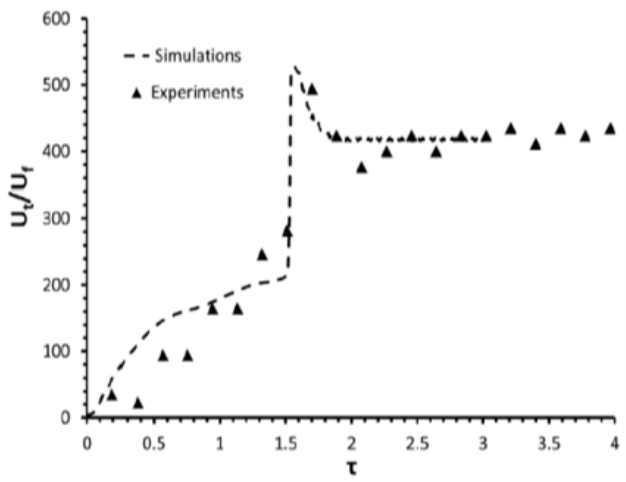

Figure 3.10: Validation: Scaled tip velocity vs the scaled time charts with both numerical and experimental results for R = 0.25 mm [86].

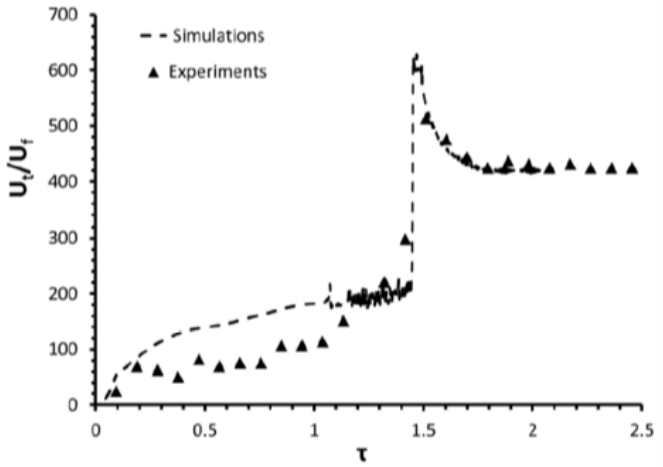

Figure 3.11: Validation: Scaled tip velocity vs the scaled time charts with both numerical and experimental results for R = 0.5 mm [86].

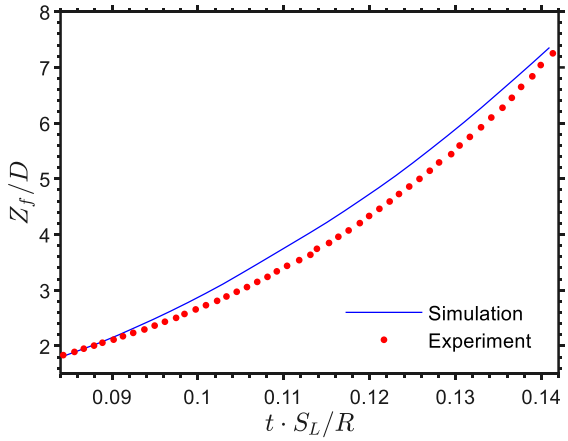

Figure 3.12: Experimental and simulation results for flame tip evolution in a channel of width 0.75 mm and blockage ratio of 2/3 [85].

3.7 Details of Parametric Study

The study is systematically designed to analyze the roles of various parameters and their interplay on propagation of non-equidiffusive flames, considering various combinations of channels widths, blockage ratios, obstacle spacing, thermal expansion ratios, and Lewis numbers. Other parameters used in the simulations include: molecular weight $m = 2.9 \times 10^{-2}\text{kg/mol}$, initial fuel density $\rho_f = 1.16\,\text{kg/m}^3$, initial fuel pressure $P_f = 100$ kPa, initial fuel temperature $T_f = 300$ K, dynamic viscosity $\eta = 1.7 \times 10^{-5}\text{kg/(m} \cdot \text{s)}$. The flame thickness $L_f = 4.22 \times 10^{-5}\text{m}$ and the laminar flame speed, $S_L = 34.7\ \text{cm/s}$, being 10^3 times smaller than the initial speed of sound in this fuel mixture $c_0 = 347\ \text{m/s}$ such that the hydrodynamics is almost incompressible at the initial stage of burning. Table 3.2 summarizes the geometry and thermo-chemical properties varied in the parametric study.

Table 3.2: Factors and values considered in the study

Factors			Values
Semi-open channel	Smooth	Channel half-width	10, 20, 30
		Thermal expansion ratio	5, 8, 10
		Lewis number	0.2, 0.5, 1.0, 1.5, 2.0
		Wall boundary condition	Adiabatic, free slip
	Obstacle laden walls	Channel half-width	24, 36, 48
		Blockage ratio	1/3, 1/2, 2/3
		Obstacle spacing	R/4
		Thermal expansion ratio	8
		Lewis number	0.2, 0.5, 1.0, 1.2, 2.0
		Boundary condition	Adiabatic, free slip
Fully open channel	Smooth	Channel half-width	10, 20, 30
		Thermal expansion ratio	5, 8, 10
		Lewis number	0.2, 0.5, 1.0, 1.5, 2.0
		Wall boundary condition	Adiabatic, isothermal (T_w = 300K), non-slip
	Obstacle laden walls	Channel half-width	12, 24, 36, 48
		Blockage ratio	1/3, 1/2, 2/3
		Obstacle spacing	R/4, R/2, R
		Thermal expansion ratio	5, 8, 12
		Lewis number	0.3, 0.5, 1.0, 1.5, 2
		Boundary condition	Adiabatic, free slip

3.7.1 Semi-open channel with slip wall

For a semi-open channel, where the aim is to analyze the impact of non-equidiffusive burning at the early stage of flame propagation, through the finger flame acceleration mechanism [51]. The channel half-width in the range $10 \leq R/L_f \leq 30$, thermal expansion ratio $5 \leq \Theta \leq 10$ and Lewis number $0.2 \leq Le \leq 2$. The nonreflecting boundary conditions are employed at the open end of the channel to prevent the reflection of the sound waves and weak shocks. The walls of the channel are taken to be free-slip and adiabatic. Various tube radii and channel half-widths were considered in the range $10 \leq R/L_f \leq 30$, which corresponds to a relatively low flame propagation Reynolds number, $Re = U_f R/\nu = R/\mathrm{Pr}L_f = 10{\sim}30$. The flame is ignited on the center line at the closed end with initial hemispherical radius r_f, of 1.5 L_f.

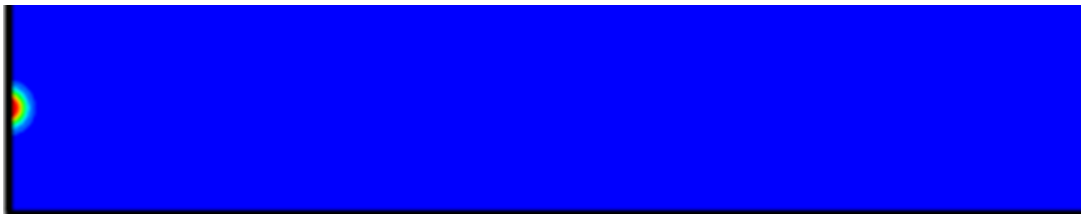

Figure 3.13: Semi-open channel for finger flame acceleration mechanism.

3.7.2 Semi-open channels with obstruction

For an obstructed channel with one end closed and the other open, with non-slip and adiabatic surfaces of the wall and obstacles, the acceleration mechanism experienced in this type of configuration is that of Bychkov [54]. The parametric study adopted here include the channel half-width R (describing the Reynolds number associated with flame propagation $Re = R/L_f\mathrm{Pr}$) in the range $R/L_f = 24, 36, 48$; the blockage rato $\alpha = 1/3, 1/2, 2/3$ and obstacle spacing $\Delta Z = R/4$. The Lewis numbers in the range $0.2 \leq Le \leq 2.0$, and the thermal expansion ratio $\Theta = \rho_f/\rho_b = 8$ are used. A flame is ignited on the center line at the closed end with a hemispherical radius $r_f = 5.1L_f$.

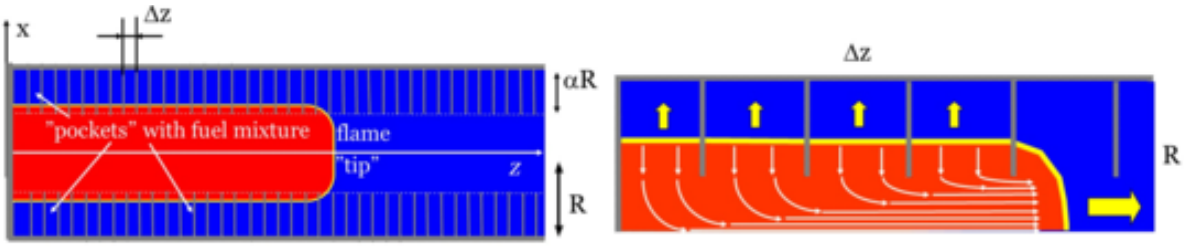

Figure 3.14: Semi-open obstructed channel illustrating the Bychkov mechanism of FA [54]

3.7.3 Open Channels with smooth wall

For channel with both ends open, the non-reflecting boundary condition is applied at both ends, while a combination of the no-slip and adiabatic or isothermal boundary conditions are applied at the channel walls. For the isothermal case, only cold wall maintained at $T_w = 300K$ is considered. Channel half-width in the range $R/L_f = 10, 20, 30$, thermal expansion ratios $\Theta = 5, 8, 10$ and the Lewis numbers in the range $0.2 \leq Le \leq 2.0$ are the governing parameters considered. The initial flame structure is imitated by the Zeldovich-Frank-Kamenetskii (ZFK)-like solution for a planar flame front [8] initiated at the distance $50\ L_f$ from the left end of the channel.

Figure 3.15: schematic of an unobstructed channel with both extremes open.

3.7.4 Obstructed channels with open ends

For the obstructed channel with open ends (Fig. 3.16), adiabatic and free-slip boundary conditions are applied on the surfaces, consisting of the wall and obstacle surfaces. Non-reflecting boundary condition is applied at both ends of the channel. Other parameters considered here include: the channel half-width $R/L_f = 12, 24, 36, 48$, the blockage ratio $\alpha = 1/3, 1/2, 2/3$, spacing between the obstacles $\Delta Z = R/4, R/2, R$, the thermal expansion ratio $\Theta = 5, 8, 12$. The Lewis number is varied in the range $0.3 \leq Le \leq 2.0$, by keeping constant $\mathrm{Pr} = 1$ and adjusting Sc accordingly. The initial flame structure is imitated by the ZFK-like solution for a planar flame front initiated at a distance $60\ L_f$ from the left extreme of the channel.

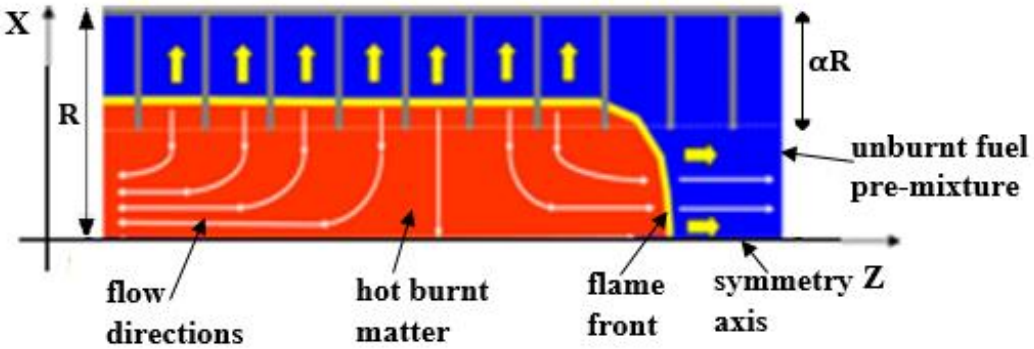

Figure 3.16: A schematic of an obstructed channel with both extremes open (only an upper half is shown) [21]

3.8 Flame Characterization

Resulting flames from the simulations are characterized by monitoring the flame tip position at every instant during the flame propagation. The flame tip velocity U_{tip} is estimated from the flame tip position Z_{tip}. The burning rate is calculated as

$$U_w = \frac{1}{2R\rho_f}\int \frac{\rho Y}{\tau_R} exp\left(-\frac{E_A}{R_p T}\right) dxdz. \tag{3.28}$$

The flame tip velocity and the burning rate is scaled by the laminar flame velocity S_L. A convenient measure of the instantaneous flow compressibility and thereby, the stage of DDT, is instantaneous Mach number associated flame propagation, which is defined as

$$Ma_{tip} = \frac{U_{tip}}{c_{tip}}, \tag{3.29}$$

where

$$c_{tip} = \sqrt{\left({C_p}/{C_v}\right) \times \left({R_p}/{M}\right) \times T_{tip}} \tag{3.30}$$

is the instantaneous speed of sound in the fuel mixture at the flame tip. It is noted that $Ma_{tip} \ll 1$ at the initial, quasi-isobaric stage of burning, while it will approach an order of unity by the onset of detonation.

4 Propagation of Non-equidiffusive Flames in Semi-open Channels with Smooth Walls

4.1 Effect of Lewis number on Morphology and Dynamics of Non-equidiffusive Flames

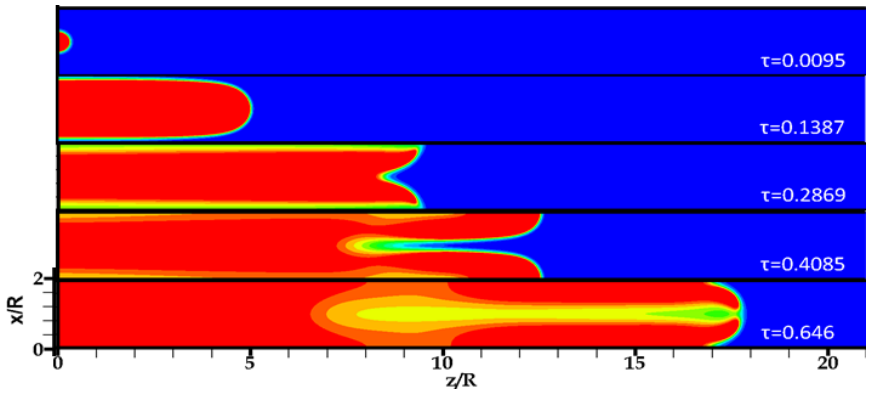

Figure 4.1: The temperature snapshots of the flame evolution with $Re = 20$, $\Theta = 8$ and $Le = 0.2$.

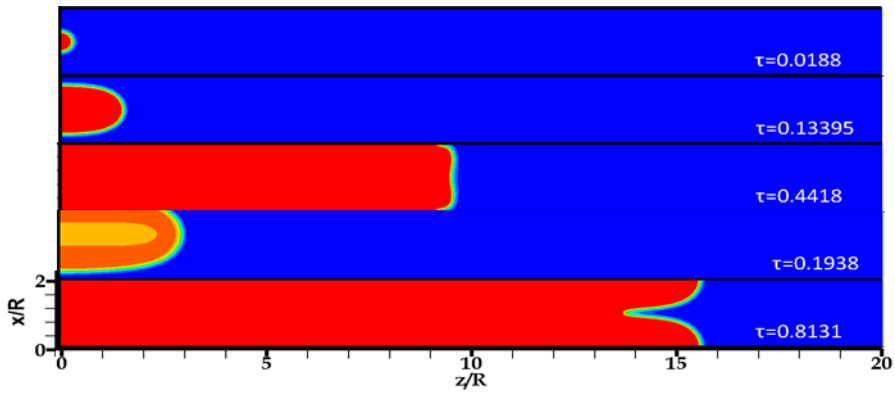

Figure 4.2: The temperature snapshots of the flame evolution with $Re = 20$, $\Theta = 8$ and $Le = 1$.

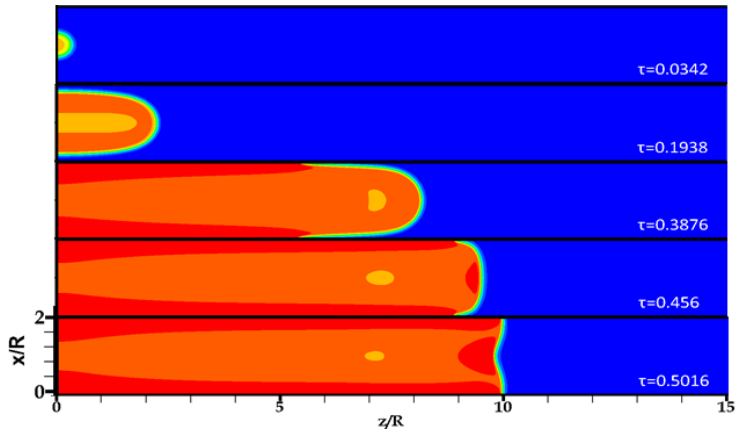

Figure 4.3: The temperature snapshots of the flame evolution with $Re = 20$, $\Theta = 8$ and $Le = 2$.

The results of parametric study on the effects of Le on the finger FA scenario in a 2D planar geometry is presented. Comparison of the flame dynamics, morphology and quantitative results of the $Le \neq 1$ flames to the $Le = 1$ ones is made. Figures 4.1 – 4.3 show the temperature snapshots of the flame evolution with various Lewis numbers, $Le = 0.2\ (4.1), 1\ (4.2), \text{and } 2\ (4.3)$ for the same $Re = 20$ and $\Theta = 8$. In all these cases, a flame embryo has been ignited at the centerline at the closed end of the channel, and it expands mainly axially because its expansion in the radial direction is inhibited by the lateral walls of the channel. As a result, the flame elongates to acquire a finger shape of the front. At this stage, the flame surface area and the total burning rate experience near-exponential growth for a limited time. This is due to such finger FA, which lasts until the lateral sides of the flame front (the flame skirt) contact the sidewalls of the channel. At the next stage, the flame tip starts decelerating, with flame morphology reverting from a concave finger flame front to a convex tulip flame shape.

In the case of $Le = 1$, the temperature evolution is uniform during flame propagation, which indeed indicates the balance of the diffusive properties. For the non-equidiffusive fuel mixtures with the mass diffusivity higher than the thermal diffusivity, i.e. Le < 1, shown in Fig. 4.1, it is observed that such flames accelerate much faster than the $Le \geq 1$ flames. The hemispherical flame expands axially, where the flame surface area, the velocity of its tip, as well as the total burning rate grow near-exponentially, promoting acceleration. The accelerating regime ends when a flame skirt contacts a sidewall of the channel. The flame front subsequently decelerates and, eventually, acquires a concave, tulip shape where the upper and lower crests almost exhibit the so-called flame "channeling". Another interesting stage of FA occurs when a secondary finger-shaped flame front is formed. The latter effect is presumably related to the onset of the diffusional-thermal instability. For $Le = 2$, Fig. 4.3, while the flame dynamics is qualitatively the same as that for $Le = 1$, it is observe that there is some local increase in the flame temperature, as the flame inverts to a tulip shape. This effect is due to more intensive burning at the convex part of the flame surface caused by the presence of diffusion-thermal instability. The appearance of a preheated localized region around the flame skirt and the flame tip is attributed to the effect of the high thermal diffusivity.

Quantitative comparison of the flames at various Le is next depicted, while the other flow parameters are kept constant. Specifically, Figs. 4.4 and 4.5 present the evolution of scaled total burning rate U_w/S_L (Fig. 4.4) and the scaled flame tip velocity U_{tip}/S_L (Fig. 4.5) for the Lewis number in the range $0.2 \leq Le \leq 2$ with the fixed $Re = 10$ and $\Theta = 8$. It is demonstrated that Le

plays a serious role in flame propagation. Specifically, due to the onset of the diffusional-thermal instability, the $Le < 1$ flames acquire the higher acceleration rate as compared to the $Le \geq 1$ cases.

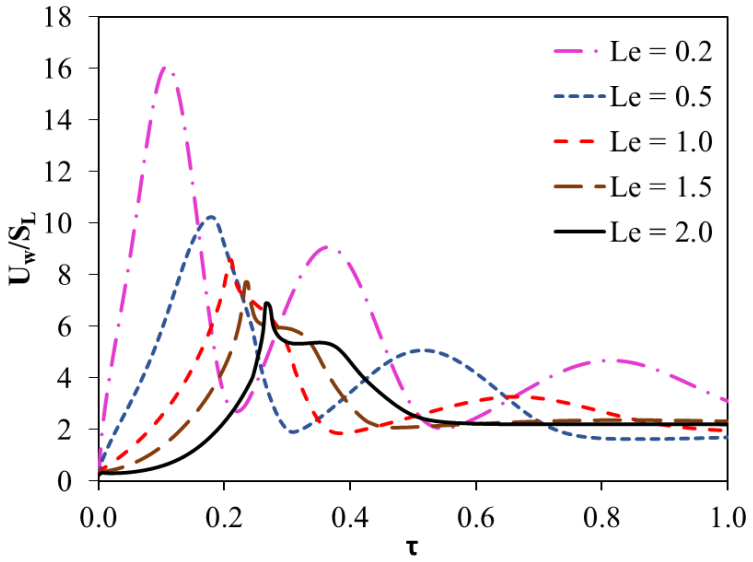

Figure 4.4: The scaled total burning rate U_w/S_L versus the scaled time $\tau = S_L t/R$ for $Re = 10$ and $\Theta = 8$.

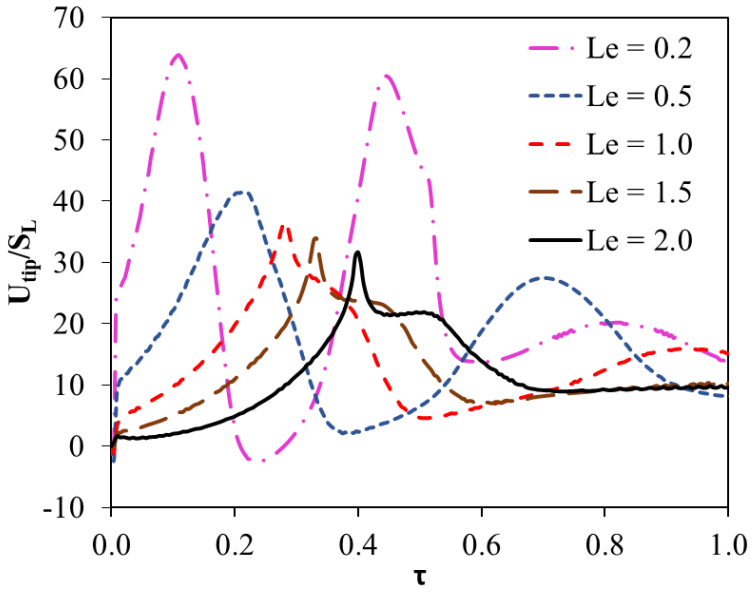

Figure 4.5: The scaled flame tip velocity U_{tip}/S_L versus the scaled time $\tau = S_L t/R$ for $Re = 10$ and $\Theta = 8$.

For a small Lewis number, $Le = 0.2$, fast FA is observed, manifesting in both the burning rate and the flame tip velocity. The peak values of the scaled burning rate and the flame tip velocity are also found to be higher as compared to all other values of Le. However, at $Le = 0.5$, while acceleration is weaker than that in the case of $Le = 0.2$ and stronger than that at $Le = 1$, the peak

values are comparable to what is seen when $Le \geq 1$. Also, in the situation of $Le < 1$, an intriguing secondary phase of finger-like FA is observed, following the distortion of the tulip flame front. On the other hand, due to an increased thickness of the flame front for $Le > 1$, such a flame accelerates slightly slower than the respective equidiffusive flame. Another difference seen is immediate sharp deceleration of a $Le \geq 1$ flame as compared to the $Le < 1$ one, and such a point on the graph corresponds to the instant, when the flame skirt contacts the channel sidewall. A response of the lateral flows to this obstruction is noticed to provide a delay in propagation of the $Le < 1$ flames.

4.2 Effects of Flame Reynold Number on Non-equidiffusive Finger Flame

The impact of Re on propagation of a flame with $Le \neq 1$ is next investigated. Figure 4.6 depicts the scaled total burning rate U_w/S_L for the flames with $Le = 0.2$ and 2, $Re = 10$ and 20. It is shown that the impact of Re in the case of $Le = 0.2$ is minor as U_w/S_L exhibits only a slight difference. In contrast, a more significant impact of Re is observed for $Le > 1$ such as a near-exponential growth during the finger FA regime. Here, the flames burning rate grow exponentially for $Re = 10$, showing less growth rate as compared to higher Re. These results are associated with the fact that the flame thickness increases with Le, thereby reducing the flame stretch. The lower flame stretch prevents adequate corrugation of the flame front, causing some reduction of the flame surface area and, thus, a lower burning rate. Similarly, a wider flame front would be easier to corrugate than a small one, explaining the higher burning rate observed for larger Re, $Re = 20$.

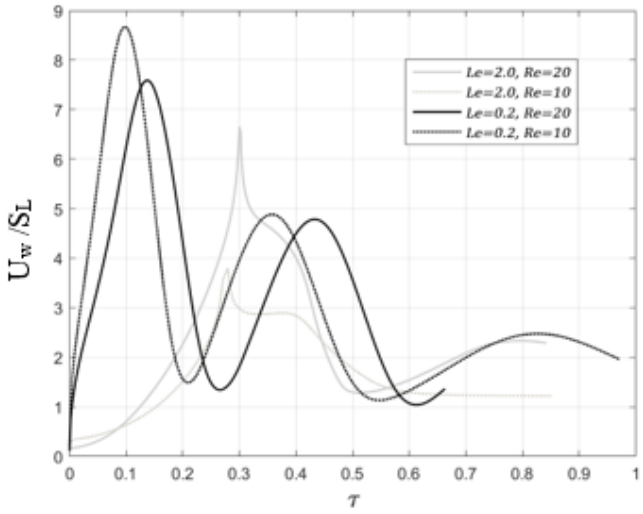

Figure 4.6: The scaled total burning rate U_w/S_L versus the scaled time $\tau = S_L t/R$ in the 2D planar geometry for $Le = 0.2, 2$ and $Re = 10, 20$.

4.3 Impact of Thermal Expansion Ratio on Non-equidiffusive Flames

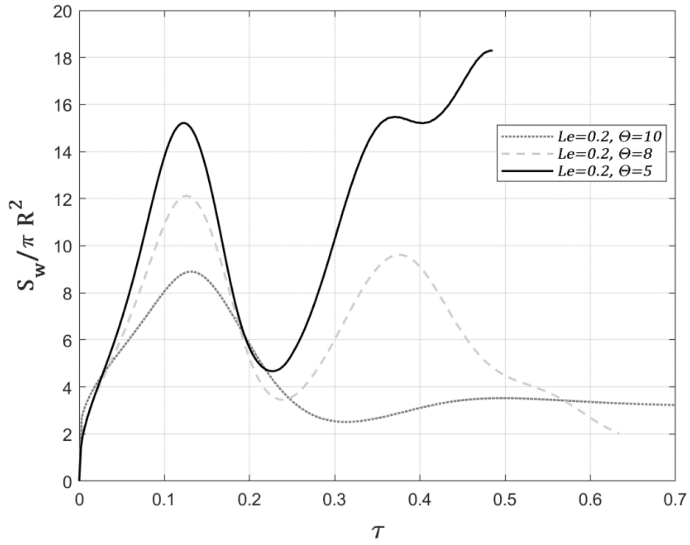

Figure 4.7: The scaled flame surface area $S_w/\pi R^2$ vs the scaled time $\tau = S_L t/R$ for $Le = 0.2$ with $\Theta = 5, 8, 10$ and $Re = 20$.

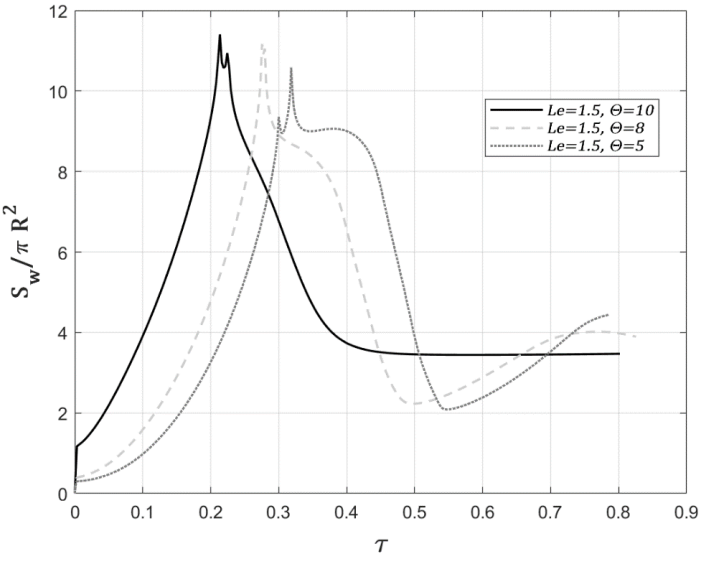

Figure 4.8: The scaled flame surface area $S_w/\pi R^2$ vs the scaled time $\tau = S_L t/R$ for $Le = 1.5$ with $\Theta = 5, 8, 10$ and $Re = 20$.

In addition, the thermal expansion ratio is varied in the range $5 \leq \Theta \leq 10$, to identify its effect on the finger FA scenario for the $Le \neq 1$ flames. The quantitative analysis of the impact of thermal expansion is presented in Figs. 4.7 and 4.8, where the time evolutions of the flame surface area are shown for $Le = 0.2$ (Fig. 4.7) and $Le = 1.5$ (Fig. 4.8), with $\Theta = 5,\ 8$ and 10 in each figure. An increase in Θ promotes acceleration of a $Le > 1$ flames in Fig. 4.7. In contrast,

we surprisingly see an opposite trend for a $Le < 1$ flame in Fig. 4.7: acceleration weakens with the increase in Θ.

5 Propagation of Non-equidiffusive Flames in Obstructed Semi-Open Channels

5.1 Flame Morphology in Obstructed Semi-open Channels

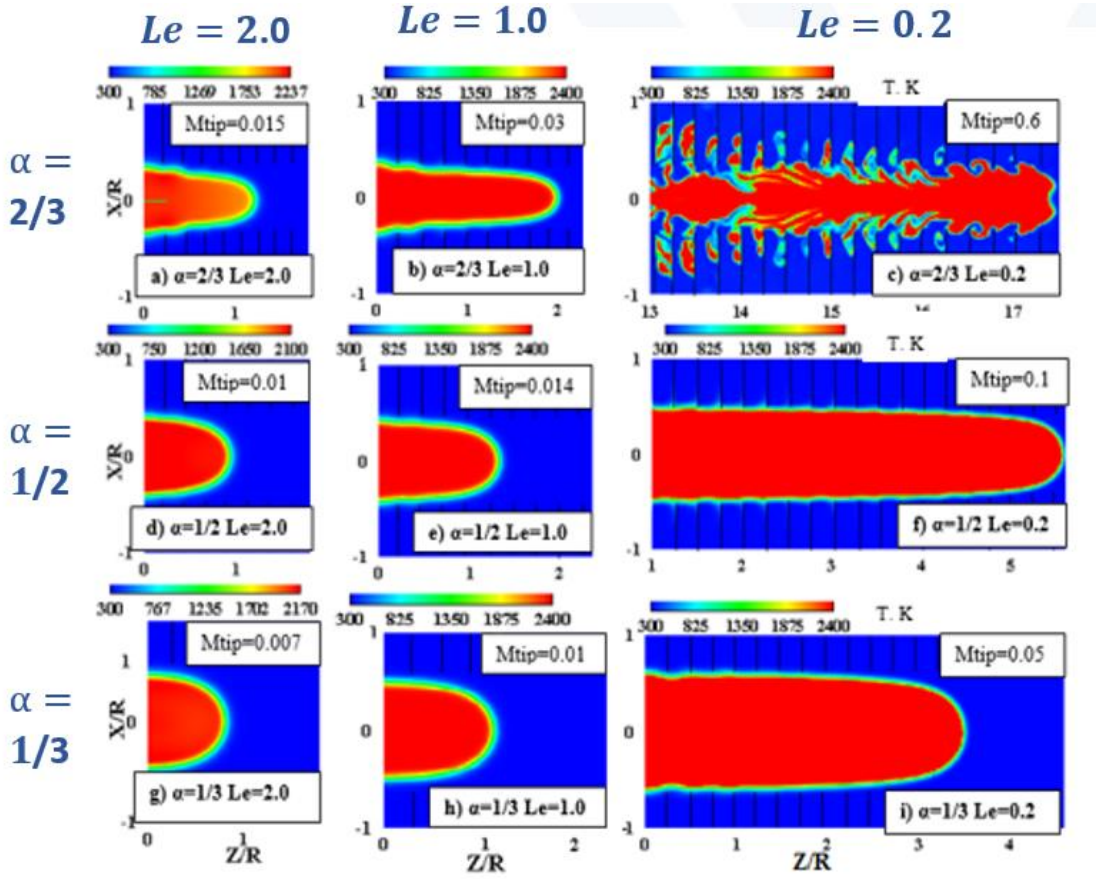

Figure 5.1: Temperature snapshots taken at the same scaled time instant, $\tau = t\, S_L / R = 0.075$ for $Re = 24\, L_f$ and various *Le* and α. (Total of nine different simulation runs, with each snapshot representing different combinations of *Le* and α).

Results of the extensive computational simulations of premixed flames with various Le in semi-open, obstructed channels of various Reynolds numbers reveals the impact of non-equidiffusivity on the shape of the flame front. Specifically, Fig. 5.1 (a-i) shows the flame shapes and positions attained at various $Le = 0.2, 1.0, 2.0$ and $\alpha = 1/3, 1/2, 2/3$ at the same scaled time instant, $\tau = 0.075$, and for the same $R/L_f = 24$ in all nine simulation runs. The respective Mach numbers

associated with flame tip at scaled time of 0.075, $Ma_{tip}|\tau = 0.075$, are also depicted. The flames are represented by the temperature snapshots, with a temperature ranging from 300 K in the fuel till 2400 K in the burnt matter. It is seen that the role of the Lewis number is paramount and as strong as that of the blockage ratio. Indeed, when both the effect of large α and nonequidiffusivity (with $Le < 1$) work together, Fig. 5.1c for α = 2/3 and $Le = 0.2$, then the flame front is drastically folded; having propagated over considerable distance, with the flame tip Mach number being as high as $Ma_{tip} = 0.6$. In contrast, a $Le > 1$ flame in a channel with small blockage ratio accelerates very slow, as observed in Fig. 5.1g for α = 1/3 and $Le = 2.0$. In other cases of Fig. 5.1, the effects of α and Le on FA compete, such that almost equivalent flame structures and M_{tip} are observed in the pairs of Figs. 5.1d and 5.1h; Figs. 5.1a and 5.1e; an even Figs. 5.1b and 5.1i.

5.2 Statistical Significance of the Effects of R, α, and Le on Flame Propagation

Analysis of variance (ANOVA) is used to determine the factors which significantly affects the propagation of a flame in obstructed channel with one end closed and the other being open. The combined effects of the factors on flame propagation are also scrutinized by statistically analyzing the interactions among the factors.

Table 5.1: Analysis of variance table for flame acceleration in obstructed semi-open channel

Factors	Sum of squares	Degree of Freedom	Mean Square	F	Prob>F (95% CL)
Half-width (R)	72.4	2	36.18	1.31	0.3144
Blockage ratio (α)	7970.8	2	3985.39	147.81	0.0371
Lewis number (Le)	9469.3	2	4734.65	175.59	0.0371
R*α	102.5	4	24.63	0.95	0.2831
R*Le	133.1	4	33.27	1.23	0.3695
BR*Le	12476.2	4	3119.06	115.68	0.0371
Error	215.7	8	26.96		
Total	30440	26			

The analysis of variance results shown in Table 5.1, indicates that at 95% confidence level ($p \leq 0.05$), the effects of blockage ratio, α and the Lewis number, Le, are found to be statistically significant ($0.0371 < 0.05$), and so is the effects of the interaction between these two factors. The three sources appear to be of equal significance in determining the flames dynamics. On the other hand, the channel width, R, is not statistically significant, as the F-value is greater than 0.05

(0.3144 > 0.05). This confirms the Reynolds independence of the Bychkov mechanism of flame acceleration as reported in previous study [54]. The interactions between the channel width and the blockage ratio, as well as between channel width and the Lewis number are found to be statistically insignificant.

5.3 Effects of Lewis number on Flame propagation

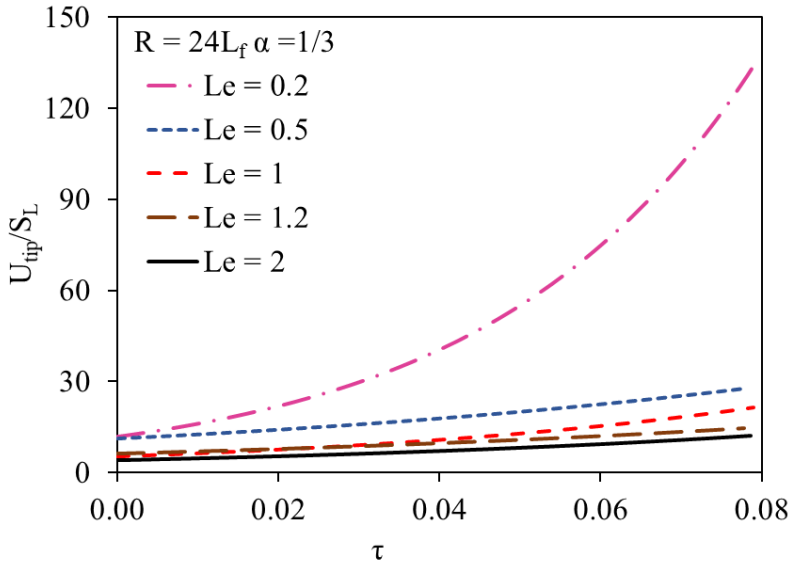

Figure 5.2: The scaled flame tip velocity U_{tip}/S_L versus the scaled time $\tau = t\,S_L/R$ for $R = 24\,L_f$ and $\alpha = 1/3$.

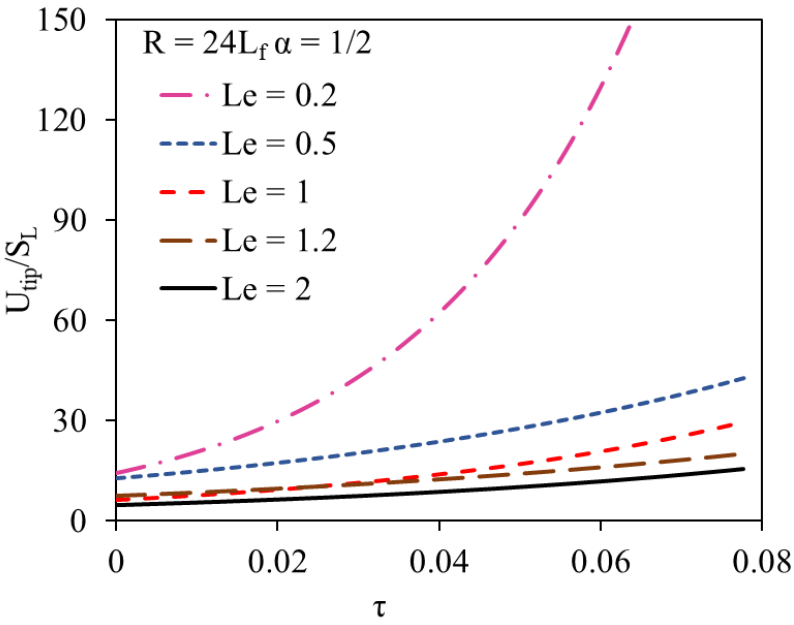

Figure 5.3: The scaled flame tip velocity U_{tip}/S_L versus the scaled time $\tau = t\,S_L/R$ for $R/L_f = 24$ and $\alpha = 1/2$.

To quantify the impacts of Le, in Figs. 5.2 – 5.5, the evolution of the scaled flame tip velocity, U_{tip}/S_L, is presented for several blockage ratios, α = 1/3 (Fig. 5.2), 1/2 (Fig. 5.3), and 2/3 (Fig. 5.4), with different $Le = 0.2, 0.5, 1.0, 1.2, 2.0$ in each plot. It is seen that the effect of Le is very strong, especially for the $Le < 1$ flames. Indeed, in all three Figs. 5.2 – 5.5, $Le = 0.2$ leads to an increase in U_{tip} almost by an order of magnitude as compared to the equidiffusive case, $Le = 1$. The effect of $Le > 1$ is substantially weaker, but $Le = 2.0$, nevertheless, noticeably moderates FA as compared to the $Le = 1$ cases. Figure 5.5 depicts the variation of the logarithm of scaled tip velocity with Le at $R/L_f = 24$ at the scaled time instant $\tau = 0.075$ (similar to Fig. 5.1). It is shown that the flame velocity increases as Le decreases for all values of α, with the greatest increase observed at $Le < 1$, and minimal changes at Le above unity.

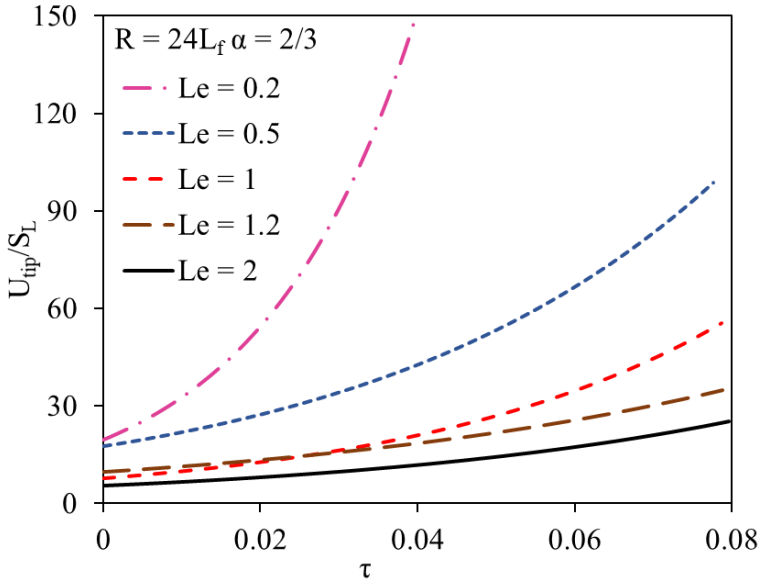

Figure 5.4: The scaled flame tip velocity U_{tip}/S_L versus the scaled time $\tau = t\,S_L/R$ for $R/L_f = 24$ and $\alpha = 2/3$.

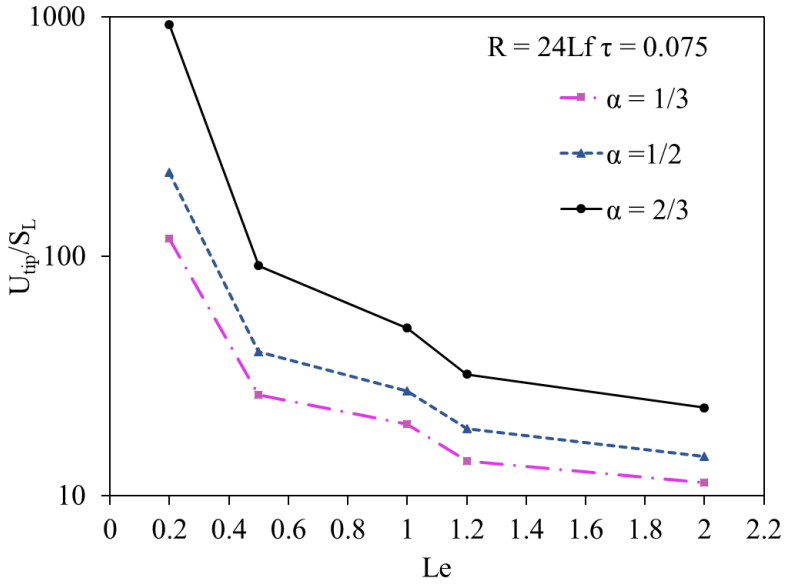

Figure 5.5: The scaled flame tip velocity U_{tip}/S_L at $\tau = 0.075$ versus Le for different values of $\alpha = 1/3, 1/2, 2/3$.

5.4 Impact of Blockage ratio on Flame propagation

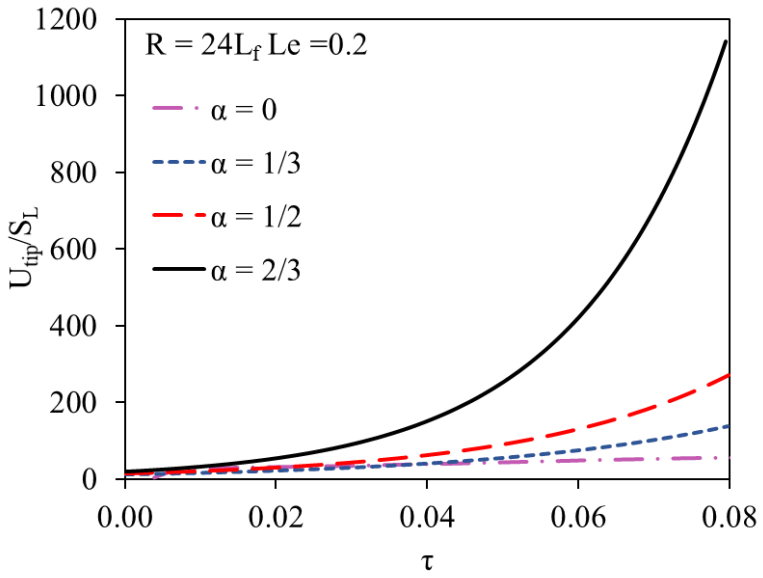

Figure 5.6: The scaled flame tip velocity U_{tip}/S_L versus the scaled time $\tau = t\,S_L/R$ for $R/L_f = 24$ and $Le = 0.2$.

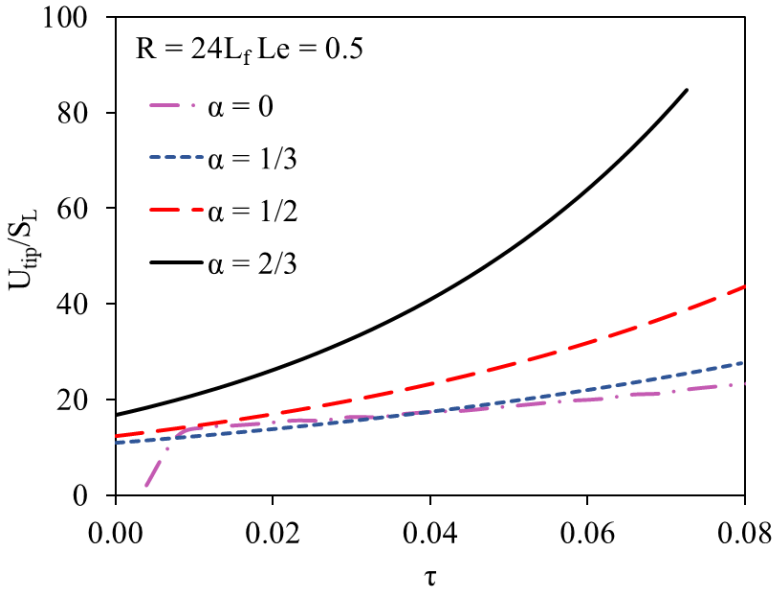

Figure 5.7: The scaled flame tip velocity U_{tip} / S_L versus the scaled time $\tau = t\, S_L / R$ for $R/L_f = 24$ and $Le = 0.5$.

Figures 5.6–5.9 illustrate the role of the blockage ratio α in acceleration of the flame tip. It is seen that α-dependence is significant and much stronger than the Re-dependence for all the Lewis numbers considered. At the same time, the impact of Le on the α-dependence is smaller than that on the Re-dependence: specifically, the α-dependence does not change sign due to Le, but there is a noticeable quantitative effect: the α-dependence is stronger for the $Le < 1$ flames. For different values of Le, the flames exhibit weaker acceleration in unobstructed channel, $\alpha = 0$, as compared to acceleration in obstructed ones.

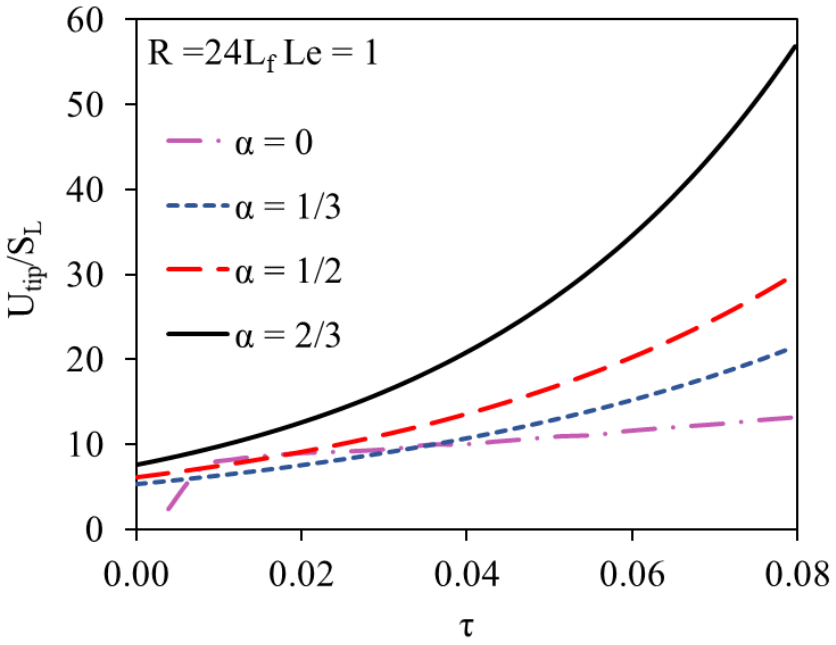

Figure 5.8: The scaled flame tip velocity U_{tip}/S_L versus the scaled time $\tau = t\,S_L/R$ for $R/L_f = 24$ and $Le = 1$.

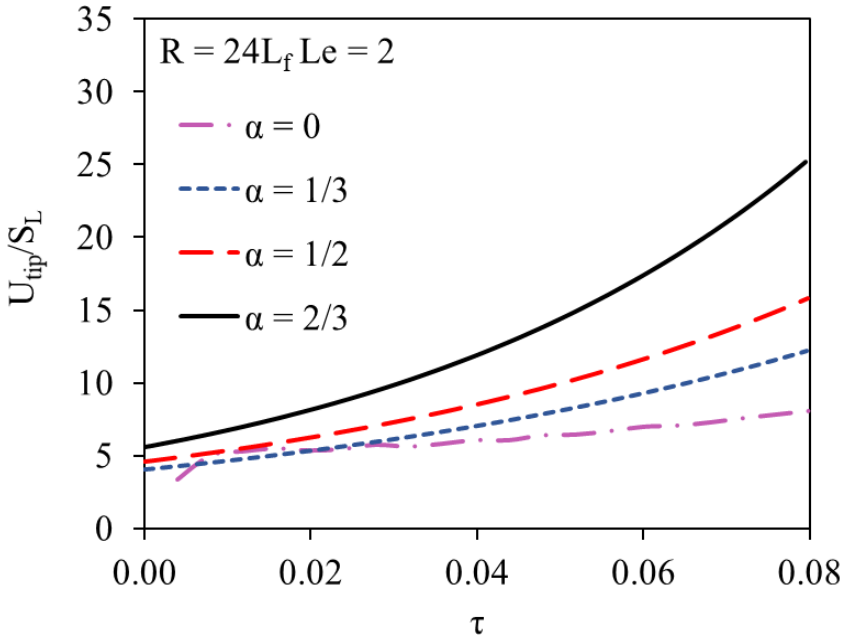

Figure 5.9: The scaled flame tip velocity U_{tip}/S_L versus the scaled time $\tau = t\,S_L/R$ for $R/L_f = 24$ and $Le = 2$.

5.5 Effect of Channel Width on flame Propagation

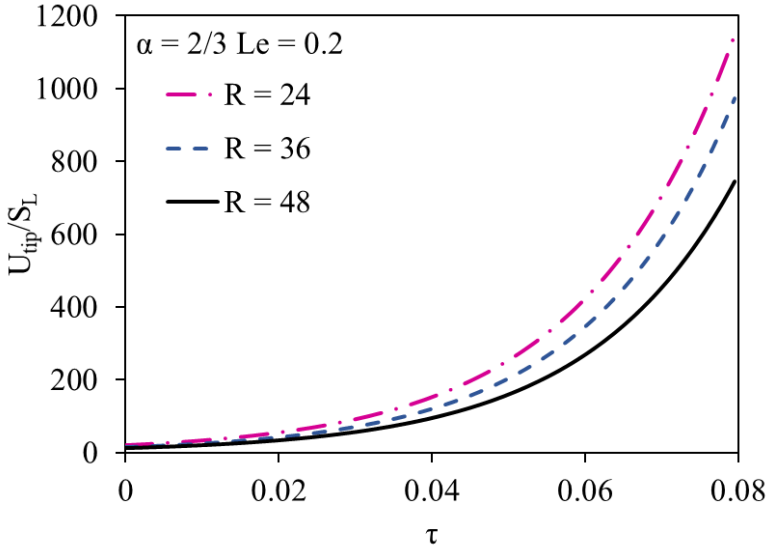

Figure 5.10: The scaled flame tip velocity U_{tip}/S_L versus the scaled time $\tau = t\,S_L/R$ for α = 2/3 and Le = 0.2.

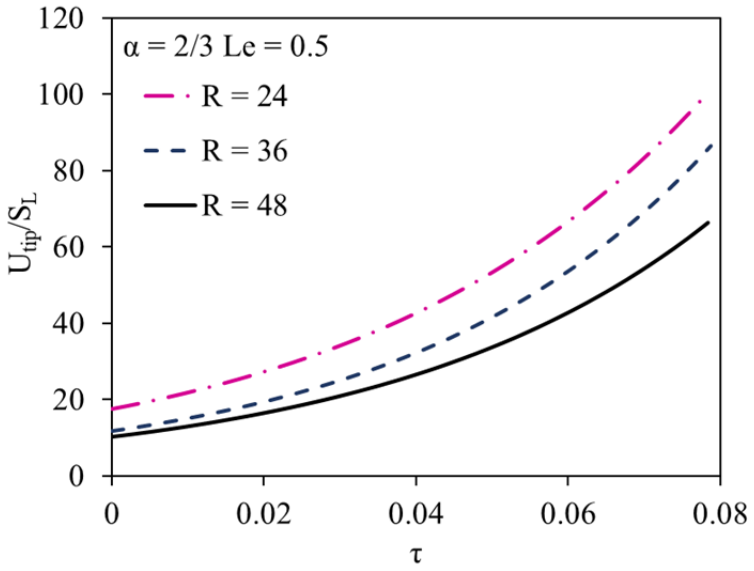

Figure 5.11: The scaled flame tip velocity U_{tip}/S_L versus the scaled time $\tau = t\,S_L/R$ for α = 2/3 and Le = 0.5.

While the effect of channel width is found to be insignificant, most especially at $Le = 1$, some effects are noticeable at $Le \neq 1$. The role of channel width for various Le and α is presented in Figs. 5.10 – 5.13. It is seen that the impact of Re is minor as all the plots for $R/L_f = 24, 36, 48$ in Figs. 5.10 – 5.13 attain very similar acceleration rates. This supports the Bychkov formulation [54] predicting Re-independent FA. On the other hand, the figures show a very intriguing result: the impact of Le modifies the Re-dependence up to the opposite one. Indeed, FA weakens with Re for

the $Le \geq 1$ flames, due to a decreasing flame stretch, but it is promoted with *Re* in the $Le < 1$ case for the opposite reason, see Fig. 5.13. This indicates the existence for a potential threshold Lewis number corresponding to the change of a trend and thus providing the complete *Re*-independence. While adiabatic walls are assumed here, it is important to note that the presence of heat losses at the walls may modify the flow behind the flame front and, thus, change the flame tip dynamics.

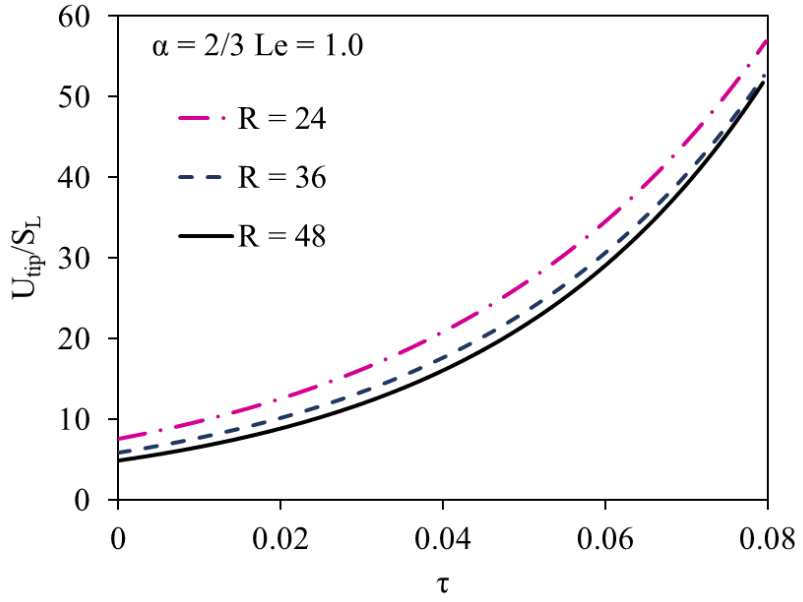

Figure 5.12: The scaled flame tip velocity U_{tip}/S_L versus the scaled time $\tau = t\,S_L/R$ for α = 2/3 and *Le* = 1.0.

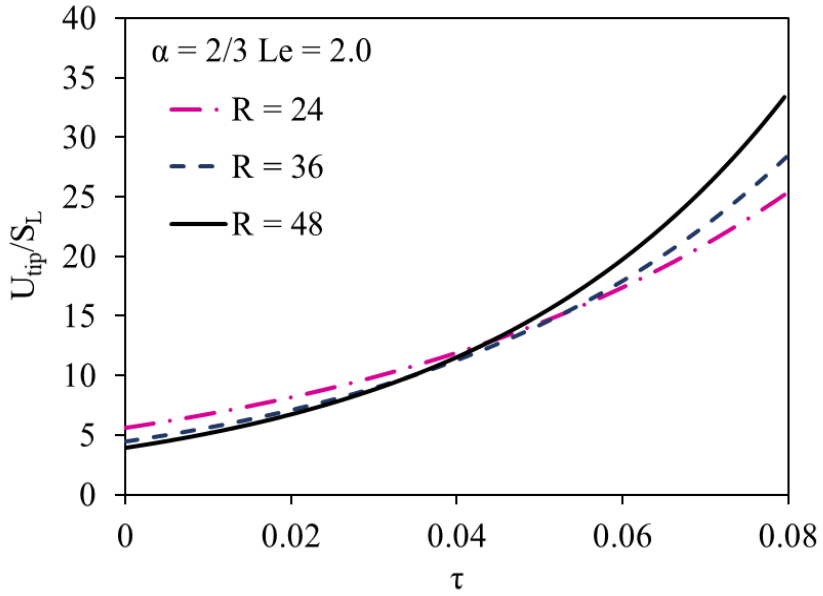

Figure 5.13: The scaled flame tip velocity U_{tip}/S_L versus the scaled time $\tau = t\,S_L/R$ for α = 2/3 and *Le* = 2.0.

5.6 Quantitative Analysis of Flame Acceleration Rate

Finally, the acceleration trends are analyzed in the cases when the exponential trends are exhibited. The exponential acceleration rate σ is related to flame tip position by $Z \approx e^{\sigma\tau}$ and was estimated as the slope from plot of scaled flame tip position Z versus scaled time τ. The resulting σ is plotted versus Le in Fig. 5.14 for Re = 24 (a), 36 (b) and 48 (c), respectively, with α = 0, 1/3, 1/2, 2/3 in each figure. The acceleration rate σ is largest for non-equidiffusive cases of $Le < 1$.

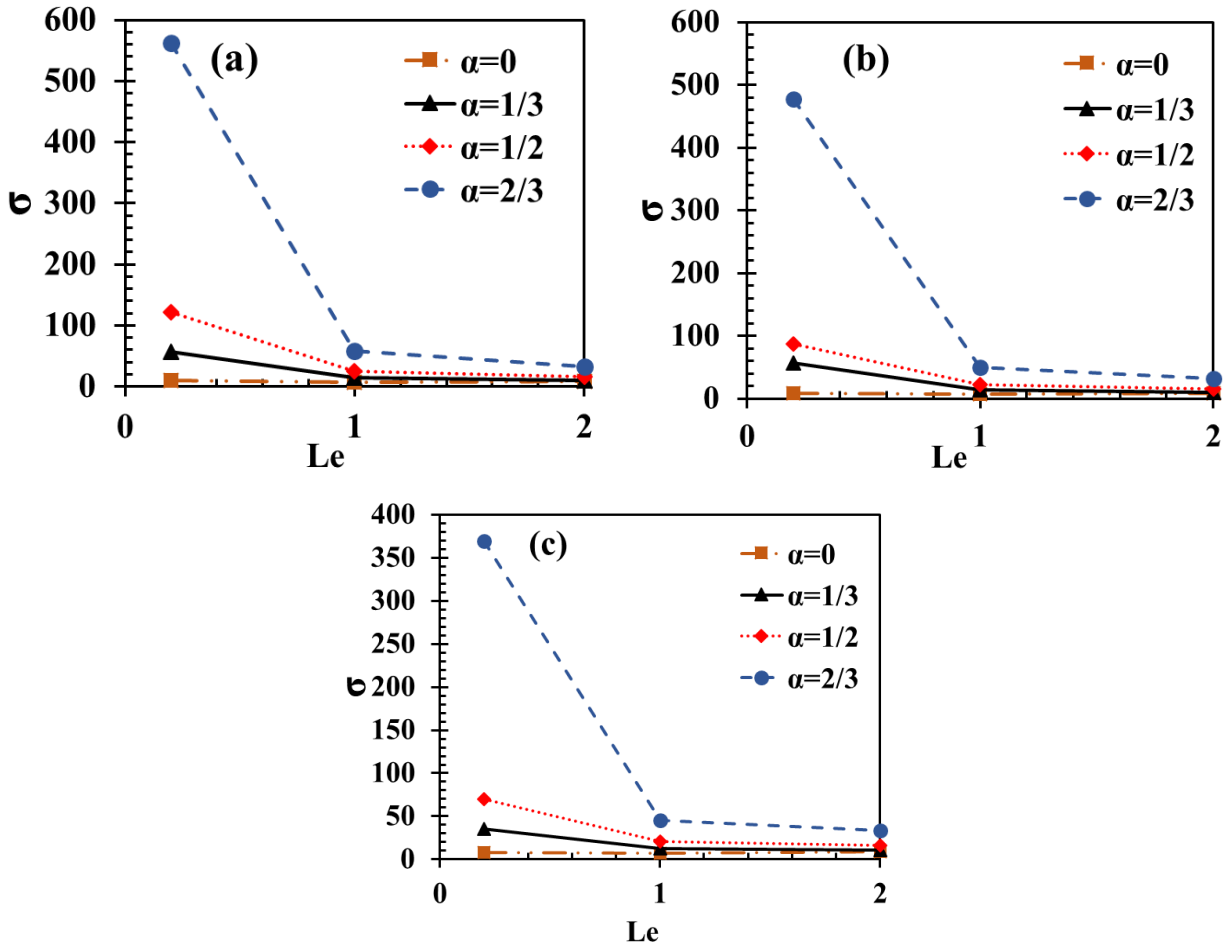

Figure 5.14: The exponential acceleration rate σ versus the Lewis number Le for R/L_f = 12 (a), 24 (b) and 48 (c) with α = 0, 1/3, 1/2, and 2/3 in each figure.

6 Propagation of Non-equidiffusive Flames in Unobstructed Channel with Open Ends

6.1 Morphology of $\Theta = 5$ Flames in Fully-Open Adiabatic Channel

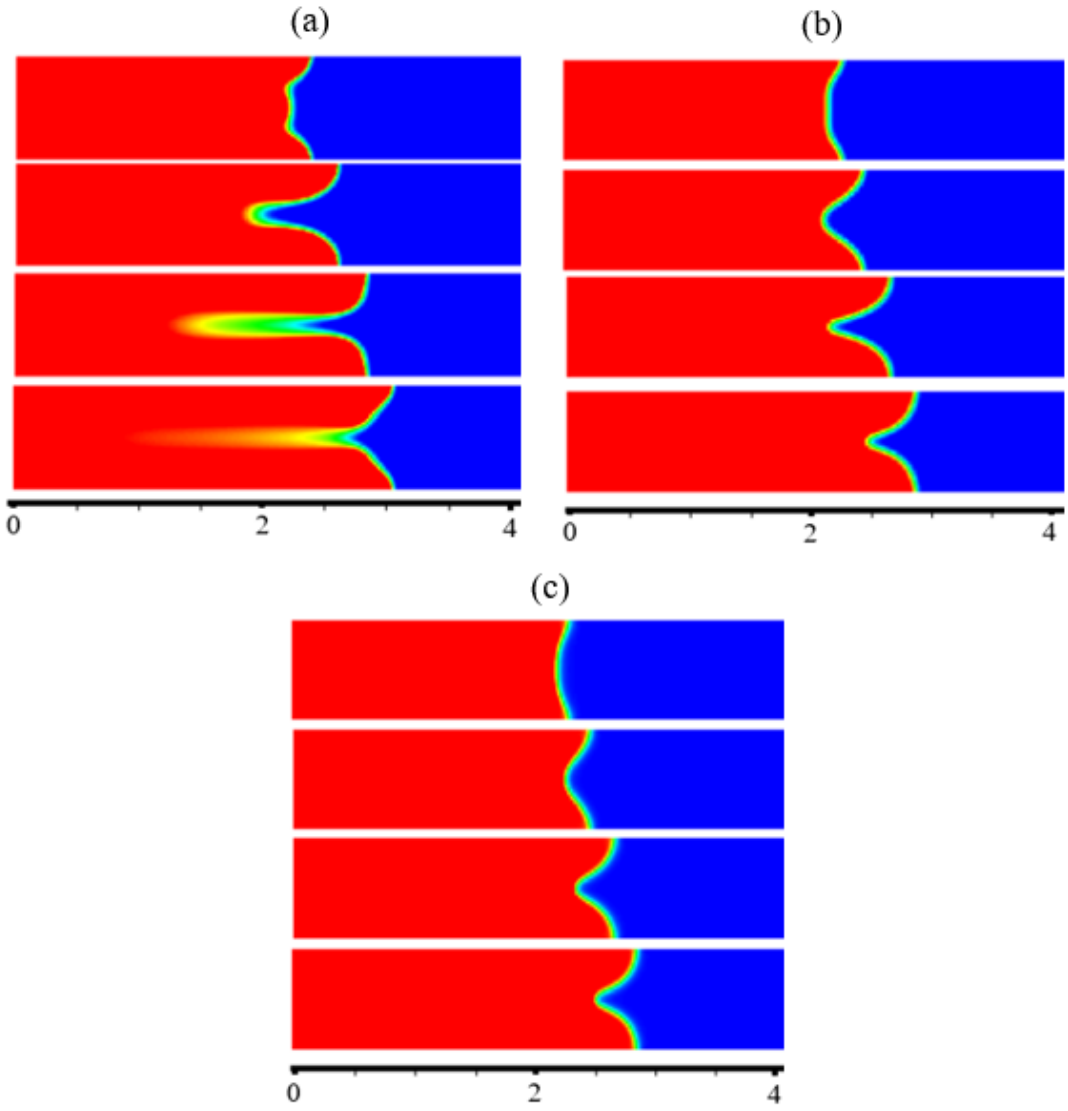

Figure 6.1 The temperature snapshots for the evolutions of a $\Theta = 5$ flame in an adiabatic channel with $R = 10\ L_f$, and $Le = 0.2$ (a), $Le = 1$ (b), $Le = 2$ (c).

The morphology of flames with various Lewis numbers, initiated as the ZFK planar flame and propagating through a channel with open ends, presents some interesting features that can help in gaining understanding of such flame dynamics. Right after flame initiation, there is distortion of the flame front due to the impact of the thermal expansion ratio and the flame-wall interactions. The evolution of a flame in channel with half-width $R = 10\ L_f$ and thermal expansion ratio $\Theta = 5$

is shown in Fig. 6.1. For the $Le = 0.2$ flame, shown in Fig. 6.1a, it is revealed that the flame front becomes corrugated showing concave shape with three leaves, such that the center is behind the other segments. As the flame propagation continues, its segments close to the wall moves further into the premixtures, while the central flame segment becomes deeper, causing formation of a cusp at the center of the channel, and thus increasing the flame surface area. This results in bifurcation, causing unburnt fuel to be entrapped between the flame segments, further increasing the surface area. The flame segments eventually collapse when the entrapped fuel is consumed. This process is repeated because of the competing momenta of the burnt gas and the fuel mixture. Since both ends of the channel are open, the flow is not restricted in any direction, and therefore, distributed towards both exits.

The cycle of the cusp formation, flame bifurcation, and the collapse of the flame segments continues, resulting in deceleration and acceleration of the flame tip. The flame tip is found to decelerate during formation of the cusp and bifurcation, and accelerates during the collapse of the segments. Such an extent of the flame front distortion, observed for a flame with $Le = 0.2$, can be devoted to the thinner flame front, which make corrugation easier, and the increased flame stretch due to the diffusional-thermal instability. For $Le = 1$, shown in Fig. 6.1b, the flame front is less distorted as compared to the $Le < 1$ flames. Here, the cusp formed in the flame is not as deep as that of the $Le < 1$ flames, and there is no bifurcation of the flame. Due to the less distorted flame front, the flame surface area is lower, and therefore, the extent to which the flame would accelerate or decelerate is reduced. The flame at $Le = 2$, shown in Fig. 6.1c, shows similar behavior as that of $Le = 1$. However, the cusp, and consequently, the flame surface area is slightly lower. Less distortion of the $Le \geq 1$ flames can be attributed to the thicker flame front, which makes the flame less susceptible to corrugation, and as well, the absence of the diffusion-thermal instability.

In a wider channel with R $= 20\ L_f$, the flame propagation still shows a similar trend as that of $R = 10\ L_f$, especially at $Le \geq 1$. While the $Le = 0.2$ flame also shows a similar behavior of a cusp formation, flame bifurcation, and a collapse of the flame segments, as described for R $= 10\ L_f$, the wider channel allows stronger corrugation of the flame front. The flame is almost divided into two halves along the center line, before the collapse of the flame segments is completed.

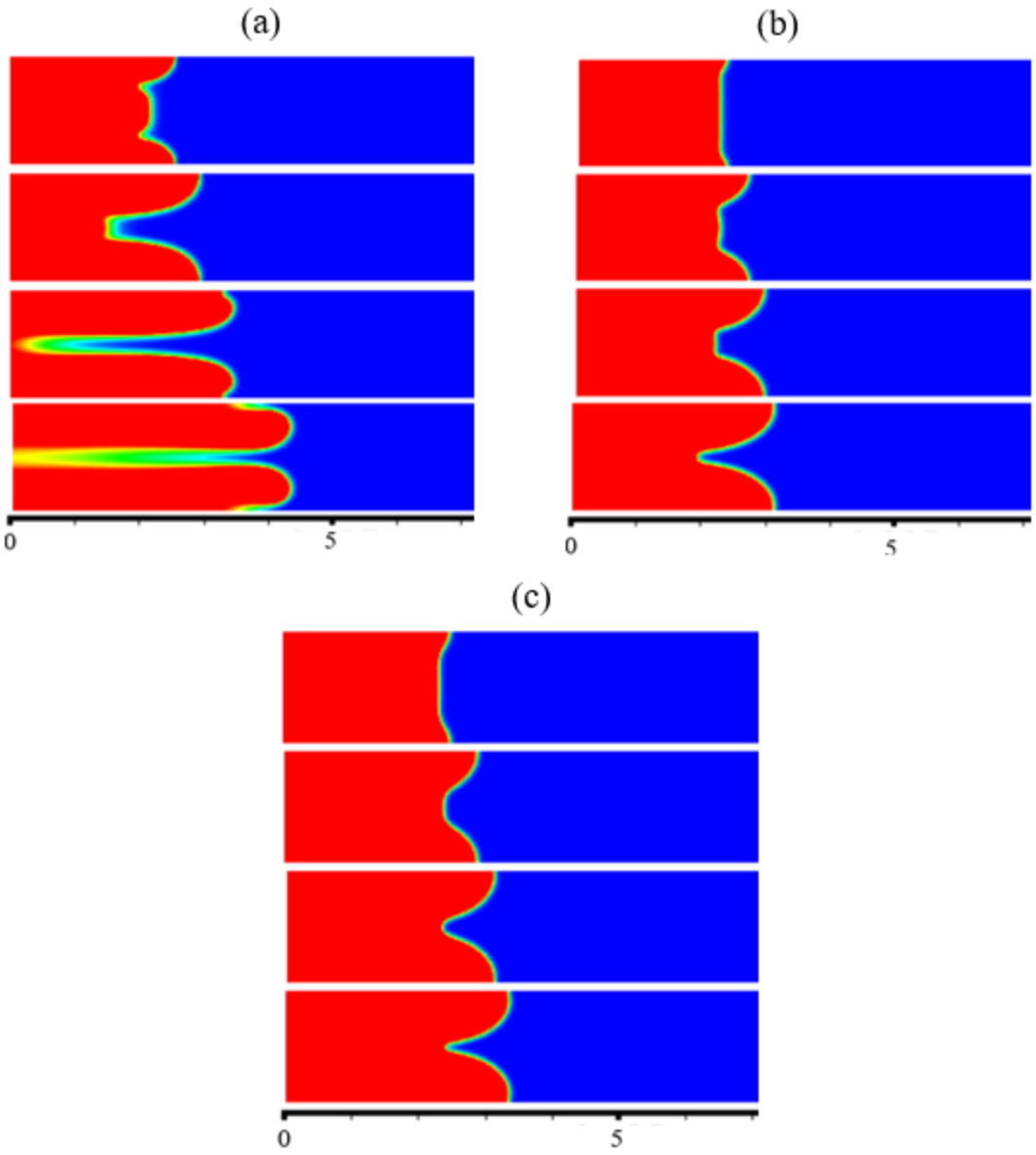

Figure 6.2: The temperature snapshots for the evolutions of the $\Theta = 5$ flames in adiabatic channels with R $= 20\ L_f$, and $Le = 0.2$ (a), $Le = 1$ (b), $Le = 2$ (c).

6.2 Dynamics of $\Theta = 5$ Flames in Adiabatic Channels with Open Ends

To describe the dynamics of a flame propagating through an open channel with adiabatic and non-slip walls, the plots of scaled flame tip position Z_{tip}/R and scaled burning rate U_w/S_L versus the scaled time $\tau = tS_L/R$ for a channel of half-width $10\ L_f$ and a flame of thermal expansion ratios 5 are shown in Figs. 6.3a and 6.3b, respectively. Both plots in Fig 6.3 shows the flame oscillating as it propagates through the channel. The oscillations are however found to be more prevalent for

a $Le = 0.2$ flame. This can be devoted to the combustion instability inherent to the low-Le flames. The oscillations observed here for the $Le = 0.2$ flame further confirms an implication of the trough formation, and the subsequent collapse of the flame segments, identified in Figs. 6.1a and 6.2 a. It is also seen that the amplitude of the oscillations decreases as the flame propagates through the channel, signifying a reduction in the flame oscillations with distance.

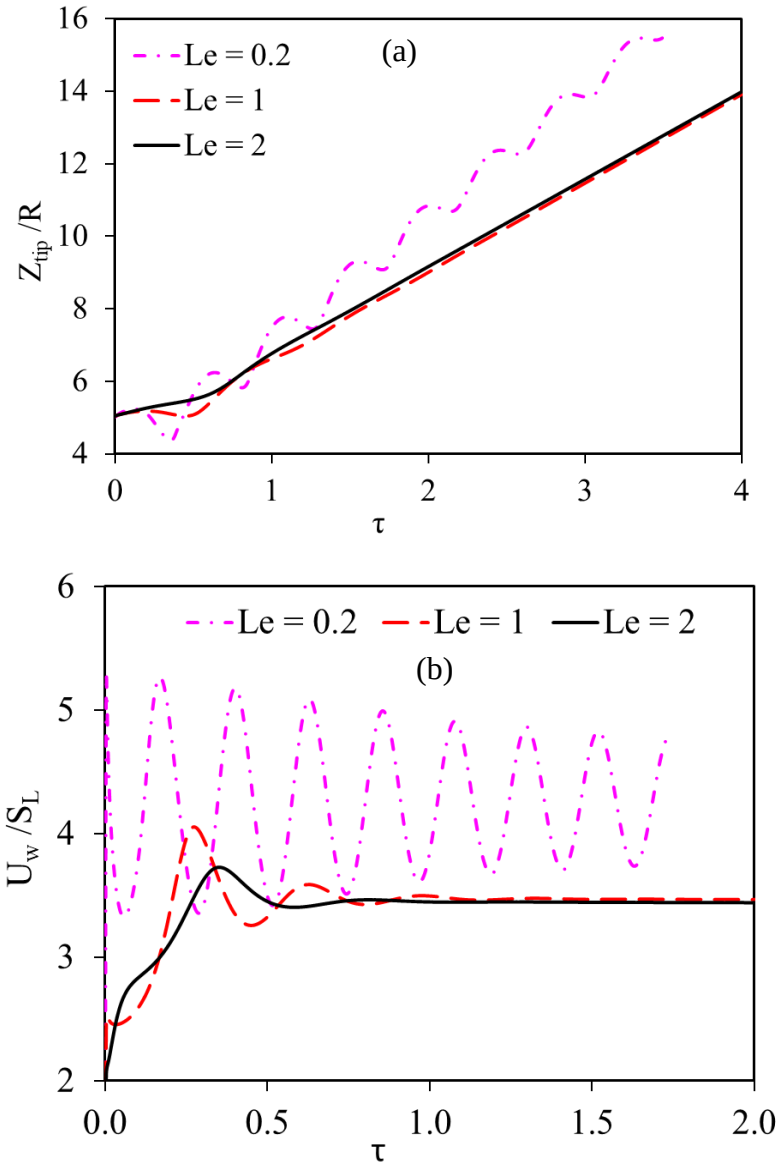

Figure 6.3: The scaled flame tip positions Z_{tip}/R (a) and the scaled burning rate U_w/S_L (b) versus the scaled time $\tau = tS_L/R$ for the $\Theta = 5$ flames with various $Le = 0.2, 1$ and 2 propagating in the adiabatic channel of $R = 10\ L_f$.

For $Le = 1$ and 2, only minor oscillations are observed at the initial stage of flame propagation. The flame is subsequently stabilized, and propagates with a constant velocity, as indicated by the

plots of the scaled flame tip position and the scaled burning rate in Figs. 6.3a and 6.3b, respectively. It is important to mention here that FA (found in a semi-open channel, with a closed left end) is not observed here. This is due to the fact that the flow is not constrained to any direction when both channel ends are open and, therefore, the fluid flow is distributed towards both ends. The resulting effect of this condition is that the opposing momenta of the burnt gas behind the flame and the fuel mixture ahead of the flame, more or less balance each other, thereby, preventing significant push from the burnt gas.

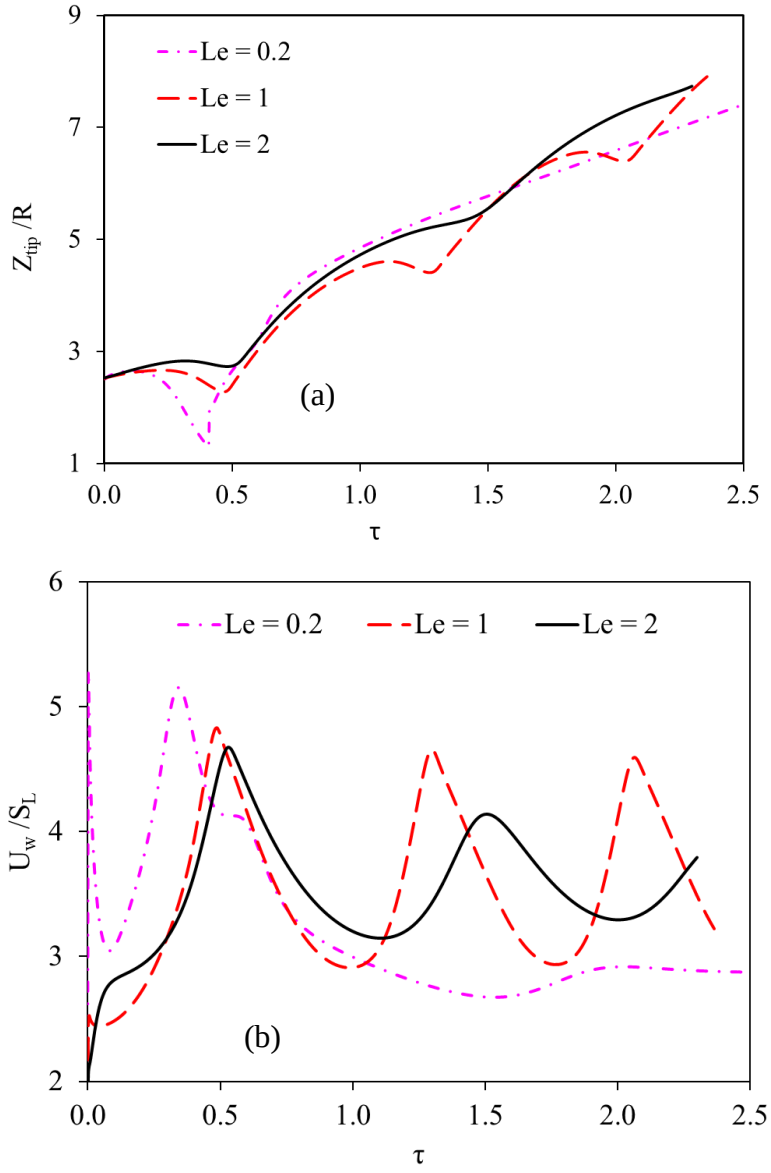

Figure 6.4: The scaled flame tip positions Z_{tip}/R (a) and the scaled burning rate U_w/S_L (b) versus the scaled time $\tau = tS_L/R$ for the $\Theta = 5$ flames with various $Le = 0.2, 1$ and 2 propagating in the adiabatic channel of $R = 20\ L_f$.

With an increased channel half-width to $R = 20\ L_f$, the plots of the scaled flame positon and the scaled burning rate versus scaled time in Figs. 6.4a and 6.4b show that the flame still oscillates through the channel. However, here the flame oscillations are observed to be of lower frequency as compared to the flame in the $R = 10\ L_f$ channel. In such a wider channel, the flame exhibits stronger oscillations when $Le \geq 1$, similar to the findings of Akkerman *et al*. [24]. This is as a result of the easier corrugation experienced by a flame in a wider channel.

6.3 Flames in Fully-Open Adiabatic Channel with $\Theta = 8$ and 10

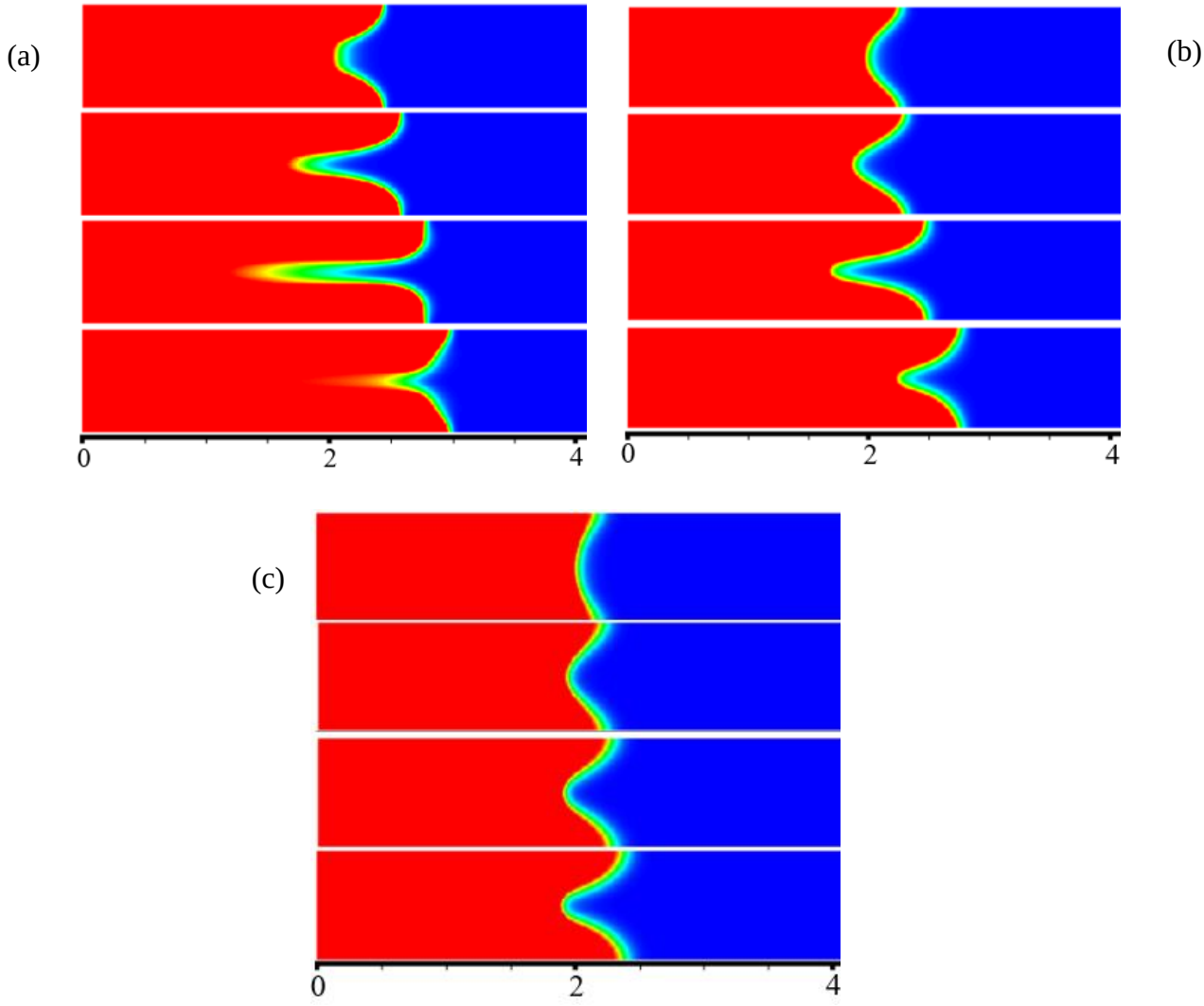

Figure 6.5: The temperature snapshots for the evolutions of the $\Theta = 5$ flames in adiabatic channels with R $= 20\ L_f$, and $Le = 0.2$ (a), $Le = 1$ (b), $Le = 2$ (c).

The thermal expansion ratio, which is an indication of the density jump across the flame front. Therefore, higher level of Darius-Landau instability is expected in the flame when the value of thermal expansion ratio is higher. This is indicated in the temperature snapshots for the $\Theta = 10$ flames in the adiabatic channels with $R = 20\ L_f$, shown in Fig. 6.5. The morphology of the flame at this condition is qualitatively similar to that exhibited when the thermal expansion ratio is 5, with higher distortion of the flame front experienced at $Le = 0.2$. The flame corrugation and, consequently, oscillations decrease as the Lewis number grows from 0.2 to 2. Figures 6.6a and 6.6b show the plots of the scaled flame tip position and the scaled burning rate versus the scaled time for flames with higher thermal expansion, $\Theta = 10$, respectively. Similar plots are also shown in Fig. 6.7 for $\Theta = 8$ flames.

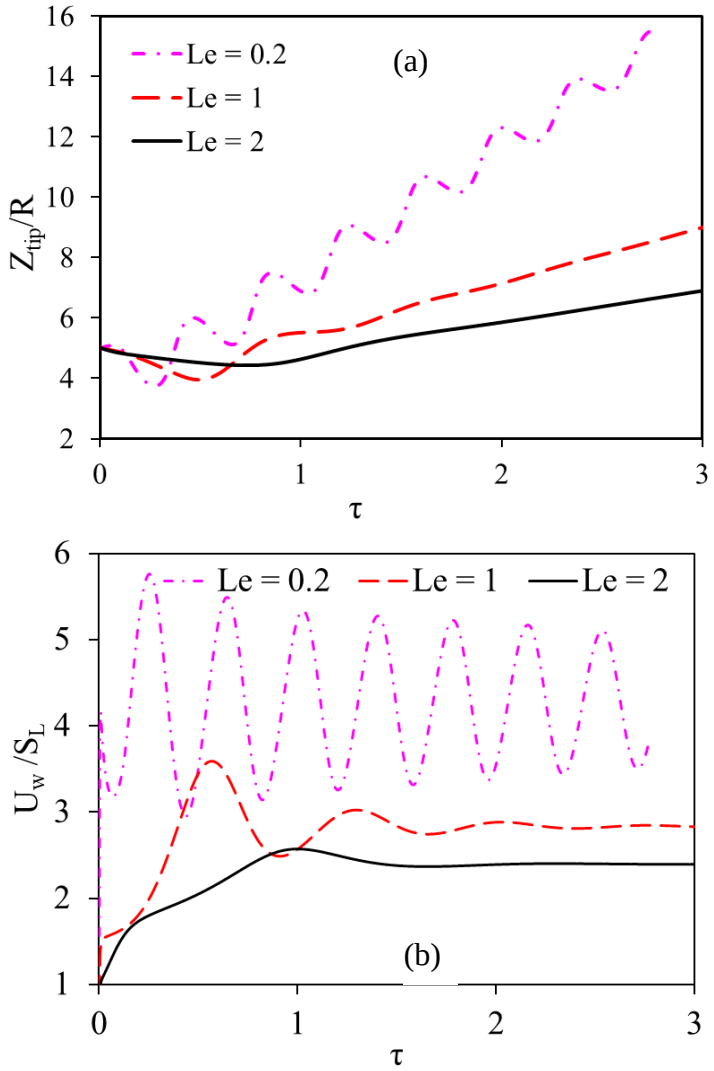

Figure 6.6: The scaled flame tip positions Z_{tip}/R (a) and the scaled burning rate U_w/S_L (b) versus the scaled time $\tau = tS_L/R$ for the $\Theta = 10$ flames with various $Le = 0.2, 1$ and 2 propagating in the adiabatic channel of $R = 10\ L_f$.

It is observed that increasing the thermal expansion ratio from 5 to 8 and 10 does not have any qualitative effect on the flame dynamics, as oscillations still remain the mode of propagation experienced. A minor quantitative difference is noticed, in terms of the oscillation parameters. Another important finding of this result is the damping effect of Le. Indeed, it is observed that, as Le grows from 0.2 to 2, the oscillation amplitude decreases. The flames with the Lewis number lower than unity show clear oscillations with decreasing amplitude and frequency as the $Le \rightarrow 1$. This reduction in the oscillation parameters are the indications of the flame stability as Le grows.

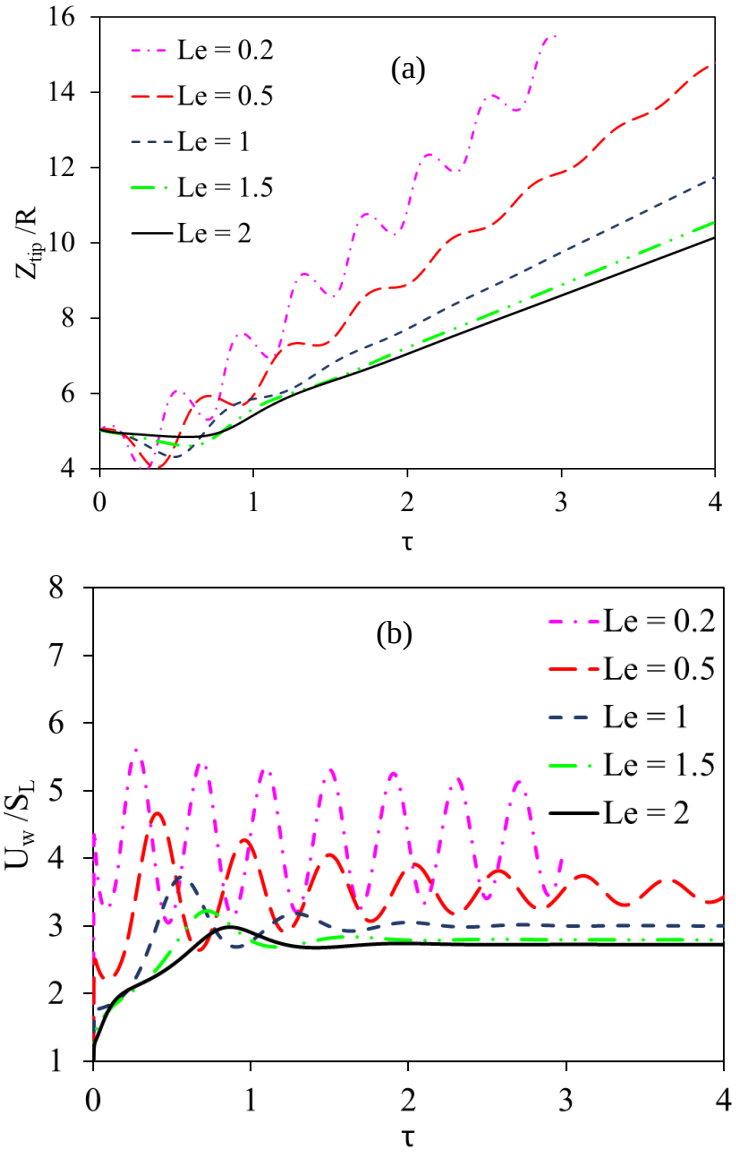

Figure 6.7: The scaled flame tip positions Z_{tip}/R (a) and the scaled burning rate U_w/S_L (b) versus the scaled time $\tau = tS_L/R$ for the $\Theta = 8$ flames with various $Le = 0.2, 0.5, 1, 1.5, 2$ in the adiabatic channel of $R = 10\ L_f$.

6.4 Propagation of Flames in Fully-Open Channels with Non-Slip and Isothermal Walls

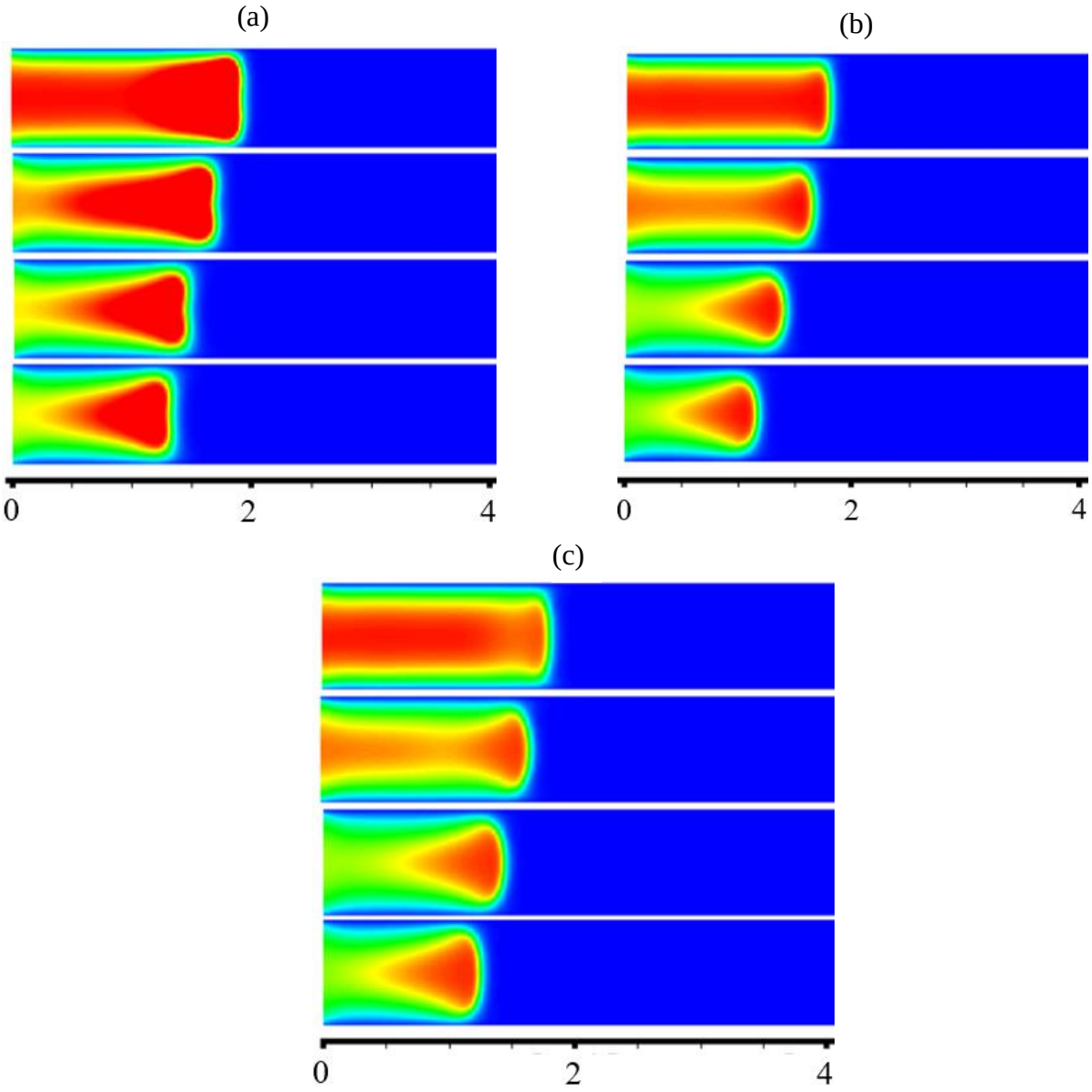

Figure 6.8: The temperature snapshots for the evolutions of the $\Theta = 8$ flames propagating in isothermal channels with R $= 10\ L_f$, and $Le = 0.2$ (a), $Le = 1$ (b), $Le = 2$ (c).

Flame propagation in fully-open channels with non-slip and isothermal boundary conditions at the wall is also scrutinized, in order to identify the effects of the changes in the thermal boundary condition on the flame. The temperature snapshots shown in Fig. 6.8 is for the $\Theta = 8$ flame with various Lewis numbers in the range of $0.2 \leq Le \leq 2$, propagating in channels of half-width $10\ L_f$.

The flame morphology when the channel wall is maintained at a temperature of 300 K as shown in Fig. 6.8 shows a flame that is qualitatively different from that seen in the adiabatic channels. After the flame is initiated using the ZFK planar approach, the flame front is observed to retract, instead of propagating into the fuel premixtures, for all the Le considered. Contraction of the flame is also observed to take place as heat is being loss to the channel wall. However, the rate at which this flame front retraction and flame contraction occurs changes with the Lewis number. For $Le = 0.2$ in Fig 6.8a, where mass diffusivity is dominant, both the retraction and contraction occur at a slower rate. The higher rate of mass diffusion into the flame front attempts to balance the heat being lost to the cold wall. When the mass diffusion balances or exceeds the thermal diffusion, we see the flame retracting and contracting slightly faster. The heat loss from the burnt gas to the cold wall, coupled with the distributed flow towards both exits, prevents the burnt gas from having the momentum required to push the fuel ahead of the flame front. Figures 6.8b and 6.8c show the flames with $Le = 1$ and $Le = 2$, where the mass diffusion equals or exceeds the thermal diffusion, respectively. The rate of flame front retraction, and flame contraction is shown to grow with Le.

The plots of scaled flame tip position and scaled burning rate for flames with $\Theta = 8$ and various Lewis numbers, propagating in a fully-open channel of half-width $R = 10\ L_f$ with isothermal wall is shown in Fig. 6.9. Evolution of the flame position shows the flame retraction earlier described. Namely, the plot of the scaled flame tip versus the scaled time, Fig. 6.9a, shows the flame tip moving towards the left open end of the channel, as opposed to travelling towards the right end, as was observed in semi-open channels as well as in adiabatic channels. The scaled burning rate versus the scaled time, Fig. 6.9b, also decreases for the $Le \geq 1$ flames. This is expected, since the flame morphology seen in the snapshots of Fig. 6.9 does not show any increase in surface area. For a wider channel, $R = 20\ L_f$, the scaled flame tip position and the scaled burning rate versus the scaled time are shown in Figs 6.10a and 10b, respectively. Again, we see the flame retreating, instead of advancing in Fig. 6.10a. However, the retraction here happened at a slower rate.

Also, a deviation from the generally observed flame behavior is obtained for a low Lewis number, $Le = 0.2$, as such a flame is seen to have changed direction at a point in the channel. The scaled flame tip, thereafter shows an upward trend (Fig. 6.10a). The same trend is revealed in the plot of the scaled burning rate shown in Fig. 6.10b. This slight changes in the flame behavior when the channel half-width is increased from $10\ L_f$ to $20\ L_f$ can be attributed to the impact of heat loss to the channel wall. While both channels have their walls kept at 300 K, the impact of the heat loss

is more significant in a narrower channel. The reason being that, the narrower the channel, the higher the surface to volume ratio, and consequently, the higher the impact of the heat loss is.

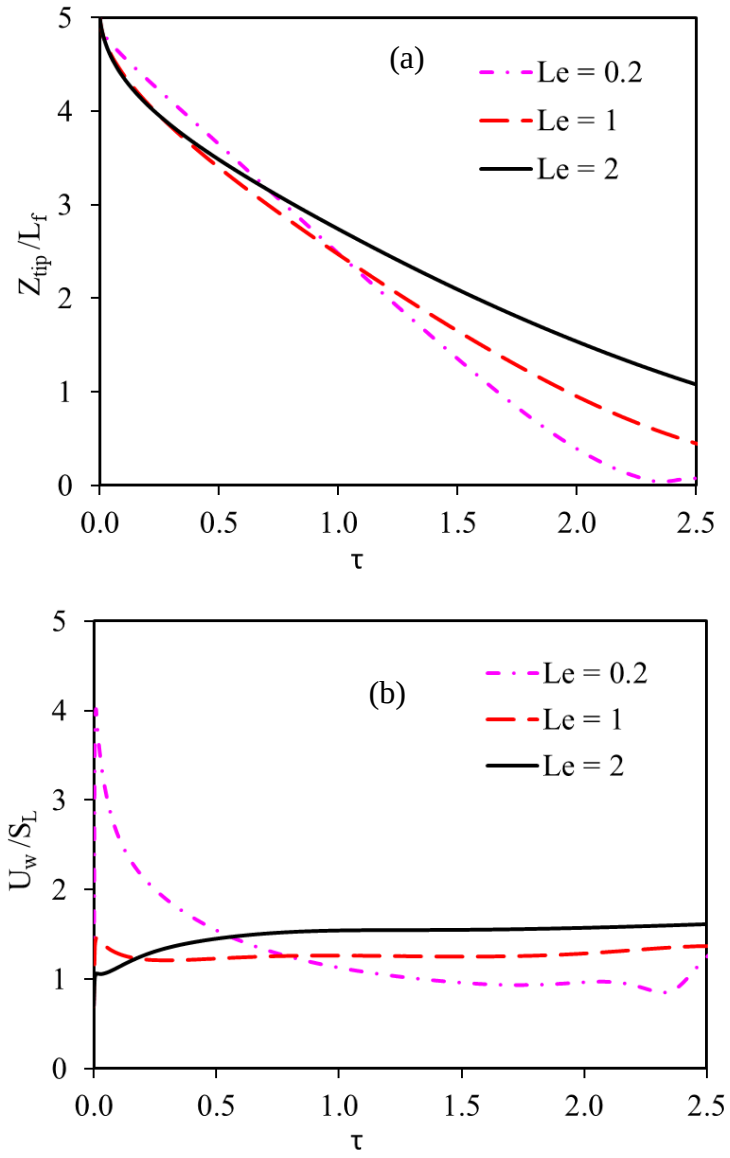

Figure 6.9: The scaled flame tip positions Z_{tip}/R (a) and the scaled burning rate U_w/S_L (b) versus the scaled time $\tau = tS_L/R$ for the $\Theta = 8$ flames with various $Le = 0.2, 1$ and 2 propagating in the isothermal ($T_w = 300$ K) channel of $R = 10\ L_f$.

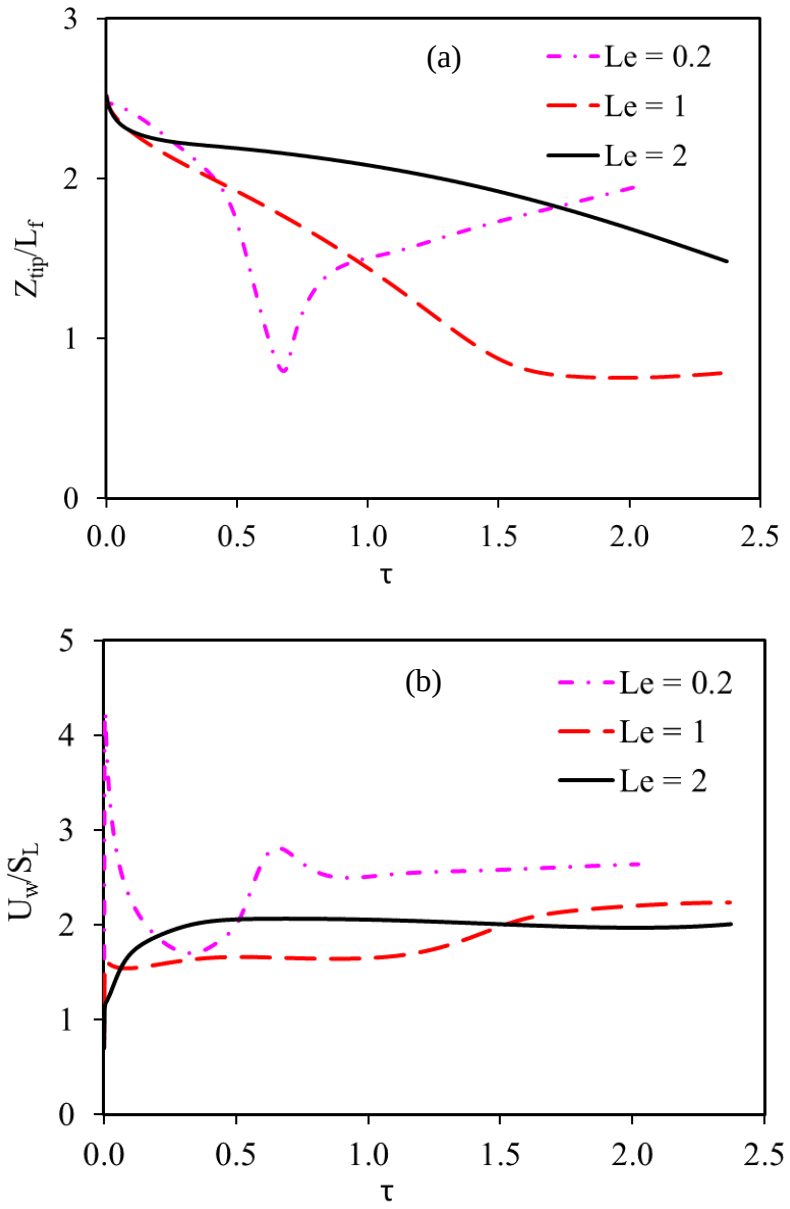

Figure 6.10: The scaled flame tip positions Z_{tip}/R (a) and the scaled burning rate U_w/S_L (b) versus scaled time $\tau = tS_L/R$ for the $\Theta = 8$ flames with various $Le = 0.2, 1$ and 2 propagating in the isothermal ($T_w = 300$ K) channel of $R = 20\ L_f$.

7 Propagation of Non-equidiffusive Flames in Obstructed Channels with Open Ends

7.1 Statistical Significance of the Effects of R, α, and *Le*

Analysis of variance (ANOVA) is used to determine the factors which significantly affects the propagation of a flame in obstructed channel where both extremes open. Combined effects of the factors on flame propagation are also scrutinized by statistically analyzing the interactions among the factors.

Table 7.1: Analysis of variance table for flame acceleration in obstructed fully open channel

Factors	Sum of squares	Degree of Freedom	Mean Square	F	Prob>F (95% CL)
Half-width (R)	99533.7	2	49766.9	2.23	0.1701
Blockage ratio (α)	327822.2	2	163911.1	7.34	0.0155
Lewis number (Le)	90691.8	2	453456.9	20.31	0.0007
R*α	79263.6	4	19815.8	0.89	0.5132
R*Le	289686.6	4	72421.6	3.24	0.0735
BR*Le	697750.5	4	174437.6	7.81	0.0072
Error	178640	8	22330		
Total	2579610	26			

Similar to the result obtained for the semi-open channel, both the blockage ratio, α and the Lewis number, Le, are found to be statistically significant in determining the flame position in a channel with both ends open, at 95% confidence level ($p \leq 0.05$). The Lewis number appears to have the highest effect with a value of 0.0007, which is smaller than 0.0155 for α. The channel width does not have a significant effect on the as the F-value is greater than 0.05 ($0.701 > 0.05$). However, the channel width seems to be more important in determining the flame position in a fully open channel than it is in a semi-open channel. Among the interactions, that between Le and α is found to be significant ($0.0072 < 0.05$). While the interaction of Le with R is not significant ($0.0735 > 0.05$), the F-value is indeed close.

7.2 Propagation of Non-Equidiffusive Flame in Narrow Channels with Low Blockage Ratio

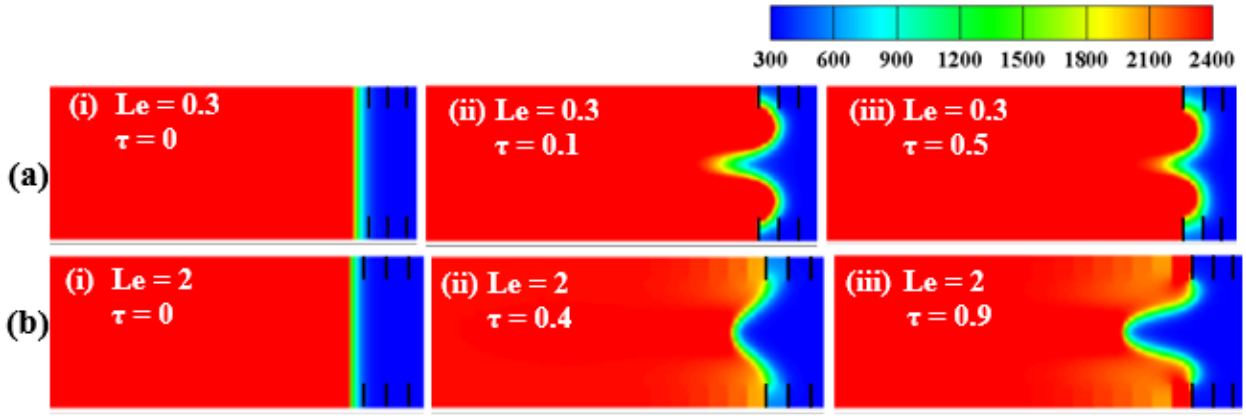

Figure 7.1: Temperature snapshots for the flame evolution with $R = 12L_f$, $\Theta = 8$, $\alpha = 1/3$, $Le = 0.3$ (a) and 2 (b).

The temperature snapshots in Fig. 7.1 shows the morphology of the flame front as the non-equidiffusive flame of $Le = 0.3$ (a) and $Le = 2$ (b) propagates through an obstructed channel. In both cases, the flames were initiated as the planar ZFK front, acquires curved shape, with the extent of curvature determined by the burning conditions. Variations in the shape of the flame front are largely dependent on the flame response to curvature caused by a rearward flow of the premixtures ahead of the flame front. Showing the temperature snapshots for $Le = 0.3$ at the scaled times that are different from that presented for $Le = 2$ is necessitated by the need to cover the full extent of the shape changes encountered in each case. At $Le = 0.3$, Fig. 7.1a, the planar flame front quickly acquires a concave shape at the center of the channel and convex shape towards the obstructed sides, resulting in increased surface area. The flame front also shows a wider preheated zone at the center of the channel, Fig. 7.1a ii. As the preheated fuel mixture is consumed, the cusp previously formed at the center of the channel decreases, Fig. 7.1a iii, causing FA as well as the reduction in concavity of the flame front. This acceleration is short lived as the distributed nature of the flow prevents the burnt gas from providing adequate push on the fuel mixture, causing the flame front to revert to the flame with a concave center and wide preheated zone, discussed earlier. The back and forth push from the burnt gas and the fuel premixtures continues, culminating in the periodic oscillation of the flame as it propagates through the channel. For $Le = 2$, Fig. 7.1b, it takes a longer time for the flame front to acquire an appreciable concave shape with a thinner preheated zone at the center, Fig. 7.1b ii. The flame curvature continues, almost forming a tulip shape, Fig. 7.1b iii,

before the fuel mixture is consumed and acceleration taking place. The process is repeated, causing periodic oscillations of the flame to occur. However, the oscillations are expected to have a higher period, as it takes longer for a flame to respond to curvature caused by a rearward premixture flow.

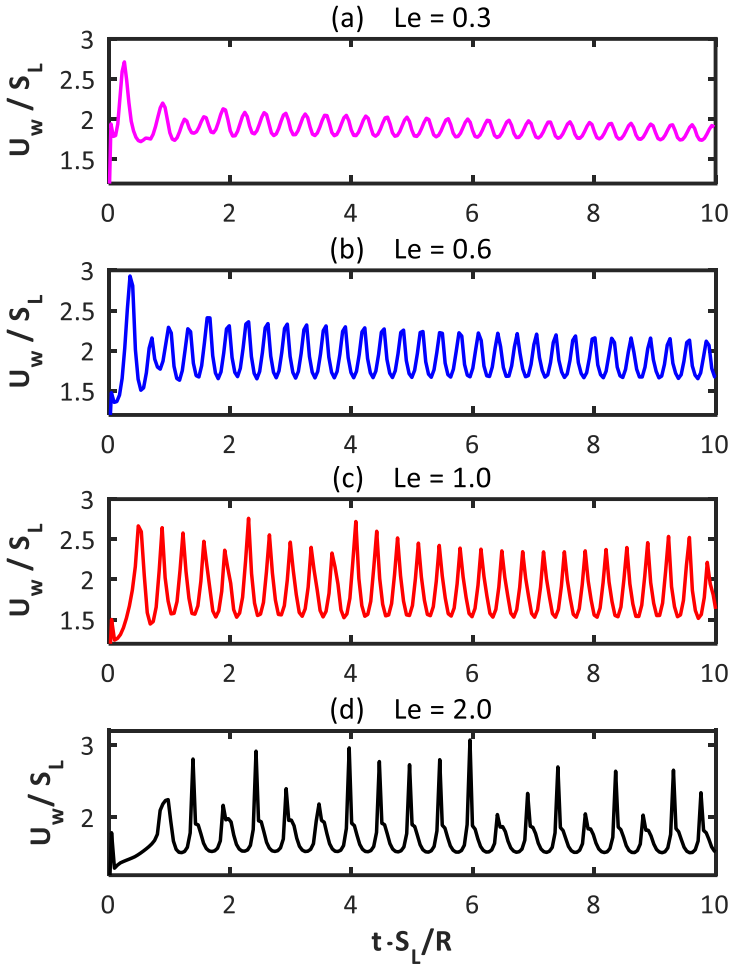

Figure 7.2: The scaled burning rate U_w/S_L versus the scaled time tS_L/R for the thermal expansion ratio $\Theta = 8$, the blockage ratio $\alpha = 1/3$, the obstacle spacing $\Delta Z = R/4$, the channel half-width $R = 12\ L_f$, and various Lewis numbers $Le = 0.3$ (a), 0.6 (b), 1 (c), and 2 (d).

Further illustration of the effect of Le on flame propagation is achieved by plotting the scaled burning rate versus the scaled time and scaled frequency (sf) of the flame oscillations for various operating conditions. Additional characterization is done by examining the physical appearance of the waveform, estimating the average oscillation frequency, and the average amplitude of the oscillations. The plots of burning rates versus scaled time for various operating conditions, provide further illustration of flame propagation as affected by Le. Figure 7.2 shows the scaled burning

rate versus scaled time for $R = 12\ L_f$, $\alpha = 1/3$, $\Theta = 8$ as well as the frequency spectra for the oscillations are shown at similar condition by plotting scaled burning rate versus scaled frequency in Fig. 7.3. The plots for the channel with the blockage ratio of 1/2 are shown in Figs 7.4 and 7.5. For clarity of the plots, each subplot pallet represents the plots related to different Lewis numbers.

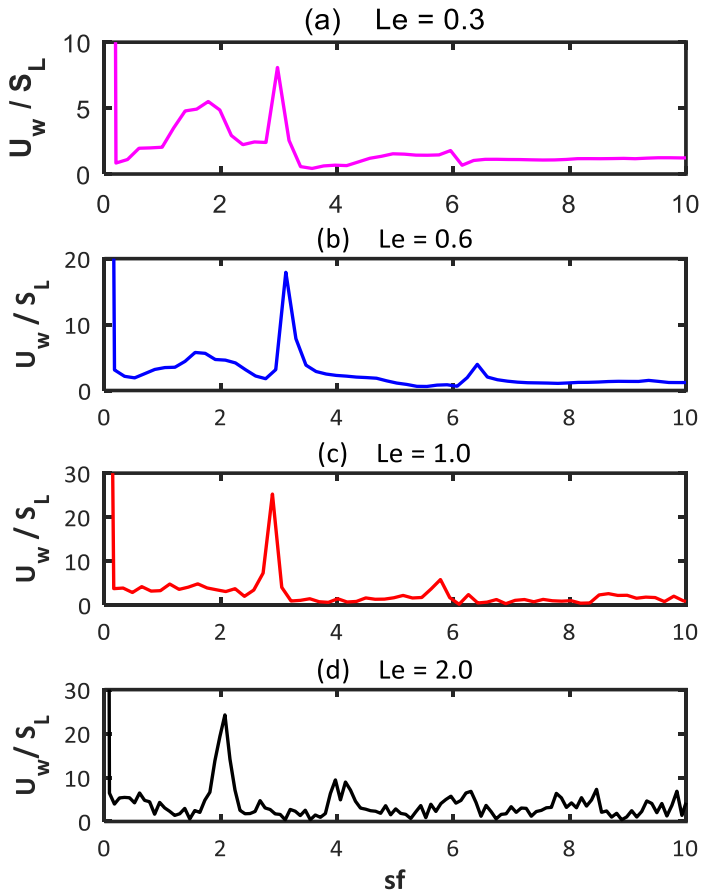

Figure 7.3: The scaled burning rate U_w/S_L versus the scaled frequency (sf) for the thermal expansion ratio $\Theta = 8$, the blockage ratio $\alpha = 1/3$, the obstacle spacing $\Delta Z = R/4$, the channel half-width $R = 12\ L_f$, and various Lewis numbers $Le = 0.3$ (a), 0.6 (b), 1 (c), and 2 (d).

For all Le considered, the flames exhibit oscillations as they propagate through a narrow channel. The oscillations, however, show varying quality in terms of the frequency and amplitude. In both Figs. 7.2 and 7.4, the waveforms produced from the flame oscillations are largely symmetric about the quasi-steady velocities, except for the flame with $Le = 2$, Fig. 7.4d, where flame spreads at a constant rate, without any oscillation. It is also observed, Fig. 7.3, that in the case of $Le < 1$, the flame oscillation amplitude decreases as the flame propagates through the channel.

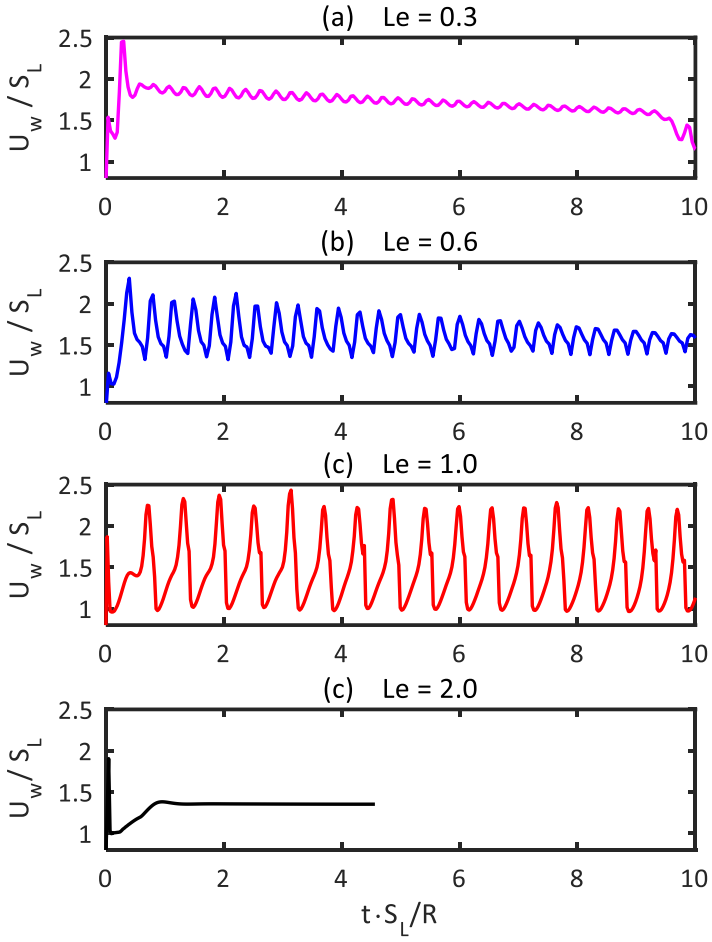

Figure 7.4: The scaled burning rate U_w/S_L versus the scaled time tS_L/R for the thermal expansion ratio $\Theta = 8$, the blockage ratio $\alpha = 1/2$, the obstacle spacing $\Delta Z = R/4$, the channel half-width $R = 12\ L_f$, and various Lewis numbers $Le = 0.3$ (a), 0.6 (b), 1 (c), and 2 (d).

The spectra analysis of the flame oscillations shown in Figs. 7.3 and 7.5 reveals that most of the high-amplitude oscillations occur at a low scaled frequency in each case. When the blockage ratio is $1/3$, Fig. 7.3, the $Le < 1$ flame shows a broad low-amplitude oscillation before a high amplitude oscillation. The amplitude of the broad pick oscillations decreases, while that of the high amplitude oscillation grows as Le increases from 0.3 to 0.6. Further increase in Le results in a disappearance of the broad pick, and an increase in the higher amplitude oscillation. At $Le = 2$, the low amplitude oscillations are also observed, at the higher scaled frequencies. Increasing the blockage ratio to $\alpha = 1/2$ results in suppression of the oscillations in the cases of $Le = 0.3$ and 2. However, multiple picks are obtained for the $Le = 0.6$ and $Le = 1$ flames, with the highest amplitude seen at $Le = 1$.

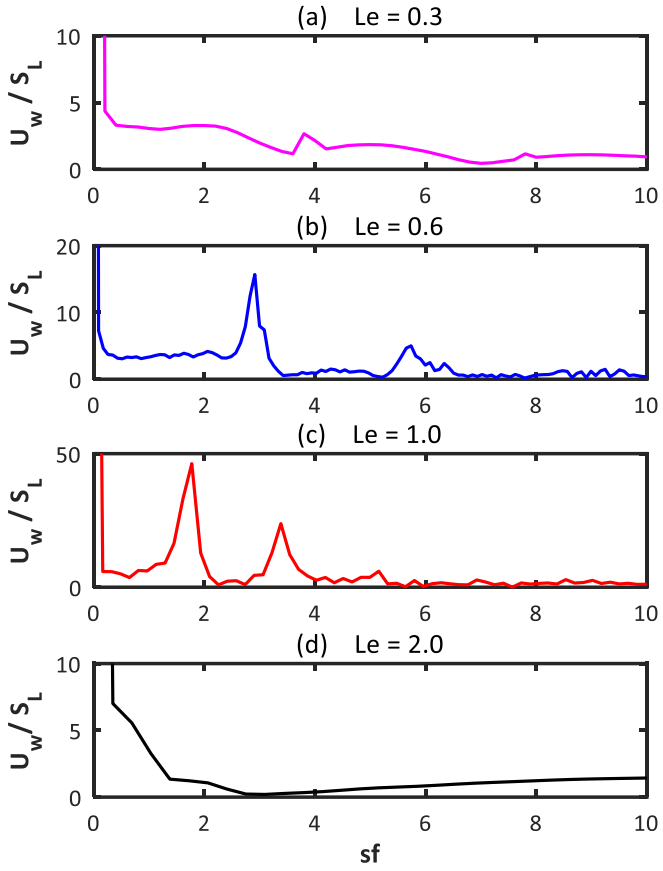

Figure 7.5: The scaled burning rate U_w/S_L versus the scaled frequency $sf = R/\tau S_L$ for the thermal expansion ratio $\Theta = 8$, the blockage ratio $\alpha = 1/2$, the obstacle spacing $\Delta Z = R/4$, the channel half-width $R = 12\ L_f$, and various Lewis numbers $Le = 0.3$ (a), 0.6 (b), 1 (c), and 2 (d).

Figure 7.6 shows that the flame oscillation amplitude increases as Le grows from $Le = 0.3$ to $Le = 1$, and then declines by increasing the Lewis number to $Le = 2$. There is no noticeable difference in the oscillation frequency, when Le grows from 0.3 to 0.6; however, further increase in Le to $Le = 2$ results in the reduction of the scaled frequency from 3 to 1.9. Similarly, in Fig. 7.7, the scaled oscillation frequency decreases from a maximum value of 3.3 at $Le = 0.3$ to zero at $Le = 2$, which signifies no oscillation. For the equidiffusive flames, this oscillatory behavior can be attributed to the hydraulic resistance of the flow ahead of the flame front and the distributed flow of the burnt gas in a channel with both open ends. While the distributed flow is still encountered in non-equidiffusive burning, additional contributions to flame dynamics from non-equidiffusivity can be caused by the finite thickness of the flame front as well as the local flame temperature and stretch.

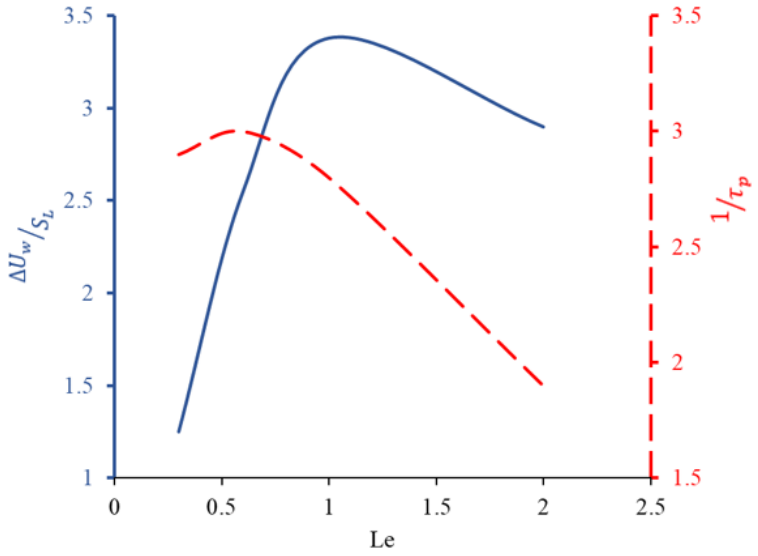

Figure 7.6: Variation of the scaled oscillation amplitude, $\Delta U_w/S_L$, and the scaled oscillation frequency, $1/\tau_p$ (here τ_p is the scaled oscillation period) with the Lewis number, Le, for the thermal expansion ratio $\Theta = 8$, the channel half-widths $R = 12\ L_f$, the blockage ratio $\alpha = 1/2$, and the obstacle spacing $\Delta Z = R/4$.

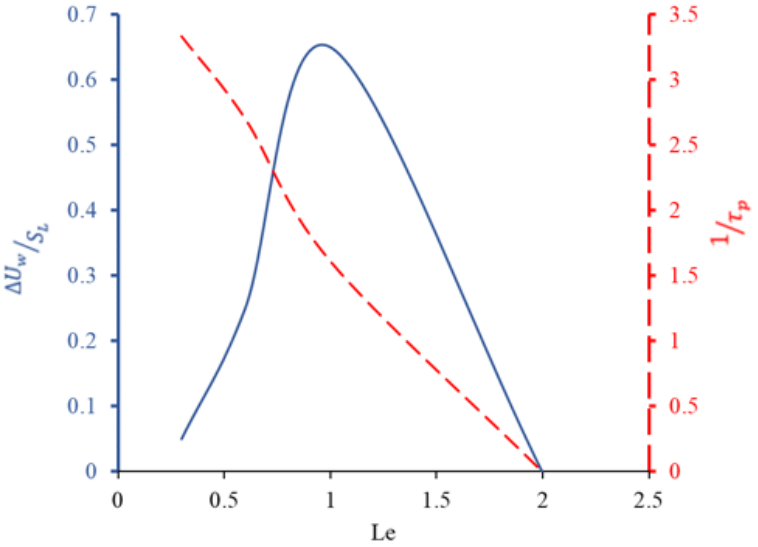

Figure 7.7: Variation of scaled oscillation amplitude, $\Delta U_w/S_L$, and scale oscillation frequency, $1/\tau_p$ (here τ_p is the scaled oscillation period) versus the Lewis number, *Le*, for the thermal expansion ratio $\Theta = 8$, the channel half-widths $R = 12\ L_f$, the blockage ratio $\alpha = 1/3$, and the obstacle spacing $\Delta Z = R/4$.

The thinner flame front and the high local flame temperature peculiar at $Le < 1$ results in faster response to the flame stretch caused by a backward flow of the unburnt premixtures, and thus, the lower amplitude and the higher frequency observed in the flame oscillations. On the other hand, a thicker flame front at $Le \geq 1$ is able to withstand the higher stretch from a backward flowing premixtures, causing a delayed response and, consequently, lower oscillation frequency and higher

amplitude, compared to $Le < 1$. We are unable to perform this comparative analysis of oscillation properties for other cases, as different regimes of propagation are encountered.

7.3 Nonequidiffusive Flame Propagation in Fully-Open Channels with High Blockage Ratio

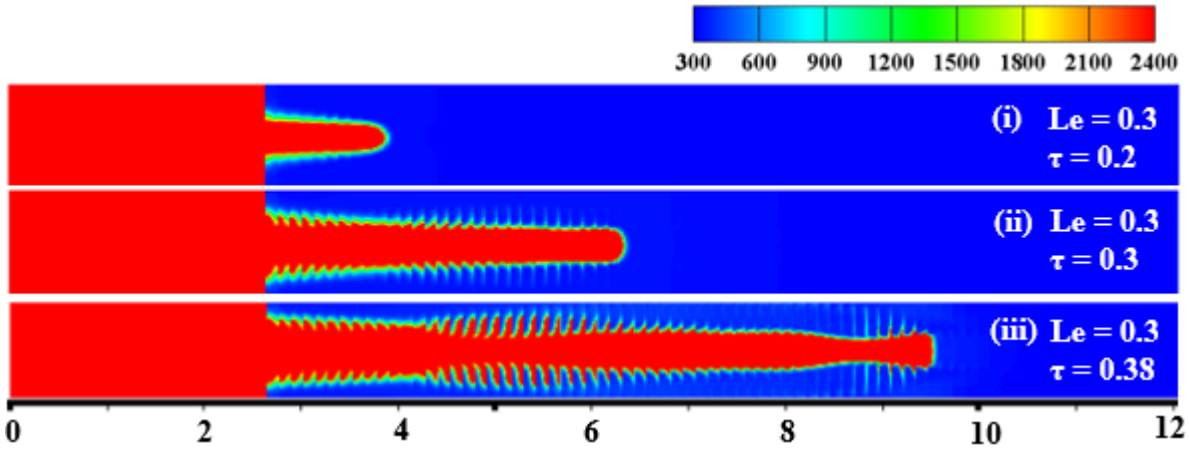

Figure 7.8: Temperature snapshots for the flame evolution, with $\Theta = 8$, $\alpha = 2/3$, $R = 12L_f$.

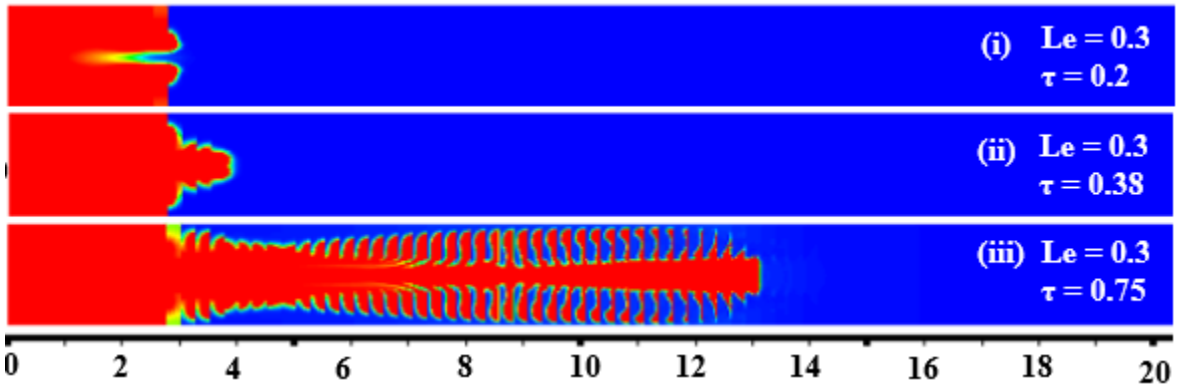

Figure 7.9: Temperature snapshots for the flame evolution, with $\Theta = 8$, $\alpha = 2/3$, $R = 24L_f$.

The color temperature snapshots for the $\Theta = 8$ and $Le = 0.3$ flame, propagating through channels with a high blockage ratio, $\alpha = 2/3$, of half-widths $R = 12\ L_f$ and $R = 24\ L_f$ are shown in Figs. 7.8 and 7.9, respectively. The flames here exhibit a propagation mode different from the oscillatory mode discussed earlier. In both cases, the flames accelerate as they propagate through the channel. For $R = 12\ L_f$, the initial ZFK planar flame swiftly forms a front with a prolonged convex shape, Fig. 7.8 i, signifying an increased surface area and thus, acceleration. However, propagation only occurs at the central, unobstructed part of the channel, with fuel in the side pockets left unburnt,

Fig. 7.68ii. While the consumption of the fuel premixture in the side pocket is delayed at the initial stage, lateral propagation is observed to increase as the flame propagates away from its ignition position, Fig. 7.8 iii. This poses the possibility of thermal explosion, as the contribution of delayed burning to the propagating front will be immense, when it finally happens. Widening the channel to $R = 24\ L_f$ results in slightly delayed FA, with a flame bifurcation just after ignition, Fig. 7.9 i.

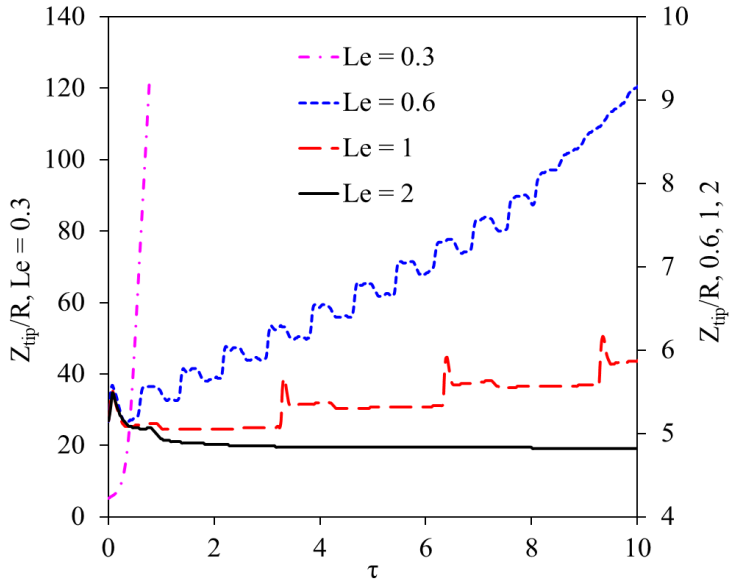

Figure 7.10: The scaled flame tip Z_{tip}/L_f versus the scaled time tS_L/R for the thermal expansion ratio $\Theta = 8$, the blockage ratio $\alpha = 2/3$, the obstacle spacing $\Delta Z = R/4$, the channel half-width $R = 12\ L_f$ for various Lewis numbers $Le = 0.3$, 0.6, 1, and 2.

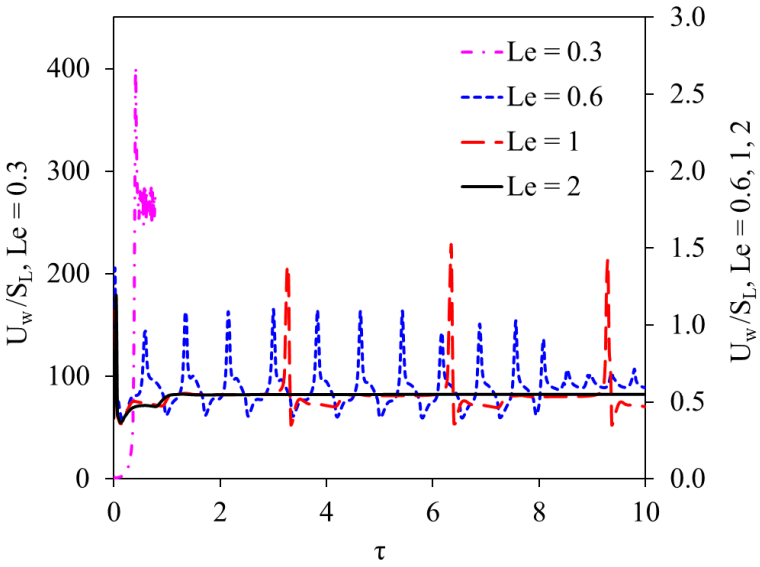

Figure 7.11: The scaled burning rate U_w/S_L versus the scaled time tS_L/R for the thermal expansion ratio $\Theta = 8$, the blockage ratio $\alpha = 2/3$, the obstacle spacing $\Delta Z = R/4$, the channel half-width $R = 12\ L_f$ for various Lewis numbers $Le = 0.3$, 0.6, 1, and 2.

A flame front changes to a convex shape, with propagation into the side pockets also occurring, Fig 7.9 ii. Due to the increased surface area, the flame accelerates and more lateral propagation also occurs away from the ignition position, Fig. 7.9 iii. Various regimes of flame propagation are clearly seen in the plots of the scaled flame tip position, Fig. 7.10, and the burning rate, Fig. 7.11.

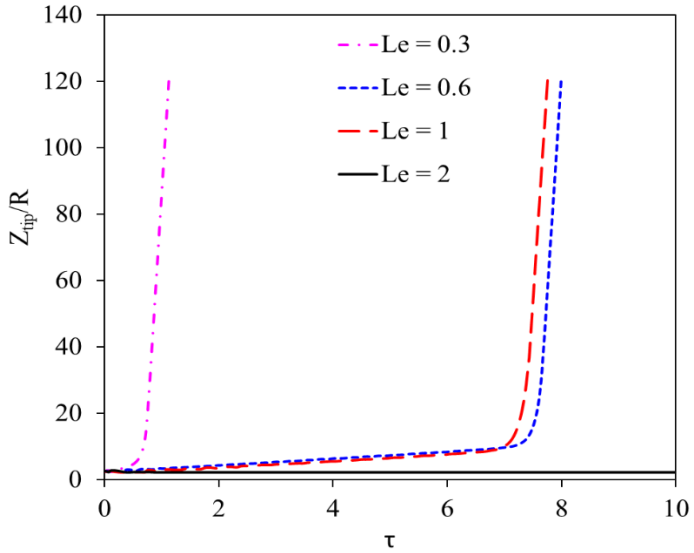

Figure 7.12: The scaled flame tip Z_{tip}/L_f versus scaled time tS_L/R for the thermal expansion ratio $\Theta = 8$, the blockage ratio $\alpha = 2/3$, the obstacle spacing $\Delta Z = R/4$, the channel half-width $R = 24\ L_f$ for various Lewis numbers $Le = 0.3$, 0.6, 1, and 2.

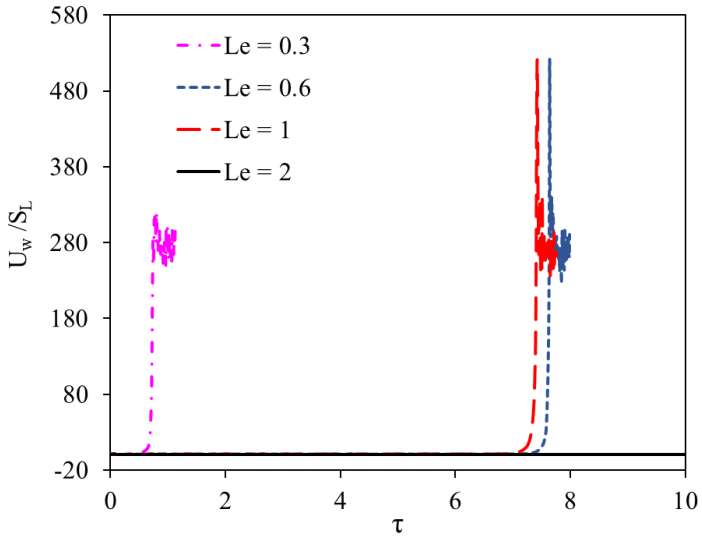

Figure 7.13: The scaled burning rate U_w/S_L versus the scaled time tS_L/R for the thermal expansion ratio $\Theta = 8$, the blockage ratio $\alpha = 2/3$, the obstacle spacing $\Delta Z = R/4$ the channel half-width $R = 24\ L_f$ for various Lewis numbers $Le = 0.3$, 0.6, 1, and 2.

At $Le = 0.3$ (see the scaled flame tip position and burning rate represented on the left vertical axis in Figs. 7.10a and 7.10b), the flame exhibits some slight initial quasi-steady propagation, and then a transition to an accelerating regime, with acceleration being quite strong. The strong and sudden acceleration observed here is similar to that reported and discussed in Ref. [22]. This is followed by slight deceleration before another round of quasi-steady oscillations, which occurs at the flame saturation velocity. Despite the effect of distributed flow, that is known to limit FA in channels with open ends, it is interesting to see that the combined effects of a low Le, $Le = 0.3$, and a high blockage ratio of $2/3$ can produce enough momentum to overcome the hydraulic resistance, and eventually transit to acceleration. At $Le = 0.6$, Fig. 7.10, and $Le = 1$, Fig. 7.11, it is observed that the flame propagates by oscillating about a quasi-steady velocity, with a much lower oscillation frequency at $Le = 1$. On the other hand, at $Le = 2$, the scaled flame tip position plot shows that the flame is not actually propagating: the flame position remains practically the same. The scaled burning rate plot in Fig. 7.11 also shows that burning occurs at a constant rate, which indicates a balance between the push effect of the burnt gas and the resisting force. The scaled flame tip position and the burning rate for $Le = 0.6, 1, 2$ are represented by the right vertical axis in Figs. 7.10 and 7.11, respectively. The plots for the evolution of the flame tip position and the burning rate for $\Theta = 8$, $\alpha = 2/3$, $\Delta Z = R/4$, $R = 24\, L_f$, depicted in Figs 7.12 and 7.13, demonstrate that a flame undergoes sudden acceleration at $Le = 0.3, 0.6, 1$. The flames however show near-steady initial propagation before such acceleration. The time of such initial propagation increases as Le grows from 0.3 to 0.6. Similar behavior is also exhibited by the $Le = 1$ flame, while neither oscillations nor acceleration is observed for $Le = 2$. Also, the maximum burning rate attained by a flame before propagation at a saturation velocity is lower for $Le = 0.3$ as compared to the cases of $Le = 0.6$ and 1. However, the saturation velocity falls within the same range for all three cases.

Establishing the occurrence of such transitions between the oscillations and the acceleration regimes under the impact of Le provides a fascinating result. Indeed, it is seen that the Lewis number has both qualitative and quantitative effects on flame propagation in channels with open ends. Another interesting phenomenon observed in this configuration is Le-coupling to the channel geometric parameters such as the channel width and the blockage ratio. For clearer understanding of these interacting effects: $Le - \alpha$ and $Le - R$ interplays are separately presented in the following.

7.4 Impact of $Le - \alpha$ Interplay on Flame Propagation in Fully-Open Obstructed Channel

In a semi-open channel, with a flame ignited at the closed end and travelling towards the open one, both parameters such as Le and α have been demonstrated, individually, to impact FA, for reasons including the changes in the flame thickness or in the local flame temperature, due to Le-variations [87,88], and also the impact of delayed burning in the pockets between the obstacle varies with the blockage ratio [54]. Now, we consider both effects cumulatively. The impact of Le on the flame, as seen here, is either enhanced or suppressed by α. Figures 7.14 and 7.15 depict the evolution of the scaled flame tip position and the scaled burning rate, receptively, for the $\Theta = 8, Le = 0.3$ flames propagating in the channels with $R = 24\ L_f$, $\Delta Z = R/4$ and three various blockage ratios.

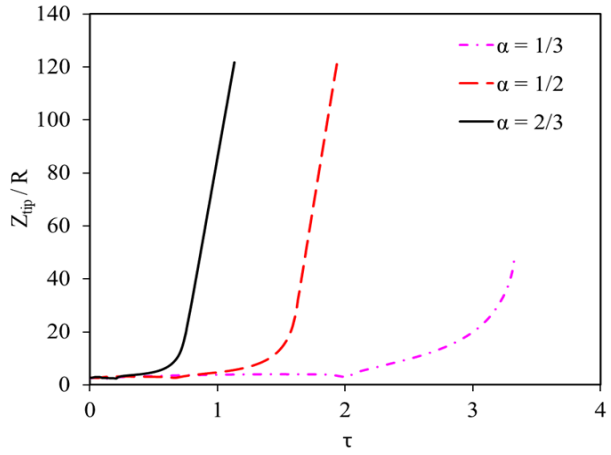

Fig 7.14: The scaled flame tip position Z_{tip}/R versus the scaled time tS_L/R for the thermal expansion ratio $\Theta = 8$, the obstacle spacing $\Delta Z = R/4$, the channel half-width $R = 24\ L_f$, various $\alpha = 1/3, 1/2, 2/3$ and $\boldsymbol{Le = 0.3}$.

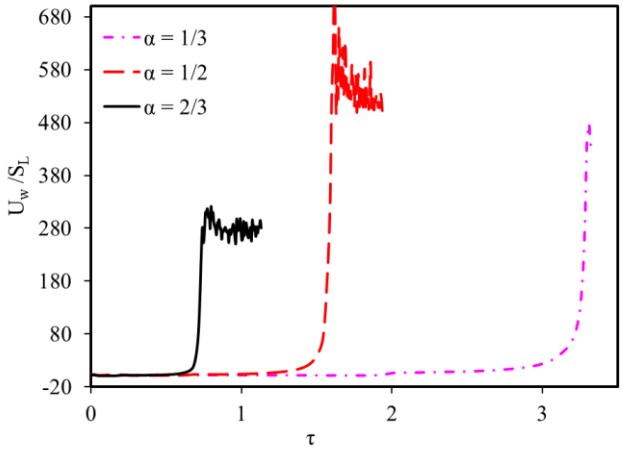

Fig 7.15: The scaled burning rate U_w/S_L versus the scaled time tS_L/R for the thermal expansion ratio $\Theta = 8$, the obstacle spacing $\Delta Z = R/4$, the channel half-width $R = 24\ L_f$, various $\alpha = 1/3, 1/2, 2/3$ and $\boldsymbol{Le = 0.3}$.

While Figs. 7.14 and 7.15 are for the $Le < 1$ flames, their respective counterparts for equidiffusive ($Le = 1$) combustion are Figs. 7.16 and 7.17, while Figs 7.18 and 7.19 are for the $Le = 2$ flames. For $Le = 0.3$ in Figs 7.14 and 7.15, the flame accelerates for all three blockage ratios considered. However, the time taken for initial propagation to until a transition to acceleration decreases as α grows from $1/3$ to $2/3$. Also, the maximum burning rate and the saturation velocities also differ.

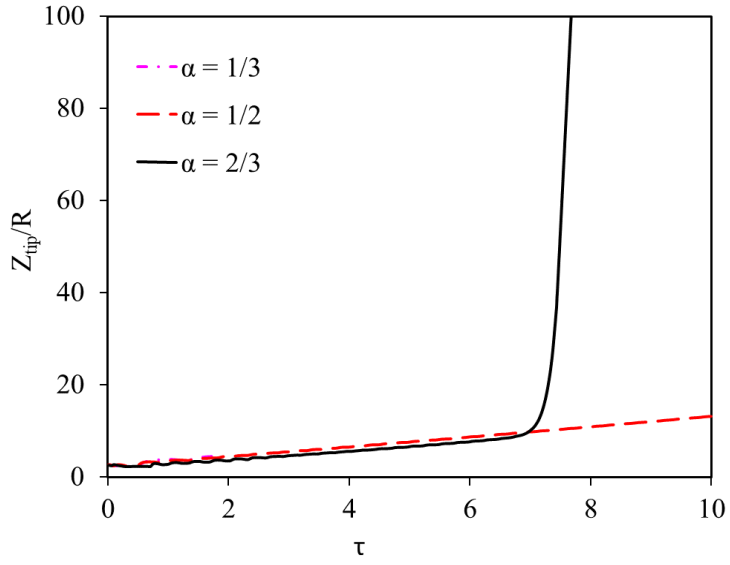

Fig 7.16: The scaled flame tip position Z_{tip}/R versus the scaled time tS_L/R for the thermal expansion ratio $\Theta = 8$, the obstacle spacing $\Delta Z = R/4$, the channel half-width $R = 24\ L_f$, various $\alpha = 1/3\,, 1/2, 2/3$ and $\boldsymbol{Le = 1}$.

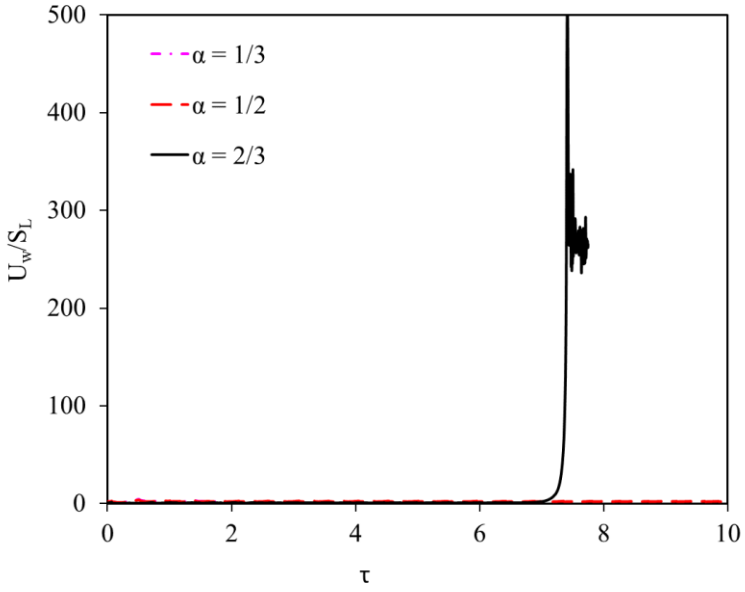

Fig 7.17: The scaled burning rate U_w/S_L versus the scaled time tS_L/R for the thermal expansion ratio $\Theta = 8$, the obstacle spacing $\Delta Z = R/4$, the channel half-width $R = 24\ L_f$, various $\alpha = 1/3\,, 1/2, 2/3$ and $\boldsymbol{Le = 1}$.

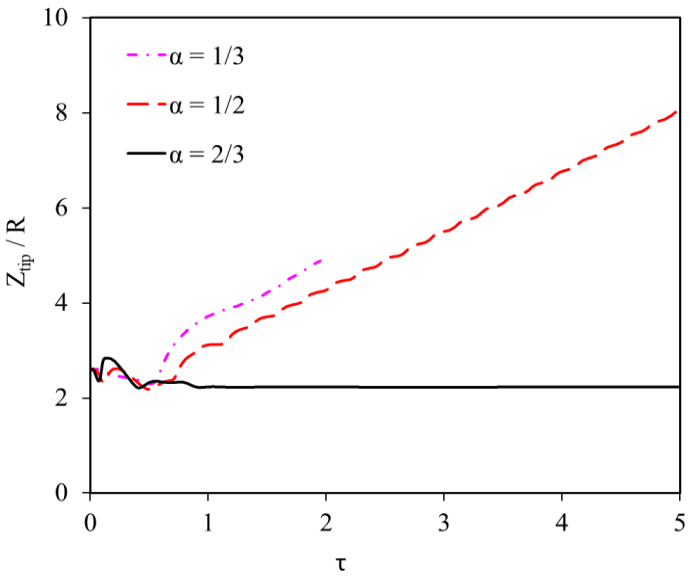

Fig 7.18: The scaled flame tip position Z_{tip}/R versus the scaled time tS_L/R for the thermal expansion ratio $\Theta = 8$, the obstacle spacing $\Delta Z = R/4$, the channel half-width $R = 24\ L_f$, various $\alpha = 1/3\,, 1/2, 2/3$ and $\boldsymbol{Le} = \mathbf{2}$.

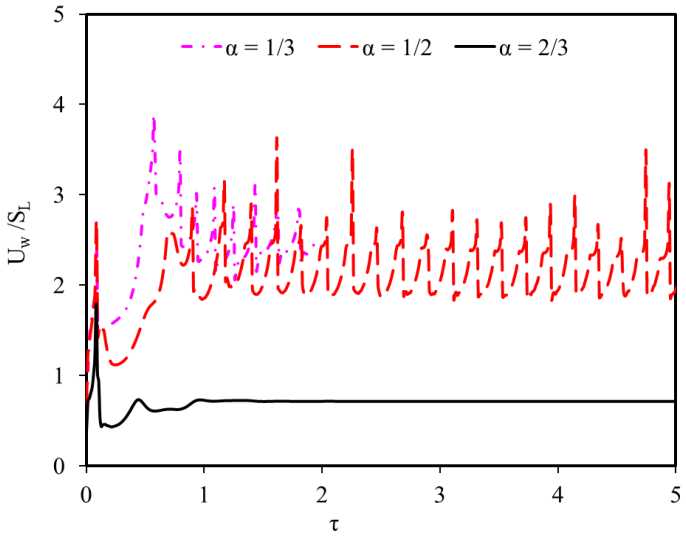

Fig 7.19: The scaled burning rate U_w/S_L versus the scaled time tS_L/R for the thermal expansion ratio $\Theta = 8$, the obstacle spacing $\Delta Z = R/4$, the channel half-width $R = 24\ L_f$, various $\alpha = 1/3\,, 1/2, 2/3$ and $\boldsymbol{Le} = \mathbf{2}$.

The decreasing trend of initial propagation period with blockage ratio, observed here, is similar to the increasing trend of the acceleration rate observed for various blockage ratios in a semi-open channel. Specifically, higher blockage ratios are found to provide faster acceleration according to the Bychkov mechanism [54,89], when other conditions are kept constant, because of the larger volume of the burnt gas released into the central unobstructed part after delayed burning in the side pockets. The decrease in the initial propagation period observed for $Le = 0.3$ with growing α

can be attributed to delayed burning interacting with other attributes of a low-Le flame such as thinner flame front, higher local heating temperature and faster flame response to flame curvature and stretch – all of which enhances FA. On the other hand, no acceleration is observed for all the blockage ratios when $Le = 2$ (Figs 7.18 and 7.19). Namely, the flame is seen to oscillate at $\alpha = 1/3$ and $1/2$, while it simply propagates at a constant velocity at higher α of $2/3$. Increasing the blockage ratio to $2/3$ in this case results in suppression of the oscillations observed at lower α. An interplay between the higher volume of gas produced from delayed burning in the sides pockets (promoting effect) and other conditions provided by $Le > 1$ (moderating effect) appear enough to balance the resisting force, therefore, resulting in flame propagation at a constant velocity. In the case of $Le = 1$, Figs. 7.16 and 7.17, transition to acceleration is only observed for $\alpha = 2/3$, with the flame propagating at a constant rate for the other two blockage ratios.

7.5 Impact of the Le-Re Interplay on Flame Propagation in Fully-Open Channel

Also, an interplay between the flame Lewis and Reynolds numbers, Le and Re, is explored in Figs. 7.20 – 7.23 by plotting the scaled flame tip position and the scaled burning rate versus the scaled time for $\Theta = 8$ and $\alpha = 2/3$ and various scaled channels half-width, $R/L_f = 12, 24, 36, 48$. While the first two figures presents the $Le = 0.3$ flames, the latter two are their counterparts for $Le = 2$.

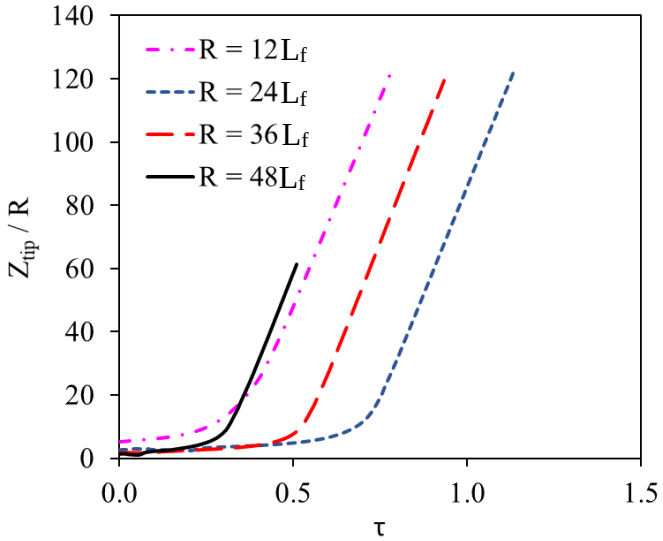

Figure 7.20: The scaled flame tip position Z_{tip}/R versus the scaled time tS_L/R for the thermal expansion ratio $\Theta = 8$, the obstacle spacing $\Delta Z = R/4$, the blockage ratios $\alpha = 2/3$, the Lewis number $\boldsymbol{Le = 0.3}$ and various channel half-widths $R = 12\ L_f, 24\ L_f, 36\ L_f, 48\ L_f$.

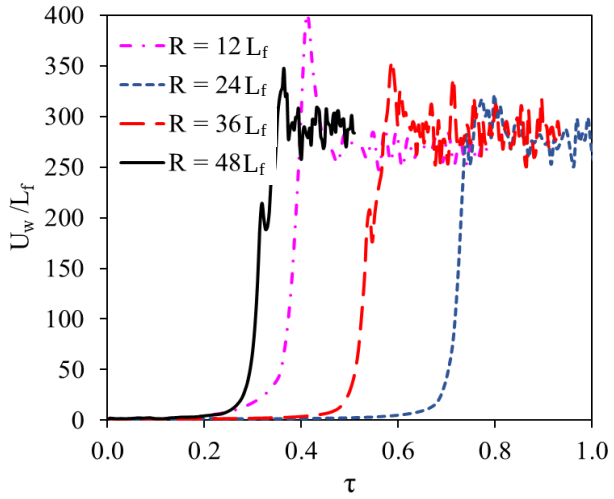

Figure 7.21: The scaled burning rate U_w/S_L versus the scaled time tS_L/R for the thermal expansion ratio $\Theta = 8$, the obstacle spacing $\Delta Z = R/4$, the blockage ratios $\alpha = 2/3$, the Lewis number $\boldsymbol{Le = 0.3}$ and various channel half-widths $R = 12\ L_f, 24\ L_f, 36\ L_f, 48\ L_f$.

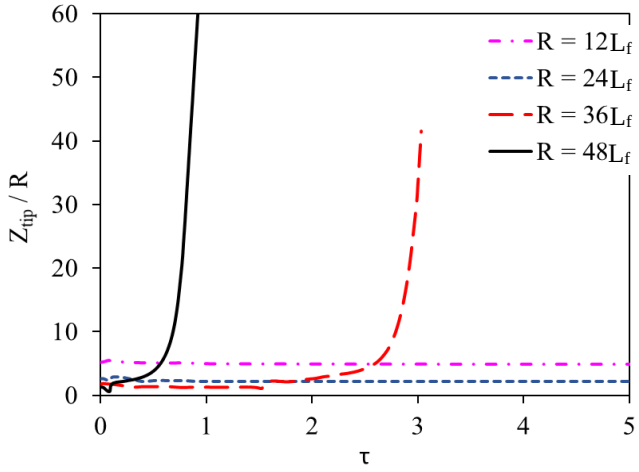

Figure 7.22: The scaled flame tip position Z_{tip}/R versus the scaled time tS_L/R for the thermal expansion ratio $\Theta = 8$, the obstacle spacing $\Delta Z = R/4$, the blockage ratios $\alpha = 2/3$, the Lewis number $\boldsymbol{Le = 2}$ and various channel half-widths $R = 12\ L_f, 24\ L_f, 36\ L_f, 48\ L_f$.

All the three propagation regimes (namely, that of initial propagation at constant velocity, that of sudden acceleration, and that of oscillations at a saturation velocity) are exhibited by the $Le = 0.3$ flames in the channels of half-width ranging from $R = 12\ L_f$ to $48\ L_f$. The acceleration rates, the maximum scaled burning rate and the saturation velocities fall within the same range for all the channels considered. This supports the Re-independence of the original Bychkov FA mechanism.

However, an interesting situation is observed in the delay time before FA, i.e. the time taken for initial flame propagation. The increase in such a delay time observed when R grows from $R = 12\ L_f$ to $R = 24\ L_f$ is reversed by further increasing R, to the value of $R = 36\ L_f$, with the time

decreasing further by increasing R to $R = 48\,L_f$. Such a delay prior to acceleration was however attributed to the effect of hydraulic resistance (viscous effect) [22], with the delay period stated to decay to zero as $R \to \infty$. This assertion however does not hold under some conditions, in this case, for $12\,L_f \le R \le 24\,L_f$. A reversal of such a trend experienced for $24\,L_f \le R \le 36\,L_f$ indicates the presence of a threshold within this region, which might depend on the Peclet number (the ratio of the channel half-width to the flame thickness) or other effects. For the $Le = 2$ flame (Fig 7.23), acceleration is observed only in the $R = 36\,L_f$ and $R = 48\,L_f$ channels, with the delay time prior to acceleration decreasing as R grows from $36\,L_f$ to $48\,L_f$. At narrower channels such as those with $R = 12\,L_f$ and $24\,L_f$, a flame propagates with a constant velocity.

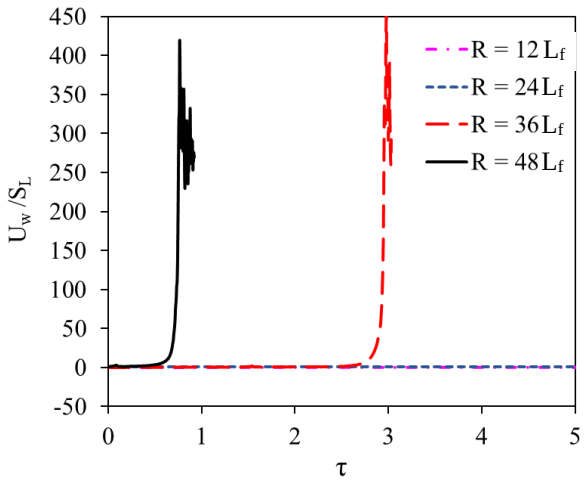

Figure 7.23: The scaled burning rate U_w/S_L versus the scaled time tS_L/R for the thermal expansion ratio $\Theta = 8$, the obstacle spacing $\Delta Z = R/4$, the blockage ratios $\alpha = 2/3$, the Lewis number $\boldsymbol{Le} = \mathbf{2}$ and various channel half-widths $R = 12\,L_f, 24\,L_f, 36\,L_f, 48\,L_f$.

7.6 Impact of Le-ΔZ Interplays on Flame Propagation in Fully Open Channel

Increasing the obstacle spacing from $\Delta Z = R/4$ to $R/2$ and R, most especially for cases of $Le < 1$, where the existence of different modes of flame propagation has been established, show that the delay time prior to acceleration is also impacted. Specifically, Fig. 7.24 shows the scaled burning rate versus the scale time for $Le = 0.3$, $\Theta = 8$, $R = 24$, and $\alpha = 1/2$, with the delay time before transition to sudden acceleration decreasing as the obstacle spacing grows from $R/4$ to $R/2$. This delay time, however, increases when the obstacle spacing is further increased to $\Delta Z = R$. While flame propagation is not affected qualitatively as the obstacle spacing varies, the changes observed in the delay time might be due to competing contributions of delayed burning in the pockets and

turbulence. Indeed, a supplementary role played by turbulence in the Byckhov mechanism of FA in obstructed conduits is known to increase as the obstacle spacing grows, and thus, expected to contribute to the reduction of the initial delay time. However, the time needed before a contribution of delayed burning is felt in the unobstructed part of the channel also increases with the obstacle spacing, due to the increased volume of fuel premixture per pocket. When α grows to $2/3$, Fig. 7.25, similar to the case of $\alpha = 1/2$, the delay time grows by increasing the obstacle spacing from $R/4$ to $R/2$, but decreased thereafter. The higher blockage ratio of $\alpha = 2/3$, however, altered the flame dynamics, and consequently, the time taken prior to sudden transition to acceleration.

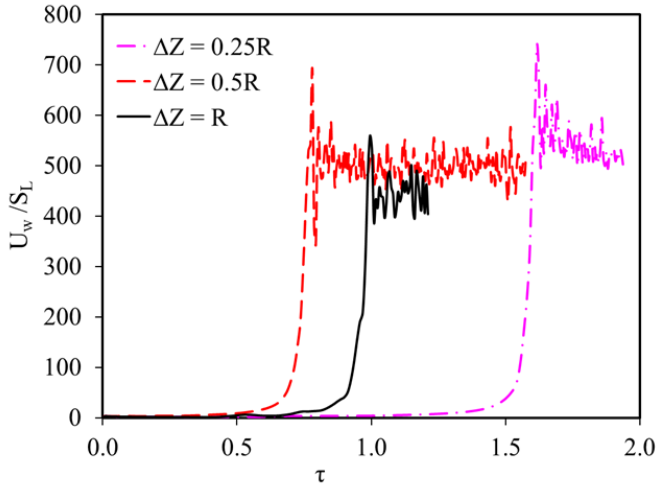

Figure 7.24: The scaled burning rate U_w/S_L versus the scaled time tS_L/R for the thermal expansion ratio $\Theta = 8$, the channel size $R = 24\ L_f$, the Lewis numbers $Le = 0.3$, blockage ratio $\boldsymbol{\alpha = 1/2}$ and various $\Delta Z/R = 1/4\,, 1/2,\ 1$.

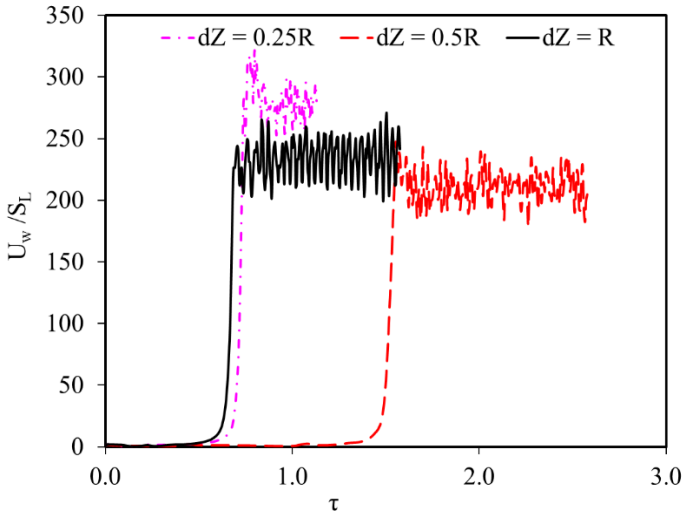

Figure 7.25: The scaled burning rate U_w/S_L versus the scaled time tS_L/R for the thermal expansion ratio $\Theta = 8$, the channel size $R = 24\ L_f$, the Lewis numbers $Le = 0.3$, blockage ratio $\boldsymbol{\alpha = 2/3}$ and various $\Delta Z/R = 1/4\,, 1/2,\ 1$.

7.7. Oscillation-to-Acceleration Transitions of Low-Le Flames in Obstructed Channels with Open Ends

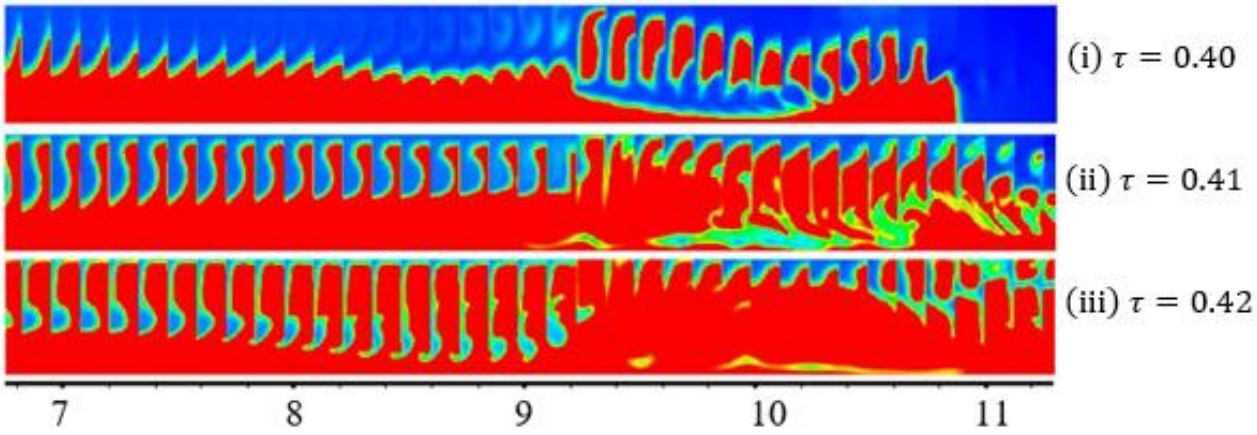

Figure 7.26: The temperature snapshots for evolution of a flame with $\Theta = 8$, $Le = 0.3$ propagating in an obstructed channel of half -width $R = 12\ L_f$ with the blockage ratio $\alpha = 2/3$ (a partial section view).

The flame evolution leading to sudden acceleration, discussed above, is illustrated by the color temperature snapshots in Fig. 7.26. Specifically, at the scaled time $\tau = 0.4$, Fig. 7.26 (i), the hot spots and the flame segments not connected to the major propagating flame segment are observed to be formed between the obstacles. Spontaneous combustion caused by this condition results in thermal explosion and formation of additional hotspots, as seen in Fig. 7. 26 (ii). The interplay of the thermal explosion and the eventual completion of delayed burning occurring upstream in the channel, Fig. 7.26 (iii), provides enough force to create sudden acceleration. Compression of the fuel mixture ahead of a propagating flame results in the increased pressure and temperature in the fuel mixture, which can cause formation of the hot spots. Figures 7.27 and 7.28 show the plots of the scaled burning rate U_w/S_L and temperature at the fuel side of the flame tip, T_{tip}, respectively. Also, depicted in Fig. 7.27 and 7.28 is the instantaneous flame tip Mach number Ma_{tip}. Here, the lines of similar color and type represent each R, while the bold lines in both figures show Ma_{tip}, faint lines represent U_w/S_L and T_{tip} in Figs. 7.27 and 7.28, respectively. These plots reveal that the three parameters follow the same trend. However, it is observed that Ma_{tip} grows first, before the other two parameters.

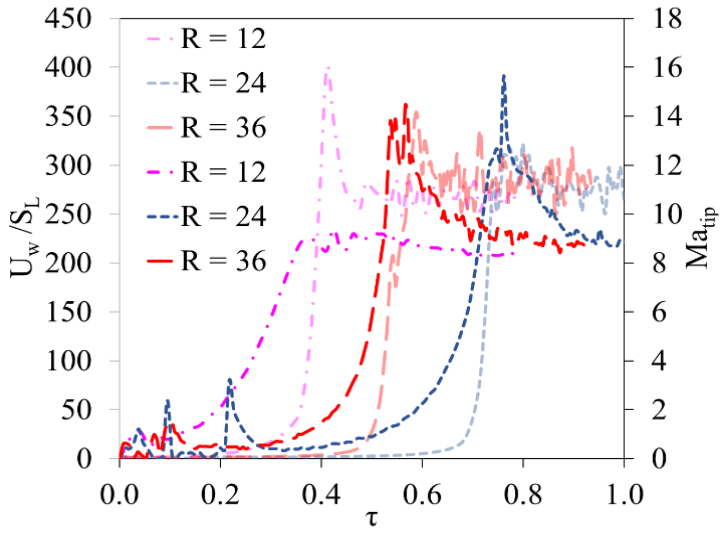

Figure 7.27: The scaled burning rate U_w/S_L and the flame tip Mach number Ma_{tip} versus the scaled time tS_L/R for the $Le = 0.3$, $\Theta = 8$ flames in the obstructed channels with $\alpha = 2/3$, $\Delta Z = R/4$, and various $R/L_f = 12, 24, 36$.

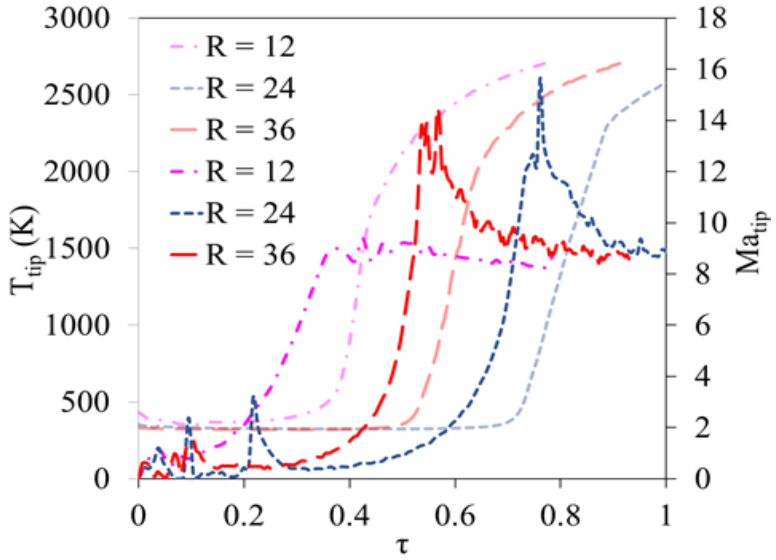

Figure 7.28: The fuel temperature at the flame tip T_{tip} and the flame tip Mach number Ma_{tip} versus the scaled time tS_L/R for the $Le = 0.3$, $\Theta = 8$ flames in the obstructed channels with $\alpha = 2/3$, $\Delta Z = R/4$, and $R/L_f = 12, 24, 36$.

At the early stage, when Ma_{tip} is low, both the flame temperature and the scaled burning rate maintain low values too. Subsequently, both T_{tip} and U_w/S_L grow swiftly, signifying a transition to sudden acceleration, when Ma_{tip} reaches a threshold value being in the range $1 \leq Ma_{tip} \leq 2$ for $R = 12\ L_f, 24\ L_f, 36\ L_f$ considered. Sudden acceleration can be devoted to compressibility in a channel as the compression of the fuel mixture ahead of the flame front results in the increased temperature and, consequently, the increased burning rate. However, while compressibility was

previously found to moderate FA in obstructed semi-open channels [82], in the present geometry, it is found to be responsible for sudden flame acceleration such as that reported in Ref. [90].

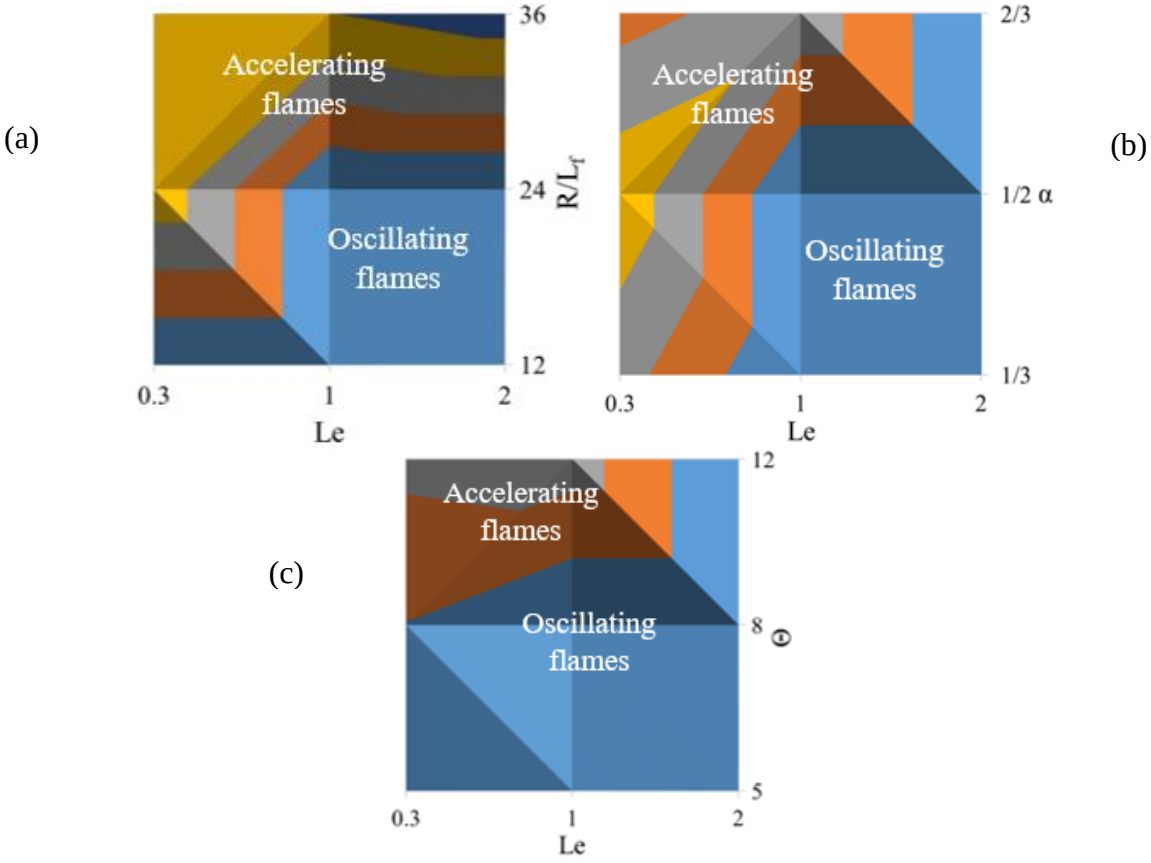

Figure 7.29: Oscillating and accelerating regimes of flame propagation for: various R, Le, $\alpha = 1/2$, $\Delta Z = R/4$ & $\Theta = 8$ (a); various α, Le, $R = 24L_f$, $\Delta Z = R/4$ & $\Theta = 8$ (b); various Θ, Le, $R = 24L_f$, $\Delta Z = R/4$, & $\alpha = 1/3$ (c).

Finally, the contour maps in Fig. 7.29 show the regimes of flame propagation, namely, acceleration and oscillations, exhibited by the propagating flame at various geometrical and thermo-chemical conditions. In Fig. 7.29a, it is shown that the tendency of the flame to accelerate increases with the channel width, for all Le. However, the critical width at which FA occurs is lower for $Le = 0.3$, as compared to the $Le \geq 1$ flames. The map of the blockage ratio α versus the Lewis number Le at $R = 24L_f$, $\Delta Z = R/4$, $\Theta = 8$ in Fig. 7.29b indicates that a flame oscillates at $Le = 2$ but accelerate at $Le = 0.3$ for all the blockage ratios. Variation of the thermal expansion ratio Θ at various Le, $R = 24L_f$, $\Delta Z = R/4$ and $\alpha = 1/3$ in Fig. 7.29c shows that an increase in Θ in from $\Theta = 5$ to $\Theta = 12$ causes only $Le \leq 1$ flames to accelerate. The impact of the higher Θ does not provide enough push to cause acceleration of the $Le = 2$ flame. In all cases considered, it is observed that the flame tendency to transit to acceleration increases as Le decreases.

8 Conclusions and Recommendations

8.1 Conclusions

The impact of non-equdiffusivity on the flame dynamics and morphology in channels of various geometrical configurations associated with different flame propagation mechanisms have been investigated by means of the computational simulations of the reacting flow equations including fully-compressible hydrodynamics, transport properties (heat conduction, viscosity and diffusion) and the chemical kinetics imitated by a first-order, one-step Arrhenius reaction. Variables explored in this parametric study include: the Lewis number, the thermal expansion ratio; the Reynolds number associated with flame propagation and defined by the channel half-width; the blockage ratio and the obstacle spacing (in obstructed geometry); and the thermal and mechanistic boundary conditions. A deviation from equidiffusivity is measured by the Lewis number, with $Le = 1$ for equidiffusive burning.

Starting with the effects of non-equidiffusivity (including such phenomena as diffusional-thermal instability and flame thickening) on finger FA at the early stage of premixed burning in a pipe with adiabatic slip walls, it is seen that the $Le < 1$ flames exhibit higher acceleration as compared with the $Le = 1$ flames. In the case of very low Le, it is shown that the flame Reynolds number Re, has only a minor effect on the burning rate and, consequently, on FA (if occurs). In contrast, the $Le > 1$ flames experience moderation of acceleration, due to a thickening of a flame front, with Re playing a more significant role in the changes that occur. It can be concluded from the fact of promoted FA observed at higher Re that easier distortion of a flame front is possible in wider channels, causing increased surface area of the flame front and thus a higher burning rate and stronger acceleration. The effect of thermal expansion ratio appears non-monotonic. Namely, an increase in Θ weakens flame acceleration at a low Le such as $Le = 0.2$. In contrast, at $Le = 1.5$, we have found that FA increases, slightly, with Θ.

The flame propagation in semi-open channel was also extended to obstructed channels in order to investigate the impact of non-equidiffusive burning on the Bychkov mechanism of FA. Specifically, the impact of Le on this acceleration mechanism is found to be as strong as that of the blockage ratio α, which was identified to be very strong for equidiffusive flames. In the case of $Le < 1$, promotion of flame acceleration is discovered. It is found that the Lewis number has an influence on the α-dependence. In contrast, moderation of FA has been observed for the $Le >$

1 flames. The interplay between $Le < 1$ and high α leads to FA with the highest acceleration rate. In addition, a unique trend is noticed for the Le-impact on Re. Specifically, the Lewis number may change a Re-dependence of FA to an opposite trend.

In continuation, the impacts of the Lewis number on flame propagation in channels with both ends open, and with smooth, no-slip, adiabatic walls are analyzed. Also scrutinized is the interplay of nonequidiffusive burning with the thermal expansion ratio Θ and the flame Reynolds number. It is found that flames oscillate at $Le < 1$, with the oscillation amplitude and frequency decreasing with Le. The low-Le flames exhibit the stages of cusp formation, flame bifurcation and the collapse of flame segments, repeatedly. As for the $Le \geq 1$ flames, the slight oscillations are seen right after initiation, following which steady flame propagation proceed. While the impact of Θ on the flame is found to be minimal, the trend of its impact at $Le = 0.2$ is reversed when $Le = 2$. An increase in the channel width produces a slight difference in the flame behavior, with the difference in morphology and dynamics more noticeable at $Le = 0.2$. Change in the thermal boundary condition to isothermal significantly changed the flame dynamics as the flames began to retract.

Finally, the effects of fuel mixture non-equidiffusivity, $Le \neq 1$ in obstructed channels with open ends are investigated. The interplays of Le with the geometrical parameter such as the channel half-width, the blockage ratio, and obstacle spacing ratio are also scrutinized. The flames undergo either oscillations, or acceleration, or a combination of both the regimes. The Lewis number was found to have both quantitative and qualitative impact on flame propagation as there are transitions from oscillation to acceleration, and vice versa, when Le changes. In conditions where oscillations are experienced for all the cases considered (namely, at thermal expansion ratio $\Theta = 8$, blockage ratio $\alpha = 1/3$, channel width; $R = 12\ L_f$, obstacle spacing $\Delta Z = R/4$), the oscillation frequency decreases while the oscillation amplitude increase with Le. The flame also showed various regimes of propagation, namely: near-steady oscillations, sudden acceleration, the oscillations around a saturation velocity or propagation with a constant velocity – depending on the impact of the Lewis number – independently, or because of its interplay with other parameters. The flames show higher tendency of exhibiting the sequence of initial flame propagation-sudden acceleration-oscillation at saturation velocity at $Le < 1$, while flame oscillation is encountered more for the $Le > 1$ flames.

The time of quasi-steady propagation of a $Le < 1$ flame is found to be affected by the changes in the channel geometric parameters. Whether a flame oscillates or accelerates is determined by the ratio of two competing forces: one from the expanding burnt gas, and the other from viscous

effect due to fuel premixture ahead of the flame front. The Lewis number is found to contribute significantly to the magnitude of the push force and the flames response to the stretch caused by the hydraulic resistance, and thus, the dynamics and morphology of the flame as it propagates. At the early stage of burning, compressibility is found not to be significant, therefore, the flame may oscillate. However, as the Mach number associated with the flame tip, Ma_{tip}, subsequently grows, accompanied by an increased fuel temperature, hot spots are formed ahead of the flame front. An interplay of the thermal explosion caused by flow compression and delayed burning in the pockets between the obstacles is found to be responsible for the sudden transition from the oscillations to acceleration.

8.2 Recommendations

The focus in this work was to investigate how the propagation of flames in channels is affected by the variations in the thermal to mass diffusivity ratio. The areas of future research directions to provide further fundamental understanding and enhanced practical applications include:

In the semi-open obstructed channels, the present work focus on the acceleration at the early stage of flame propagation. Given the strong acceleration associated with the flame propagation in this mechanism, the possibility of detonation is high. It is therefore important to investigate what the impact of non-equidiffusivity on the DDT process and eventual detonation propagation would be. Incorporation of the detailed chemistry in the analysis is also deemed essential, as chemistry plays a key role in the DDT process.

Also, part of the present work involves situations where channel ends remain open all through the flame propagation process. However, many situations in practice requires the conditions at the ends to change from time to time as the flame propagates. It is therefore necessary to investigate the effect of Lewis number on the flame when there are dynamic changes at the channel ends.

Lastly, it is desired to apply the results of the present study in designing combustion devices, such as in pulse detonation engine, micro gas turbine for powering microdevices and in the performance improvement of fire prevention equipment for residential and industrial usage.

Reference

[1] G. Ciccarelli, S. Dorofeev, "Flame acceleration and transition to detonations in ducts," *Prog. Energy Combust. Sci.*, vol. 34, pp. 499–550, 2008.

[2] S. T. Aruna, A. S. Mukasyan, "Combustion synthesis and nanomaterials," *Curr. Opin. Solid State Mater. Sci.*, vol. 12, no. 3–4, pp. 44–50, 2008.

[3] S. Demir, V. Bychkov, S. H. R. Chalagalla, V. Akkerman, "Towards a predictive scenario of a burning accident in a mining passage," *Combust. Theory Model.*, vol. 21, no. 6, pp. 997–1022, 2017.

[4] S. B. Dorofeev, "Flame acceleration and explosion safety applications," *Proc. Combust. Inst.*, vol. 33, no. 2, pp. 2161–2175, 2011.

[5] G. Thomas, G. Oakley, R. Bambrey, "An experimental study of flame acceleration and deflagration to detonation transition in representative process piping," *Process Saf. Environ. Prot.*, vol. 88, no. 2, pp. 75–90, 2010.

[6] "Fossil Fuels Account for Lowest Share of U.S. Energy Consumption in More than a Century," 2018. [Online]. Available: https://e360.yale.edu/digest/fossil-fuels-account-for-lowest-share-of-u-s-energy-consumption-in-more-than-a-century.

[7] "What is U.S. electricity generation by energy source?," 2019. [Online]. Available: https://www.brookings.edu/blog/up-front/2019/03/06/what-is u/?utm_campaign=Economic Studies&utm_source=hs_email&utm_medium=email&utm_content=70695290.

[8] C. K. Law, *Combustion Physics*. New York: Cambridge University Press, 2006.

[9] G. D. Surywanshi, B. B. K. Pillai, V. S. Patnaikuni, R. Vooradi, S. B. Anne, "4-E analyses of chemical looping combustion based subcritical, supercritical and ultra-supercritical coal-fired power plants," *Energy Convers. Manag.*, vol. 200, p. 112050, 2019.

[10] M. Ayoobi, I. Schoegl, "Numerical analysis of flame instabilities in narrow channels : Laminar premixed methane/air combustion," *Int. J. Spray Combust. Dyn.*, vol. 9, no. 3, pp. 155–171, 2017.

[11] A. Liu, Y. Yang, L. Chen, W. Zeng, C. Wang, "Experimental study of biogas combustion and emissions for a micro gas turbine," *Fuel*, vol. 267, p. 117312, 2020.

[12] K. Wang, W. Fan, W. Lu, Q. Zhang, F. Chen, C. Yan, Q. Xia "Propulsive performance of a pulse detonation rocket engine without the purge process," *Energy*, vol. 79, pp. 228–234, 2015.

[13] L. Wang, H. Ma, Z. Shen, D. Chen, "Flame Quenching by Crimped Ribbon Flame Arrestor : A Brief Review in in," vol. 38, no. 1, pp. 27–41, 2019.

[14] L. R. Boeck, A. Kink, D. Oezdin, J. Hasslberger, T. Sattelmayer, "Influence of water mist on flame acceleration, DDT and detonation in H_2-air mixtures," *Int. J. Hydrogen Energy*, vol. 40, no. 21, pp. 6995–7004, 2015.

[15] M. Han, Y. Ai, Z. Chen, W. Kong, "Laminar flame speeds of H2/CO with CO2 dilution at normal and elevated pressures and temperatures," *Fuel*, vol. 148, pp. 32–38, 2015.

[16] H. Wei, T. Zhu, G. Shu, L. Tan, Y. Wang, "Gasoline engine exhaust gas recirculation - A review," *Appl. Energy*, vol. 99, pp. 534–544, 2012.

[17] S. Wang, C. Ji, B. Zhang, X. Cong, X. Liu, "Effect of CO2 dilution on combustion and emissions characteristics of the hydrogen-enriched gasoline engine," *Energy*, vol. 96, pp. 118–126, 2016.

[18] R. Gabriel, J. E. Navedo, R. Chen, "Effects of Fuel Lewis Number on Nitric Oxide Emission of Diluted H 2 Turbulent Jet Diffusion Flames," *Combust. Flame*, vol. 121, pp. 525–534, 2000.

[19] N. Ren, D. Zeng, K. V. Meredith, W. Yi, S. B. Dorofeev, "Modeling of flame extinction/re-ignition in oxygen-reduced environments." pp. 3951–3958, 2019.

[20] R. Chen, M. Chaos, A. Kothawala, "Lewis number effects in laminar diffusion flames near and away from extinction," *Proc. Combust. Inst.*, vol. 31, pp. 1231–1237, 2007.

[21] A. Adebiyi, E. Ridgeway, R. Alkandari, A. Cathreno, D. Valiev, V. Akkerman, "Premixed flame oscillations in obstructed channels with both ends open," *Proc. Combust. Inst.*, vol. 37, no. 2, pp. 1919–1926, 2019.

[22] V. Bychkov, J. Sadek, V. Akkerman, “Analysis of flame acceleration in open or vented obstructed pipes,” *Phys. Rev. E*, vol. 95, no. 1, 2017.

[23] V. Akkerman, C. K. Law, V. Bychkov, L. E. Eriksson “Analysis of flame acceleration induced by wall friction in open tubes,” vol. 22, p. 053606, 2010.

[24] V. Akkerman, V. Bychkov, A. Petchenko, L. E. Eriksson, “Flame oscillations in tubes with nonslip at the walls,” *Combust. Flame*, vol. 145, no. 4, pp. 675–687, 2006.

[25] M. Silvestrini, B. Genova, G. Parisi, F. J. Leon Trujillo, “Flame acceleration and DDT run-up distance for smooth and obstacles filled tubes,” *J. Loss Prev. Process Ind.*, vol. 21, no. 5, pp. 555–562, 2008.

[26] C. Wang, F. Huang, E. K. Addai, X. Dong, “Effect of concentration and obstacles on flame velocity and overpressure of methane-air mixture,” *J. Loss Prev. Process Ind.*, vol. 43, pp. 302–310, 2016.

[27] Z. Shilong, F. Yuxin, L. Haojie, J. Bingyue, “Effects of a jet turbulator upon flame acceleration in a detonation tube,” *Appl. Therm. Eng.*, vol. 115, pp. 33–40, 2017.

[28] C. Dong, M. Bi, Y. Zhou, “Effects of obstacles and deposited coal dust on characteristics of premixed methane-air explosions in a long closed pipe,” *Saf. Sci.*, vol. 50, no. 9, pp. 1786–1791, 2012.

[29] V. B. Akkerman, V. V. Bychkov, R. J. M. Bastiaans, L. P. H. de Goey, J. A. van Oijen, L. E. Eriksson, “Flow-flame interaction in a closed chamber,” *Phys. Fluids*, vol. 055107, 2016.

[30] P. Chen, G. Luo, Y. Sun, Q. Lv, “Impacts of plate slits on flame acceleration of premixed methane/air in a closed tube,” *J. Energy Inst.*, pp. 1–10, 2017.

[31] A. P. Singh, V. R. Kishore, Y. Yoon, S. Minaev, S. Kumar, “Effect of wall thermal boundary conditions on flame dynamics of CH_4-air and H_2-air mixtures in straight microtubes,” *Combust. Sci. Technol.*, vol. 189, no. 1, pp. 150–168, 2017.

[32] N. Yilmaz, A. B. Donaldson, and R. E. Lucero, “Experimental study of diffusion flame oscillations and empirical correlations,” *Energy Convers. Manag.*, vol. 49, pp. 3287–3291,

2008.

[33] R. Ortiz-Imedio, A. Ortiz, J. C. Urroz, P. M. Dieguez, D. Gorri, L. M. Gandia, I. Ortiz, "Comparative performance of coke oven gas, hydrogen and methane in a spark ignition engine," *Int. J. Hydrogen Energy*, 2020.

[34] T. Lee, J. Park, D. Han, K. T. Kim, "The dynamics of multiple interacting swirl-stabilized flames in a lean-premixed gas turbine combustor," *Proceedings of the Combustion Institute*, vol. 37, no. 4. pp. 5137–5145, 2019.

[35] P. Wolanski, "Detonation engines," *J. KONES*, vol. 18, no. 3, pp. 515–521, 2011.

[36] A. Heidari, J. X. Wen, "Flame acceleration and transition from deflagration to detonation in hydrogen explosions," *Int. J. Hydrogen Energy*, vol. 39, no. 11, pp. 6184–6200, 2014.

[37] X. Rocourt, I. Sochet, B. Pellegrinelli, "Small-scale flame acceleration and application of medium and large-scale flame speed correlations," *Int. J. Hydrogen Energy*, vol. 42, no. 2, pp. 1327–1336, 2017.

[38] D. A. Kessler, V. N. Gamezo, E. S. Oran, "Simulations of flame acceleration and deflagration-to-detonation transitions in methane-air systems," *Combust. Flame*, vol. 157, no. 11, pp. 2063–2077, 2010.

[39] A. Chinnayya, A. Hadjadj, D. Ngomo, "Computational study of detonation wave propagation in narrow channels," *Phys. Fluids*, vol. 25, p. 036101, 2013.

[40] W. Rudy, M. Kuznetsov, R. Porowski, A. Teodorczyk, J. Grune, K. Sempert, "Critical conditions of hydrogen-air detonation in partially confined geometry," *Proc. Combust. Inst.*, vol. 34, no. 2, pp. 1965–1972, 2013.

[41] W. Han, Y. Gao, C. Wang, C. K. Law, "Coupled pulsating and cellular structure in the propagation of globally planar detonations in free space," vol. 27, p. 106101, 2015.

[42] E. S. Oran, V. N. Gamezo, "Origins of the deflagration-to-detonation transition in gas-phase combustion," *Combust. Flame*, vol. 148, no. 1–2, pp. 4–47, 2007.

[43] W. Han, Y. Gao, C. K. Law, "Flame acceleration and deflagration-to-detonation transition in micro- and macro-channels : An integrated mechanistic study," *Combust. Flame*, vol.

176, pp. 285–298, 2017.

[44] M. Cross, G. Ciccarelli, “DDT and detonation propagation limits in an obstacle filled tube,” *J. Loss Prev. Process Ind.*, vol. 36, pp. 380–386, 2015.

[45] G. B. Goodwin, R. W. Houim, E. S. Oran, “Effect of decreasing blockage ratio on DDT in small channels with obstacles,” *Combust. Flame*, vol. 173, pp. 16–26, 2016.

[46] R. Porowski, A. Teodorczyk, “Experimental study on DDT for hydrogen-methane-air mixtures in tube with obstacles,” *J. Loss Prev. Process Ind.*, vol. 26, no. 2, pp. 374–379, 2013.

[47] I. Brailovsky, G. I. Sivashinsky, “Hydraulic Resistance as a Mechanism for Deflagration-to- Detonation Transition,” vol. 499, pp. 492–499, 2000.

[48] G. O. Thomas, “Flame acceleration and the development of detonation in fuel-oxygen mixtures at elevated temperatures and pressures,” *J. Hazard. Mater.*, vol. 163, no. 2–3, pp. 783–794, 2009.

[49] C. K. Law, C. J. Sung, “Structure, aerodynamics, and geometry of premixed flamelets,” vol. 26, pp. 459–505, 2000.

[50] C. Clanet, G. Searby, “On the ‘Tulip Flame’ Phenomenon,” *Combust. Flame*, vol. 105, no. 1–2, pp. 225–238, 1996.

[51] V. Bychkov, V. Akkerman, G. Fru, A. Petchenko, L. Eriksson, “Flame acceleration in the early stages of burning in tubes,” *Combust. Flame*, vol. 150, no. 4, pp. 263–276, 2007.

[52] D. Valiev, V. Bychkov, V. Akkerman, C. K. Law, L. E. Eriksson, “Flame acceleration in channels with obstacles in the deflagration-to-detonation transition,” *Combust. Flame*, vol. 157, no. 5, pp. 1012–1021, 2010.

[53] V. Akkerman, D. Valiev, “Moderation of Flame Acceleration in Obstructed Cylindrical Tubes due to Gas Compression,” *Phys. Fluids*, vol. 30, p. 106101, 2018.

[54] V. Bychkov, D. Valiev, L. E. Eriksson, “Physical mechanism of ultrafast flame acceleration,” *Phys. Rev. Lett.*, vol. 101, p. 164501, 2008.

[55] V. N. Gamezo, T. Ogawa, E. S. Oran, “Flame acceleration and DDT in channels with

obstacles: Effect of obstacle spacing," *Combust. Flame*, vol. 155, no. 1–2, pp. 302–315, 2008.

[56] B. Ponizy, A. Claverie, B. Veyssière, "Tulip flame - the mechanism of flame front inversion," *Combust. Flame*, vol. 161, no. 12, pp. 3051–3062, 2014.

[57] D. M. Valiev, V. Akkerman, M. Kuznetsov, L. E. Eriksson, C. K. Law, V. Bychkov, "Influence of gas compression on flame acceleration in the early stage of burning in tubes," *Combust. Flame*, vol. 160, no. 1, pp. 97–111, 2013.

[58] A. Dejoan, V. N. Kurdyumov, "Thermal expansion effect on the propagation of premixed flames in narrow channels of circular cross-section: Multiplicity of solutions, axisymmetry and non-axisymmetry," *Proc. Combust. Inst.*, vol. 37, no. 2, pp. 1927–1935, 2019.

[59] D. M. Valiev, V. Bychkov, V. Akkerman, L. E. Eriksson, C. K. Law, "Quasi-steady stages in the process of premixed flame acceleration in narrow channels," *Phys. Fluids*, vol. 25, no. 096101, 2013.

[60] A. Adebiyi, R. Alkandari, D. Valiev, V. Akkerman, "Effect of surface friction on ultrafast flame acceleration in obstructed cylindrical pipes," vol. 9, p. 035249, 2019.

[61] G. Ciccarelli, C. T. Johansen, M. Parravani, "The role of shock-flame interactions on flame acceleration in an obstacle laden channel," *Combust. Flame*, vol. 157, no. 11, pp. 2125–2136, 2010.

[62] G. Ciccarelli, C. J. Fowler, M. Bardon, "Effect of obstacle size and spacing on the initial stage of flame acceleration in a rough tube," *Shock Waves*, vol. 14, no. 3, pp. 161–166, 2005.

[63] L. R. Boeck, M. Kellenberger, G. Rainsford, G. Ciccarelli, "Simultaneous OH-PLIF and schlieren imaging of flame acceleration in an obstacle-laden channel," *Proc. Combust. Inst.*, vol. 36, no. 2, pp. 2807–2814, 2017.

[64] A. Teodorczyk, P. Drobniak, A. Dabkowski, "Fast turbulent deflagration and DDT of hydrogen-air mixtures in small obstructed channel," *Int. J. Hydrogen Energy*, vol. 34, no. 14, pp. 5887–5893, 2009.

[65] A. Di Stazio, C. Chauveau, G. Dayma, P. Dagaut, “Oscillating flames in micro-combustion,” *Combust. Flame*, vol. 167, pp. 392–394, 2016.

[66] J. Yang, F. M. S. Mossa, H. W. Huang, Q. Wang, R. Woolley, Y. Zhang, “Oscillating flames in open tubes,” *Proc. Combust. Inst.*, vol. 35, no. 2, pp. 2075–2082, 2015.

[67] D. Patel, N. Chakraborty, “Effects of Fuel Lewis Number on Localised Forced Ignition of Globally Stoichiometric Stratified Mixtures : a Numerical Investigation,” *Flow, Turbul. Combust.*, pp. 1083–1105, 2016.

[68] S. D. Salusbury, J. M. Bergthorson, “Maximum stretched flame speeds of laminar premixed counter-flow flames at variable Lewis number,” *Combust. Flame*, vol. 162, no. 9, pp. 3324–3332, 2015.

[69] D. Lapalme, R. Lemaire, P. Seers, N. Ouest, “Assessment of the method for calculating the Lewis number of H_2/CO/CH_4 mixtures and comparison with experimental results,” *Int. J. Hydrogen Energy*, vol. 42, no. 12, pp. 8314–8328, 2017.

[70] N. Bouvet, F. Halter, C. Chauveau, Y. Yoon, “On the effective Lewis number formulations for lean hydrogen / hydrocarbon / air mixtures,” *Int. J. Hydrogen Energy*, vol. 38, no. 14, pp. 5949–5960, 2013.

[71] A. Clarke, “Calculation and consideration of the Lewis number for explosion studies,” *Trans. Inst. Chem. Eng.*, vol. 80, pp. 0957–5820, 2002.

[72] S. Bilgili, B. Demirgok, D. Valiev, V. Bychkov, V. Akkerman “Effect of Lewis number on flame acceleration in channels,” in *9th U.S. National Combustion Meeting*, 2015.

[73] V. N. Kurdyumov, “Lewis number effect on the propagation of premixed flames in narrow adiabatic channels: Symmetric and non-symmetric flames and their linear stability analysis,” *Combust. Flame*, vol. 158, no. 7, pp. 1307–1317, 2011.

[74] L. Kagan, G. Sivashinsky, “Effect of Lewis number on flame propagation through vortical flows,” *Combust. Flame*, vol. 142, pp. 235–240, 2005.

[75] S. Chakraborty, A. Mukhopadhyay, S. Sen, “Interaction of Lewis number and heat loss effects for a laminar premixed flame propagating in a channel,” *Int. J. Therm. Sci.*, vol. 47,

pp. 84–92, 2008.

[76] Z. Zhou, Y. Shoshin, F. E. Hernández-pérez, J. A. Van Oijen, L. P. H. De Goey, "Effect of Lewis number on ball-like lean limit flames," *Combust. Flame*, vol. 188, pp. 77–89, 2018.

[77] S. H. Yoon, T. J. Noh, O. Fujita, "Effects of Lewis number on generation of primary acoustic instability in downward-propagating flames," *Proc. Combust. Inst.*, vol. 36, no. 1, pp. 1603–1611, 2017.

[78] L. Berger, K. Kleinheinz, A. Attili, H. Pitsch, "Characteristic patterns of thermodiffusively unstable premixed lean hydrogen flames," *Proc. Combust. Inst.*, vol. 37, no. 2, pp. 1879–1886, 2018.

[79] N. Chakraborty, M. Klein, "Influence of Lewis number on the surface density function transport in the thin reaction zone regime for turbulent premixed flames," *Phys. Fluids*, vol. 20, p. 065102, 2009.

[80] N. Chakraborty, R. S. Cant, "Effects of Lewis number on turbulent scalar transport and its modelling in turbulent premixed flames," *Combust. Flame*, vol. 156, no. 7, pp. 1427–1444, 2009.

[81] N. Chakraborty, R. S. Cant, "Effects of Lewis number on scalar transport in turbulent premixed flames Effects of Lewis number on scalar transport in turbulent premixed flames," *Phys. Fluids*, vol. 21, 2009.

[82] V. Bychkov, V. Akkerman, D. Valiev, C. K. Law, "Influence of gas compression on flame acceleration in channels with obstacles," *Combust. Flame*, vol. 157, no. 10, pp. 2008–2011, 2010.

[83] Y. Zeldovich, R. Barenblatt, V. Librovich, G. Makhviladze, *Mathematical Theory of Combustion and Explosions*. 1985.

[84] V. V Bychkov, S. M. Golberg, M. A. Liberman, L. E. Eriksson, "Propagation of curved stationary flames in tubes," *Phys. Rev. E*, vol. 54, no. 4, pp. 3713–3724, 1996.

[85] A. Sahoo, "Flame Acceleration in an Obstacle-Laden Tube," Indian Instituted of Technology, Madras, 2017.

[86] O. J. Ugarte-Almeyda, “Effect of boundary conditions on propagation and morphology of premixed flames in narrow conduits effect of boundary conditions on propagation and morphology of premixed flames in narrow conduits,” p. Doctoral Thesis, 2015.

[87] A. Adebiyi, O. Abidakun, G. Idowu, D. Valiev, V. Akkerman, “Analysis of nonequidiffusive premixed flames in obstructed channels,” *Phys. Rev. Fluids*, vol. 4, no. 6, p. 063201, 2019.

[88] M. Alkhabbaz, O. Abidakun, D. Valiev, and V. Akkerman, “Impact of the Lewis number on flame acceleration at the early Stage of burning in pipes,” *Phys. Fluids*, vol. 31, 083606, pp. 1–10, 2019.

[89] O. J. Ugarte, V. Bychkov, J. Sadek, D. Valiev, V. Akkerman, “Critical role of blockage ratio for flame acceleration in channels with tightly spaced obstacles,” *Phys. Fluids*, vol. 28, no. 9, 2016.

[90] J. Yanez, M. Kuznetsov, V. Bykov, “Sudden acceleration of flames in open channels driven by hydraulic resistance,” *arXiv:1208.6453 [physics.flu-dyn]*, pp. 1–6, 2013.